Master of Science Thesis

Manufacturing and Quality Characterisation of pre-preg fibre-placed Composite Lattice Structures

Jotham Lee

TU Delft

Manufacturing and Quality Characterisation of pre-preg fibre-placed Composite Lattice Structures

Jotham Lee

4724399

in partial fulfilment of the requirements for the degree of

Master of Science

Faculty of Aerospace Engineering,

Aerospace Structures & Materials

at the Delft University of Technology,

to be defended publicly on Wednesday August 28, 2019 at 9:30 AM

Supervisor:	Prof. Dr. ir. C. Kasspoglou	TU Delft
Thesis committee:	Prof. Dr. ir. O.K. Bergsma,	TU Delft
	Prof. ir. M.J. Schuurman,	TU Delft
	Ir. B.J.R. Smeets,	ATG Europe

TU Delft

1. Front Matter

1.1 Abstract

Composite lattice structures (CLS) offer high performance and demonstrate significant mass savings in space structure applications. Local modifications of regular lattice designs have the potential to further improve the lattice performance. This research explored the micro-structural quality features of CLSs manufactured with pre-preg fibre-placement, and how quality is impacted by lattice modifications.

Modifications to a regular lattice for a representative case of an attachment point load are identified using a topology optimisation tool. Three lattice modifications techniques were identified: rib width variations, rib angle variations and additional ribs. A sample lattice with modifications was manufactured and evaluated by C-scan, CT techniques and micro-sections. An explanation of quality features in CLS is described and quantified using a presented characterisation model based on node transition waviness.

Using the presented explanation, a quantitative quality model was developed to relate lattice design geometry to manufactured quality for this process. The model was used to design and manufacture a second panel with improved implementation of lattice modifications. The quality model was improved and shown to explain more than 75% of all observed quality variation in the two panels with a linear regression. Future work and limitations the of the quality model are discussed.

1.2 Table of Contents

1.3 List of Figures

1.4 List of Tables

1.5 Acknowledgements

This research was carried out with the support of ATG Europe, where I completed an internship prior to this MSc thesis. Thus it has been a sustained journey of learning and discovery, and I would like to thank those that helped, guided and motivated me along the way. If I have seen further, it is by standing on the shoulders of giants. I would like to thank Ir. Bart Smeets for his time as my daily supervisor, particularly in the early days when the learning curve approximated a step function. To the others, thank you for the making the work environment so enjoyable.

In parts when the path lead in many directions, my supervisor at the Delft University of Technology provided the questions and insight I needed. Later, where we came close to a precipice, he brought me back to the right track. For making time, being enthusiastic and pushing when needed, I would like to thank Professor Christos Kassapoglou.

I would like to thank Professor Otto Bergsma for being part of the graduation committee. As lecturer of a core course, he was a first point of contact at my time in TU Delft. I would also like to thank Professor Michiel Schuurman for being part of the graduation committee. His lecturing of the Forensic Engineering course exposed me to new concepts and problems in engineering that exemplify the challenges I came to expect at TU Delft.

For those that were involved in manufacturing composite samples, such as the staff at Delft Aerospace Structures and Materials Laboratory, Fred, Victor, Gertjan and Durga to name a few, thank you for your help. To the various colleagues and interns that laid ply after ply of pre-preg tapes with me, I know it's boring after the first few but, really, just a few more before lunch and… thank you for your support.

I would also like to thank Ir. Wim Verwaal and Ellen Meijvogel-de Koning from the faculty of Civil Engineering and Geosciences for spending the afternoon with me to carry out a CT scan of a lattice node. It was during the many hours poring over the results that a breakthrough came to understand the compaction and consolidation of a node. Your assistance was essential to this work.

2. Introduction

Composite lattice structures generally refer to thin walled cylindrical or conical shells that are comprised of a system of ribs aligned at a positive and negative angle to the shell axis, and a system of ribs circumferential to it. Composite lattice structures may also have a skin, but generally do not behave as skin stiffened structures, as the grid is the primary load carrying element. Lattice structures have natural applications in space engineering as inter-stage adapters and satellite structures due to their high stiffness/mass performance. This is presented in the table below.

Table 1 Comparison of weight savings achieved with composite lattice designs

Application	Mass Saving	Baseline structure
Conical Payload Adapter [1]	60%	Aluminium prototype
Upper Inter-stage [1]	20%	Stringer-stiffened aluminium prototype
Lower Inter-stage [1]	38%	Stringer-stiffened aluminium prototype
Communications Satellite Central cylinder* [2]	27%	Aluminium honeycomb sandwich with CFRP face sheets
Ballistic missile payload Shroud [3]	61%	Aluminium shroud

* Based on finite element analysis estimate for requirement load cases

Several lattice arrangements are available, the choice of which is based on specific performance requirements and manufacturing limitations. Design optimization of the lattice geometry can improve the performance of the grid for particular load cases, and has been the subject of significant work in the industry. The ability to manufacture structures and the effect of the process on the performance of the manufactured lattice are essential factors in effective design efforts. The specific manufacturing process of interest in this research is pre-preg tape laying with expansion tooling, as this process can result in a high fibre volume fraction structure (FvF), thus maximising the mass efficiency.

This manufacturing process has been tested for regular grid geometries with good results, including destructive testing and analysis correlation. The quality of structure produced with this manufacturing method is known for certain geometries. However, irregular design geometry may lead to differences in the quality of the manufactured panel that the design process would need to account for, but so far cannot. Irregular designs may result in microstructural details that are significantly different from what is currently achieved with regular lattice designs, namely the characteristic fibre waviness, low void content and minor rib width deviations as noted by Smeets [4]. If these features are found to be sensitive to lattice geometry changes, the analysis method which accounts for them will need to adapt depending on the particular lattice geometry.

Irregular geometry lattice designs could provide performance improvement in cases where additional loads are required to be integrated into the structure. For example, load introduction points could be locally reinforced by including additional members, or locally modifying the grid pattern. Deeper understanding of the manufacturing process and its effect on manufactured quality will improve design freedom by providing a basis for what

geometries are possible with the manufacturing method, and what quality of structure can be expected.

3. State of the art

Lattice structures have been in development for decades with research coming from USA [5], Russia [1] and Japan [6]. Since 2000, increasingly reliable methods have been developed by institutions and universities to analyse grid structures, allowing designers to explore the potential of lattice structures for high performance applications. The trend has moved from analytical tools, mainly based on Smeared Stiffness Theory, towards the Finite Element Method (FEM). Totaro began with a preliminary design for a launcher structure based on numerical optimisation before being further developed with a FEM model [7]. Pavlov developed a semi-automated approach to optimise lattice structures using FEM and the multiple requirements of a satellite central cylinder [2]. The main advantages of the FEM are the level of geometric detail that can be accounted for, as well as the results it can provide for multiple load cases and failure modes. Whereas analytical methods are limited in applicability to certain geometries or global buckling modes, detailed FEM analysis provides more flexibility to account for variations such as curved surfaces, cut-outs or mid-structure attachments, all of which are critical considerations for global analysis of lattice structures in the context of practical design requirements.

However, some areas of lattice analysis using FEM are less clear. As noted by Huybrechts, areas of grid structure analysis that are not well understood analytically and are not typically captured by FEM models are the effect of nodal offset (Figure 3-1), rib-skin attachment (Figure 3-2), and rib behaviour at and near nodes [3]. Nodal offsets are a modification to the lattice layout thought to facilitate the manufacturing process by minimising the build-up at node regions.

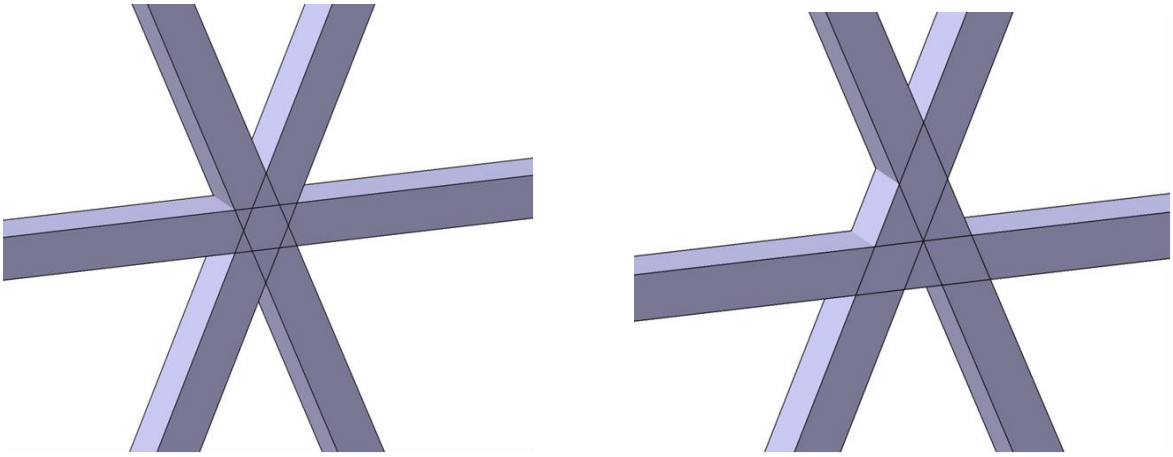

Figure 3-1 Nodal offset modification for 3 members meeting at a node: (left) zero offset where 3 members overlap and (right) offset node eliminates 3 member overlap, resulting in 3 regions with 2 member overlap

These detailed areas require special attention to capture the behaviour of the structure in the form of modifications to the FEM model. However, the particular modifications can be specific to the grid geometry, manufacturing method or the loading case. Therefore significant effort is required to test manufactured structures and correlate the performance to FEM models and obtain accurate predictions in detailed design analysis. Such correlation efforts are costly and impractical when considering the number of possible variations to grid structure.

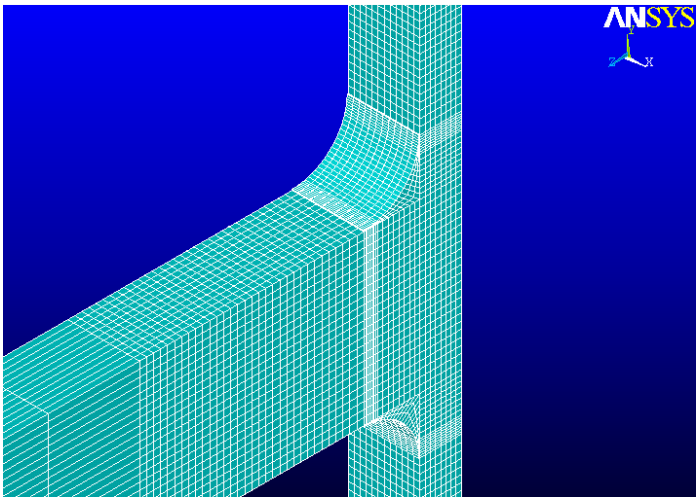

Figure 3-2 FEM model of a rib-skin attachment to capture separation behaviour leading to skin-buckling failure [5]

Details of the grid structure geometry are heavily dependent on the manufacturing method used. Very little data is available on the effects of various manufacturing processes on grid structure behaviour. As noted by Huybrechts *"some examples are skin print through (mark-off) near ribs where rubber tooling deforms the skin, wavy fibres in ribs due to lateral compaction, resin rich/dry areas at or near nodes, and non-uniform fibre volume fraction from rib top to rib bottom"* [3]. These phenomena show that the details of the process are both complex and not understood in detail.

Regarding pre-preg tape laying, recent developments have produced regular grid pattern designs using expansion tooling [8], as shown in Figure 3-3, but do not investigate the structural quality differences in relation to other lattice designs or manufacturing techniques i.e. filament winding with resin infusion.

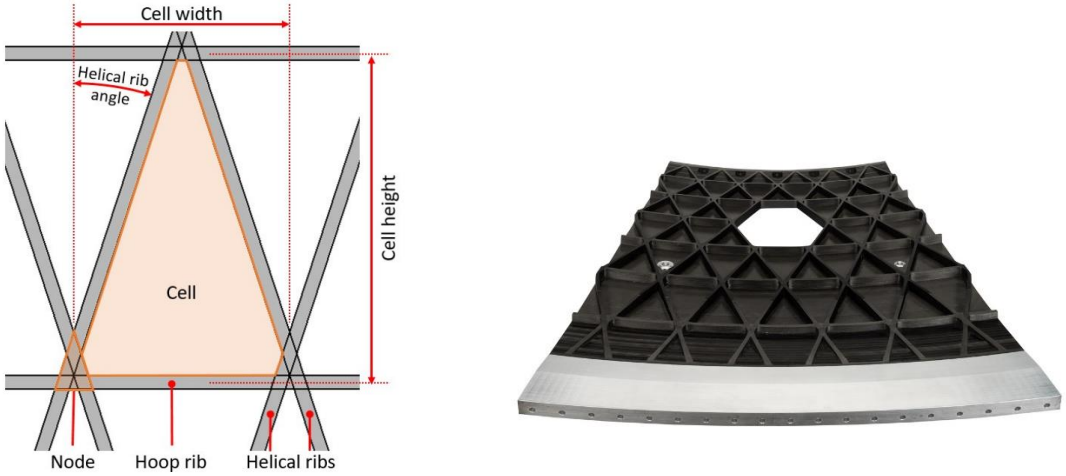

Figure 3-3 Typical grid nomenclature (left) Regular Isogrid manufactured by ATG Europe by pre-preg tow placement (right) [8]

3.1 Grid Geometries

The geometries for regular grids can be described by ribs arranged in 2-4 directions. Following the nomenclature described in Figure 3-3, grids typically have helical angles between 10-35°, as angles outside this range result in poorly performing lattice solutions

[9]. The position of hoop ribs in the circumferential direction determines the geometry of the resulting cells.

In some cases, demonstrated in the previous figures, the hoop ribs cross the helical ribs at the point where the helical ribs intersect each other (with a nodal offset). This produces a node region where the three tows are close to one another and results in regular triangular cells almost equal in size. This architecture is generally associated with lattice designs from the USA [5] and industry development efforts [8], and has been used with pre-preg tape laying [8], automated tape laying and filament winding [10].

Other design ideas arrange the helical ribs such that the hoop-helical intersection occurs at the mid-point between helical-helical intersections, as shown in Figure 3-4. This results in a large hexagonal cell, smaller triangular cells and binary lattice intersections. This design type is utilized by Russian structures, where it is typically produced using wet filament winding [1].

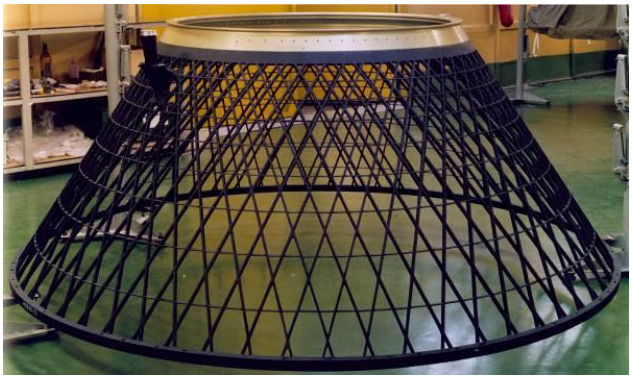

Figure 3-4 Conical payload adapter with binary lattice intersections, produced with wet filament winding [9]

3.1.1 Irregular geometries

Specific load cases might benefit from an arrangement of additional ribs in a globally optimised regular structure. Such additional ribs could provide increased stiffness or load carrying capacity, as shown by Bakhvalov to provide a load path between attachment points on interface rings [9]. Additional members interrupt the regular pattern of a lattice structure, resulting in divided and smaller cells. The additional intersections will reduce the length of some members. This may also result in mixed intersection modes, where additional members form node regions at some points in the lattice. The effect on the quality of the lattice was not discussed, although mechanical testing was said to agree with FEM predictions with an accuracy of 10%, suggesting that quality effects of placing additional elements are limited for this the wet filament winding technique.

Figure 3-5 Lattice cylinders with irregular helical rib pattern, produced by wet filament winding [1]

The lattice modifications described above represent a relatively simple design change that can be incorporated to the manufacturing process, offering a performance benefit. To date, irregular lattice designs have not been seen with lattice structures produced with pre-preg tape laying, while the effort in design and manufacturing modification would be similar to the filament wound counterparts.

3.2 Manufacturing Process

3.2.1 Continuous Tape Laying with Expansion Tooling

In a review of the manufacturing theory of grid stiffened structures for a simple rib element [11], Huybrechts proposes a simplified theory for the governing behaviour of expansion tooling (generally silicone rubber is used) as a starting point for tooling design to achieve suitable compaction during cure. This theory is demonstrated with simple, single rib elements, with good correlation. Essentially it provides the required tooling size or a suitable scale factor based on the processing conditions and the material properties of the silicone in use. This theory of tooling sizing suggests minimum dimensions for rib geometry that would be limited by the expansion of the tooling to take up compaction of the tow width to the rib geometry. The impact of this constraint is explored in the *Discussion* section.

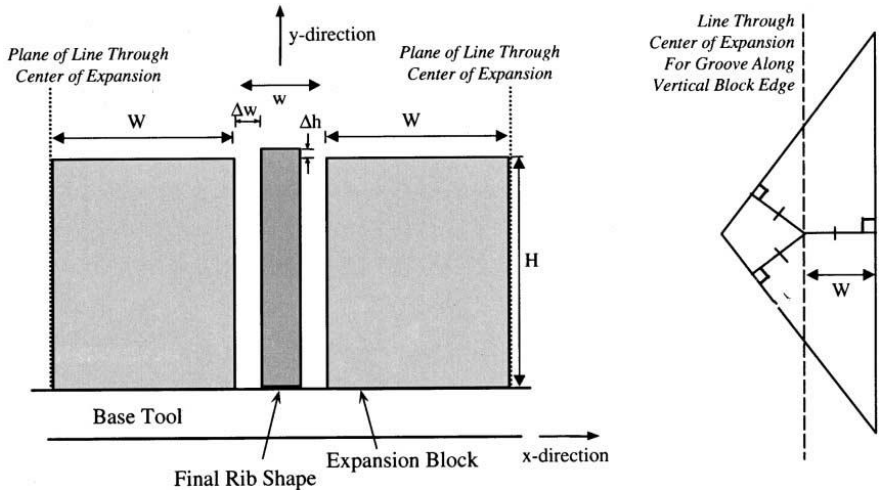

Figure 3-6 Expansion block model proposed by Huybrechts [11]

However, for practical lattice structures, that is systems of ribs in a flat panel or body of revolution, it is found that the rib geometry can deviate from the nominal design [4]. Some areas of the rib experience greater compaction compared to other areas. This suggest that a more complex process is active in practical structures consisting of multiple elements.

3.2.2 Tow Consolidation

The theory of compaction and consolidation of pre-preg composites has been investigated in order to achieve high FvF and low void content [12]. The key features of the investigation relate to the effective pressure applied to the resin, which is the applied pressure less the elastic response of the fibre network. For this reason, the processing of composite lattice structures presents challenges as the build-up of fibres is not constant, where there can be two or three times the number of plies at node regions, compared to the unidirectional ribs.

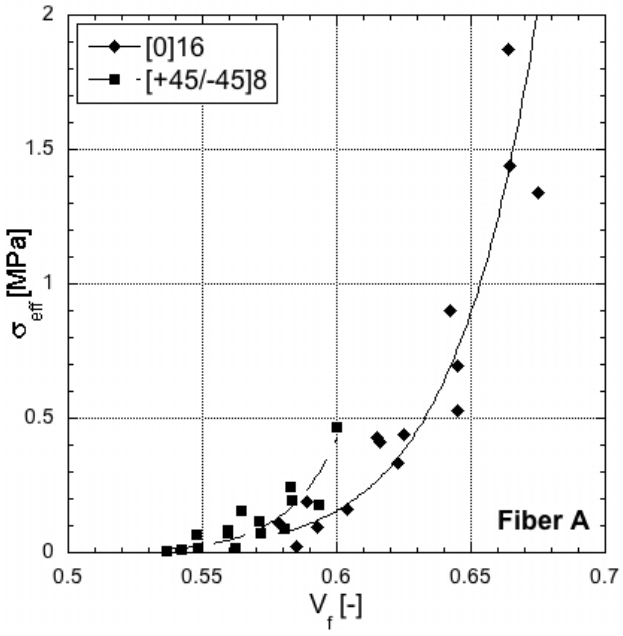

Figure 3-7 Compaction curve for an intermediate modulus carbon fibre pre-preg, 0° and ±45° [12]

Compaction experiments show stacking of crossed-plies will increase the pressure required to achieve high FvF composites as the elastic response of the fibre network cross-ply laminates is greater compared to uni-directional laminates [13]. Therefore significant differences in consolidation response exist in the ribs compared to the node region. This factor increases the complexity of the compaction process of composite lattices.

Attempts have been made to build a holistic framework for composite processing [14] which aid the detailed understanding of the consolidation process. The model consists of a nonlinear compressible fibre network and an incompressible fluid phase and attempts to account for coupling effects at the preform and ply level. However the application of this framework has not been verified with experimental results to the knowledge of this researcher. It is also unclear if these models are applicable to lattice structures using unidirectional tows with expansion tooling.

3.3 Evaluation of quality

3.3.1 Transition areas

Some work is published regarding the microstructural quality at the transition point from rib to node for the filament wound processes. Totaro found resin rich pockets in the nodal regions in a filament wound resin infused composite lattice [7]. Beside the resin pockets, Totaro noted the difficulty in controlling the final dimensions of the ribs, with the dimensions being up to 20% lower than nominal. The suspected cause was stated as the interaction with the expansion tooling and the level of tension applied to the fibres during layup.

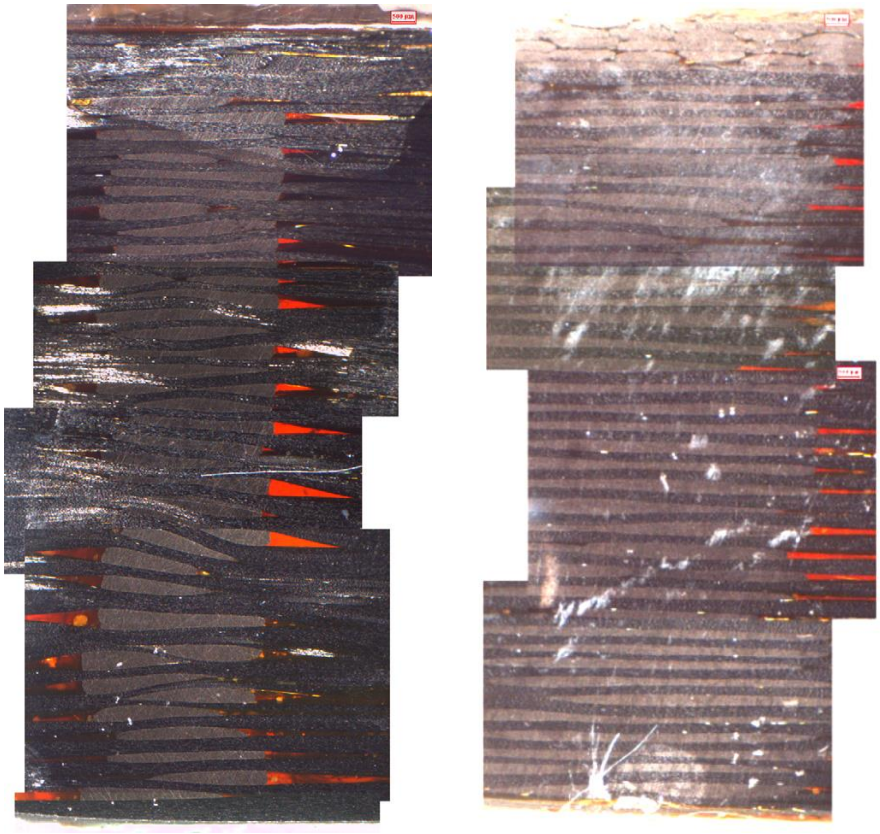

Figure 3-8 Microstructural quality of a dry-wound resin infused node of a lattice structure with resin shown in red, helical-hoop (left) [7] and helical-helical (right) [15]

Besides the resin pockets, Totaro does not discuss other features of the transition area identified as a helical-hoop nodal region. However, it is clear from the microstructure image that there is some distribution in the fibre orientation in the transition area. In conference proceedings [15], Totaro presents another image of a node region identified as a helical-helical transition. Comparing the images highlights differences in fibre orientation, resin pocket size and shape. This disparity was not discussed on the conference slides but it demonstrates that factors in design and/or manufacturing result in distinct microstructural characteristics in different lattice regions.

3.3.2 Fibre waviness

Previous manufacturing efforts with pre-preg tows found the presence of fibre waviness at rib-node transitions manufactured with fibre-placement and expansion tooling [4]. Smeets noted that the plies deviated from the intended orientation with intensity that diminished further away from the node transition. Out-of-plane waviness can be

observed in micro-sections of the transition. Also visible are resin rich pockets that are present at the transition.

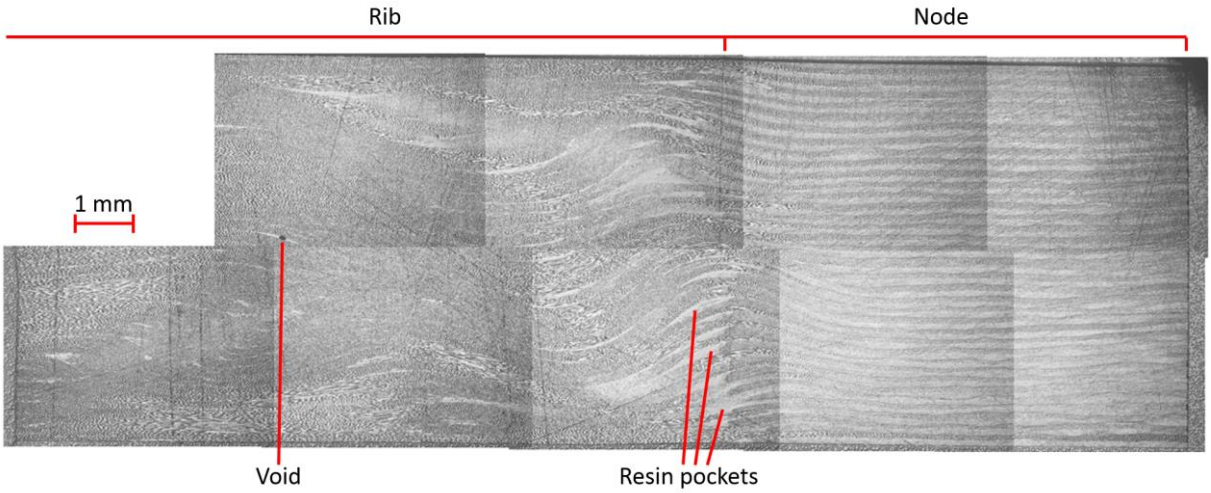

Figure 3-9 Micro-structure of rib-node transition for pre-pre fibre-placed lattice [4]

The sensitivity of this feature to the lattice geometry and tooling design is of great importance, as fibre waviness generally results in significantly deteriorated mechanical performance of traditional composites, such as compressive strength [16]. Since the origin of the waviness is not well understood, there are no details available concerning the sensitivity of fibre distortion at the rib-node transition in relation to the lattice design. Thus it is difficult to estimate if the observed waviness will be improved or deteriorated by other lattice geometries. The details of rib-node transition waviness have not been compared for different manufacturing methods in literature to the knowledge of this researcher e.g. dry winding and infusion versus pre-preg tapes with expansion tooling, and it is possible that they do not exhibit the same characteristics. One general comparison was made by Terashima [6] between pre-preg and wet winding processes and is discussed in the *Discussion* section.

The manufacture and characterisation of waviness defects in traditional composite laminates has been the subject of several studies [17, 18, 19]. Fibre waviness can be described using a sine approximation where the mean fibre position is parallel to the longitudinal axis of the fibre:

$$y = A \sin\frac{2\pi x}{L}$$

The intensity of fibre waviness can be described using the ratio of amplitude to wavelength *A/L*.

In some studies [20], manufacture techniques are used to deliberately and precisely introduce waviness of different severities into a laminate layup. The cured laminate part can then be tested and correlated to simulations to estimate a “knockdown” factor based on measured waviness severity. The knockdown for a uni-directional GFRP laminate with various waviness severities is shown in Figure 3-10.

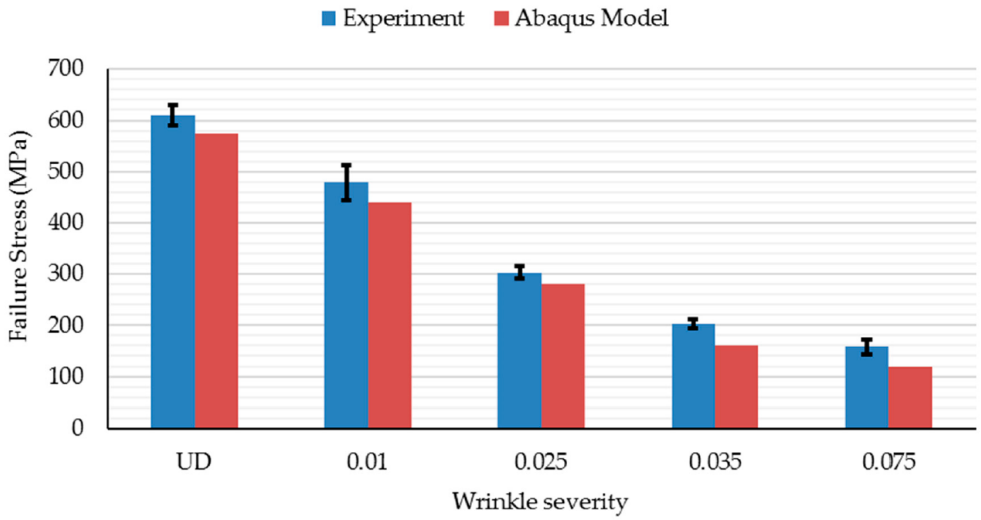

Figure 3-10 Comparison of compressive strength of GFPR laminates with various waviness severity [20]

Generally, localised waviness in manufactured specimens resulted from plies that were oversized for the laminate that contained them. This forced the plies into a smaller area and lead to fibre buckling before the laminate was cured and resulted in-plane and out-of-plane fibre waviness [19]. An example of the tool used is presented in Figure 3-11. Pre-preg plies are laid over the arc of the former such that the plies on the lower layers had a shorter path than the outer plies. After layup, the laminate is flattened between two surfaces and results in the upper plies buckling to accommodate the constant thickness.

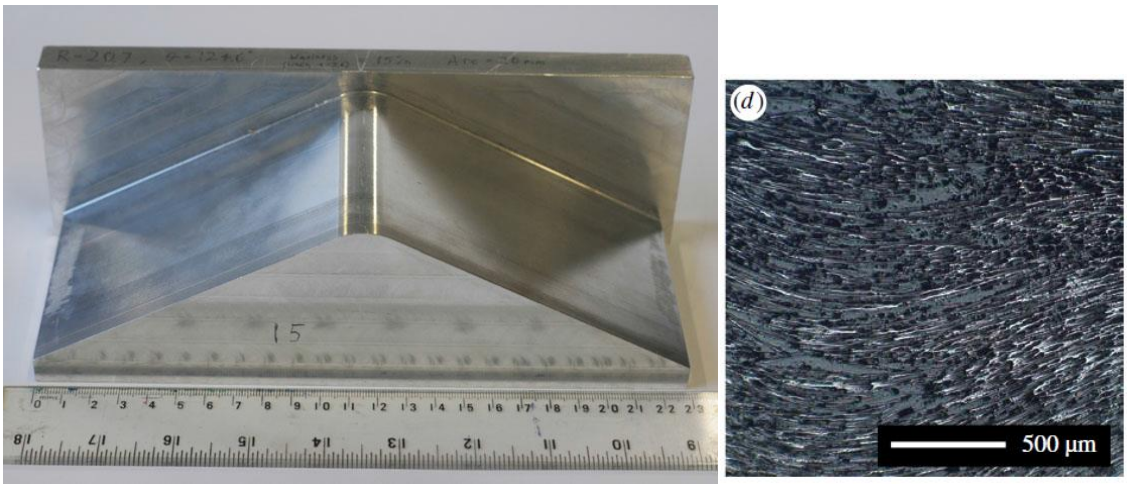

Figure 3-11 A layup former to manufacture specimens and microscope image showing in-plane waviness [19]

Another technique that resulted in manufactured ply waviness was ply drops, as investigated by Wang [18]. Using this method, and by varying the parameters described in Figure 3-12, specimens with a waviness severity between 5-28% were produced. The main factors tested were: g – the gap between the discontinuous plies, T_i – the thickness or step size of the discontinuous layers and N_i – the number of plies traversing the step. This is not necessarily fibre buckling, and produces waviness without the local thickness of the laminate changing, the applicability of this to lattice structure rib-node transitions is evaluated in the *Discussion* section.

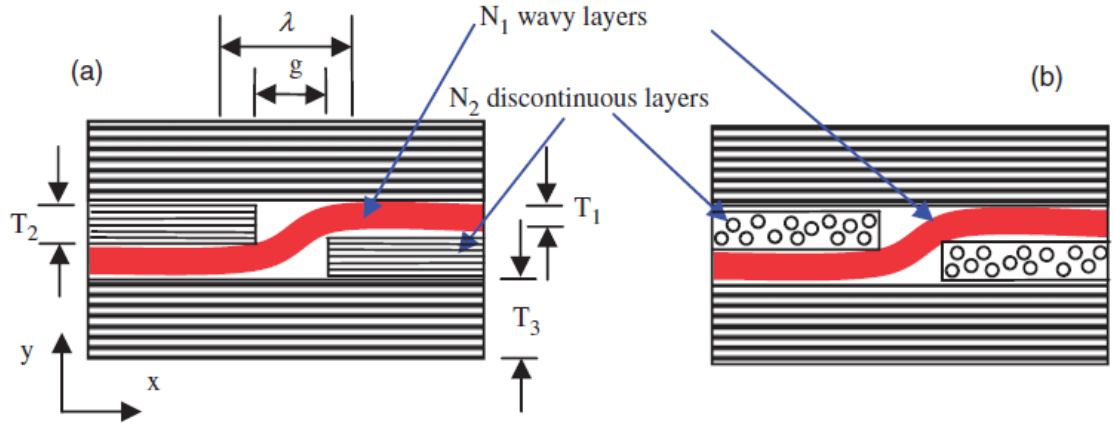

Figure 3-12 Fabrication of waviness using discontinuous plies [18]

3.3.3 Waviness Measurement

Several non-destructive methods are available for detecting fibre waviness. Advanced ultrasonic testing is able to identify and characterise, among other defects, in-plane and out-of-plane fibre waviness [21]. This technique analyses C-scan images from different depths of the composite using 2D-Fast Fourier Transforms to determine the directionality in 2D space. The distribution of the analysis results can show how the fibres in a particular ply or depth are oriented, and can be used to determine the severity of alignment distortion.

Computed micro-tomography is another method that can provide detailed characterisation of fibre directionality in carbon composites due to the high resolution [22]. This technique rotates a sample in the path of an x-ray source and records the transmitted radiation with a digital detector, a projected radiograph. The cross-section images are used to reconstruct a 3D image of the sample. Fibre directionality can be computed from individual cross-sections using the same analysis techniques as described above. CT inspections have been performed on lattice structures manufactured with a pre-preg and wet winding process to evaluate their quality by Terashima [6]. The study cites the paucity of voids and mentions the lack of fibre misalignment in regard to high quality. CT scanning appears to be an effective inspection tool for lattices.

Figure 3-13 CT Inspection of a wet-wound filament lattice structure and corresponding lattice location [6]

Destructive techniques can be simpler and include direct measurement using protractors on micrographs of sectioned composites, or using angular reticules on microscopes.

Digital image analysis (Fourier transform misalignment analysis, as discussed above) is also a possible technique to measure fibre directionality in micrographs. These are described in [18].

3.4 Discussion

3.4.1 Geometry and manufacturing method

The difference in grid design noted in the *Grid Geometries* section could be related to limitations in the manufacturing method rather than perceived structural efficiency, as this design choice is generally not discussed. The trade-off in structural quality and manufacturing complexity was explored by Terashima *"Basically, we tried some pre-preg-based processes and wet winding processes, and compared them by compressive tests and CT inspections. As a result, we chose the wet winding process for the full scale demonstrator, which was considered to be the most well-balanced in the quality and manufacturing cost"* [6]. The exact quality differences the process produced are not discussed in detail but allude to void content and fibre misalignment, while emphasis is placed on the low-cost aspects of semi-automated wet winding and the use of an internally heated mandrel that eliminates the requirement of an autoclave or conventional oven.

One difference between the processes is that the wet winding method designs relies on a lower FvF in the ribs compared to the nodes as shown in the table below.

Table 2 FvF at lattice locations compared for two manufacturing processes

FvF at Lattice Location	Wet Winding, vacuum bag & heated mandrel [6]	Pre-preg & autoclave [4]
Ribs	30.7 – 35.9%	63.1 – 63.4%
Node Intersections	57.6 – 59.7%	61.8 – 62.0%

Using the wet-winding method there is a greater availability of resin in the structure which might allow more freedom in lattice design regarding cell size or rib length, as resin would more easily be able to fill any deviations in fibre orientation and minimise void formation.

The variation in rib FvF between the manufacturing processes will directly impact the stiffness and strength of a lattice structure as it changes the rib element stiffness and buckling behaviour. For a given material, a higher FvF improves the elastic modulus in the fibre direction that will benefit the performance of a lattice structure. However, Smeets noted that higher FvF are linked to reduced rib dimensions [4]. Rib height reductions will significantly reduce the rib buckling load in compression, as noted by Huybrechts [23], and may change the failure mode from material failure to local buckling failure. Therefore, a detailed understanding of the cause of rib width variations and the sensitivity of this phenomenon to different lattice geometries will aid the designer and analyst in evaluating the performance of lattice designs.

Returning to manufacturing aspects, accuracy in winding may mean the formation of a node region, where three tows meet at a point is problematic. Vasiliev noted that early trials in the 1980s that used free winding without the guide of the expansion tooling resulted in poor rib surface quality [1]. Filament wound lattice structures where tows are located by grooves in a silicone expansion tools may therefore favour designs with binary intersections.

Another difference in the manufacturing process that may influence the quality of the manufactured structure is the tension applied during layup. It was noted by Totaro [7] that the tension applied could have an influence on the manufactured rib geometry, whereas a fibre-placed manufacturing method will have very little or no tension applied. Automated fibre placement may be able to apply tension to a pre-preg layup.

Therefore it is possible that lattice designs suitable for wet winding or dry winding with resin infusion may not be applicable to the fibre-placed manufacturing method, or that the quality produced by wet winding method may be unachievable with fibre placement.

Regarding lattice geometry, small cells may be an issue for expansion tooling due to a minimum size required for the expansion of the tool to equal the required compaction of the rib. If the cell is below the minimum size, the expansion tool will interfere with the un-compacted tows at room temperature. Solutions to overcome a minimum size limit could be explored to open the possibilities for cell geometry design with tow placement.

3.4.2 Uni-directional tows consolidation at nodes

In regard to consolidation, node regions have a significant difference in layup and compaction pressure compared to rib regions. Where the plies cross over, it is believed that there will be an increased elastic response from the reinforcement compared to the ribs, since this area approximates a cross ply laminate as discussed in the *Tow Consolidation* section. On the other hand, in the rib sections where the fibres are not supported, the elastic response should differ as this area approximates a uni-directional laminate. Therefore it is expected that effective resin pressure in the two regions is not equal and could therefore result in resin flow. If a consolidation model cannot account for these distinct regions of resin pressure and reinforcement response, it may not be applicable to describe the consolidation process of lattice designs.

Based on Huybrechts' consolidation model, compaction pressure from the silicone tooling should be equal around the cell. However, it is known that the details of rib geometry for pre-preg fibre-placed lattices deviates from the design geometry [4]. Therefore the assumption of equal pressure could be invalidated depending on the cell geometry or size. Some geometries may result in larger deviations from the design that influence the quality of the manufactured structure.

Furthermore, the consolidation from the caul plate will, at least initially, not be equal at all points in the lattice due to the build-up at rib intersections or node regions. Other parameters may be required to describe the effect of the silicone tooling and the caul plate on the composite.

An important factor to consider for industrial processes is the tolerance required for tooling design. If the method described is applicable for realistic cell shapes, it is not clear what tolerance would be applied for the tooling size. Additionally, research has not shown what the effect of manufacturing lattice structures with tooling that deviates from the proposed size, either under or oversized. It is not clear what the sensitivity of the process is to these deviations.

It is likely that tooling which significantly deviates from the "ideal" size would result in lattice dimensions that show a systematic deviation from the design beyond what might be attributed to resin migration effects discussed above. Undersized tooling could possibly result in lower rib heights, while oversized tooling could produce greater rib heights. Variation in tooling sizes could reduce the quality of transitions by a mechanism that is not currently understood. Better understanding of the interaction of the silicone expansion tooling with the composite structure will help define the limits and tolerances

of the manufacturing process that will contribute to the production of high quality lattice structures.

3.4.3 Applicability of fibre waviness experiments to lattice structures

Of the methods of manufacturing traditional composite laminates with controlled fibre-waviness reviewed in the *Fibre waviness* section, the most relatable method to composite lattice structures is the constant thickness ply-drop method, as lattice structures generally have a constant rib height. However the constant thickness ply drop method is primarily experiencing out-of-plane consolidation, whereas the rib-node transition of a lattice structure experiences simultaneous out-of-plane consolidation from the caul plate and in-plane compaction from the expansion tooling. The resulting waviness of lattice structures seems to be more complicated compared to the manufactured waviness samples, as the waviness cannot be reliably described with a single sine function. Rather, the intensity of the waviness diminishes at a distance from the node transition as shown in Figure 3-14, suggesting that a modified sine function would be more appropriate.

Figure 3-14 Comparison of fibre path for manufactured waviness sample with typical measurements (left) and waviness observed at a node transition with possible measurements (right)

A decaying sine function could approximate the fibre path at distances from the node region that describes the observed amplitude, wavelength and decay period. Such a characterisation would be useful to quantitatively compare the differences of transition regions.

Despite the differences in waviness characteristics, the factors that contribute to increased waviness described in by Wang [18] may still be relevant, namely: the thickness of the discontinuous step and the thickness of the plies that traverse the step. Such factors may be of interest in the design and manufacture of irregular lattice structures.

3.4.4 Fibre directionality characterization methods

Ultrasonic scanning may have difficulties inspecting the thin sections of ribs (generally 5mm or less in width), as edge effects could interfere with the area of interest. Furthermore, it is possible that other defects such as voids or resin pockets may form in the same location as the fibre waviness. The ability of ultrasonic methods to distinguish and quantify these features is unknown in the context of lattice structures.

Micro-section analysis has been explored in this work and shown to be effective in observing the fibre waviness in the rib sections, nodes and transition areas. Clearly this has the disadvantage of destroying the samples such that they cannot be tested afterwards.

Computed micro tomography has the potential to show lots of detail but may require additional preparation given the irregular shape of a node section. Furthermore,

significant post-processing of data is necessary to interpret the resulting images, which may become impractical if a large number of samples need to be characterized.

3.5 Conclusion

Composite lattice structures are shown to be high performance solutions in space engineering applications. Some examples of irregular lattice structures are thought to further improve performance for specific loading scenarios. However manufacturing irregular structures with pre-preg fibre-placement has not been researched. Lattice design likely has an effect on the quality of the produced lattice structure for a given material. Regarding pre-preg fibre-placement, rib geometry, such as the width of ribs, angle of ribs, cell size and the design of nodes could be important factors for the quality of the produced lattice structures as these will affect the compaction and consolidation of the tows. The sensitivity or relation of these factors is not discussed in literature.

The governing theory of tow consolidation with expansion tooling has been explored with a simplified model, with possible limitations identified. The sensitivity of tooling size, and its effect on the lattice quality is not known.

The quality of manufactured lattice structures can be characterised using a variety of techniques, the most simple of which are destructive techniques. Lattice structures produced using pre-preg tows and expansion tooling have been shown to have complex localised fibre misalignments in the transition region between ribs and nodes. The applicability fibre waviness theories for traditional laminates is unknown for composite lattices due to the complex compaction behaviour.

Characterising the severity and extent of these regions based on the geometry of a cell would be a useful tool for designers considering particular lattice geometries, as fibre misalignments are related to a reduction of mechanical performance of the structure. Improved understanding of the mechanism that results in such quality should lead to more accurate analysis predictions, and serve to diminish one the remaining barriers to composite lattice analysis. Furthermore, such understanding could lead to improvements in the design or manufacture process to result in higher quality lattice structures.

4. Concept exploration

It is desirable to develop a method to determine localised modifications to a regular lattice structure in order to accommodate specific point loads efficiently. Such a method would be useful to generate lattice arrangements that improve the strength or stiffness performance for specific load cases. Ideally the method would be flexible enough to allow a variety of lattice configurations and load cases to be considered and produce several modification possibilities with improved performance. A designer could then evaluate which modifications would best fit the general requirements and manufacturing limitations.

A topology optimisation approach was considered suitable for this task for the following reasons:

- Automated and requires minimal input from the designer. The optimisation can take input from existing models rather than requiring additional models to be setup.
- Quickly produce lattice concepts within FEM software already being used for analysis of lattice structures. No additional programs or packages are required.
- Flexibility to accommodate lattice configuration and load cases. Numerical optimisation methods may require adaptation to work with specific geometry or load cases.

This section will describe the design case considered, the topology optimisation approach, results interpretation and a brief trend study of the lattice modifications identified.

4.1 Topology Optimization Approach

This section describes the approach taken for using the ABAQUS Tosca topology optimisation tool applied to lattice structures. The goal of the optimisation efforts is to produce cell-level lattice modifications and rib sizing guidance for a generalised point load case. Effectivity, the tool should guide designers to modified cell shapes or suggest which rib elements should be reinforced in order to improve the strength performance of the lattice structure in the region around an attachment. Modifications to the lattice geometry outside of the optimisation area will not be considered. Complex, sub-cell sized truss like structures should be evaluated in from a manufacturability perspective, and will be generally be rejected.

4.1.1 Design case

In order to develop a method for lattice modifications utilising topology optimisation, it was necessary to setup a realistic design case with a regular lattice geometry and a defined point load. Recent work at ATG included a design proposal for a composite lattice structure in the application of a communications satellite central tube [2]. Such a design includes multiple load attachment points in the lattice structure with specified loads.

The introduction of point loads in composite lattice structures has been the subject of prior research at ATG [4]. The key findings are the use of a laminate patch integrated into the ribs and nodes of the lattice that completely or partially fills a cell, and an aluminium insert that facilitates a bolted connection. The design specifies a minimum size for the aluminium insert, as well as the laminate patch thickness and size.

Representative communication satellite loads, regular lattice configuration and attachment requirements were used as a design case for the optimisation process. These are detailed in Table 3.

Table 3 Lattice configuration and attachment point requirements

Lattice Geometry	
Grid Angle	22°
Rib Width	4.4 mm
Rib Height	6 mm
Helical Spacing	70 mm
Load Introduction	
Patch Thickness	4 mm
Layup	Quasi-isotropic
Bolt size	10 mm
Insert Diameter	26 mm
Attachment Loads	
x-component	1.5 kN
y-component	7.5 kN
z-component	Not considered

The out-of-plane z-component loads were not considered for this exercise. Out-of-plane loads in lattice structures are most closely related to the rib height design parameter, and are less sensitive to the in-plane design features. Since the topology optimisation is primarily interested in lattice geometries that are described by the in-plane features, and do not vary through the thickness, the z-component load was omitted. Bending loads were not considered for the same reasons.

The patch is thinner than the full height of the ribs, and is placed such that it is flush with one face of the lattice structure. The applied load is therefore not aligned with the mid-plane of the lattice, and some bending forces result from the applied in-plane load. This is typical for attachment load cases. From a structural analysis perspective, this results in critical stresses and strain on one surface of the lattice, where the bending normal reaction and in-plane loads are aligned.

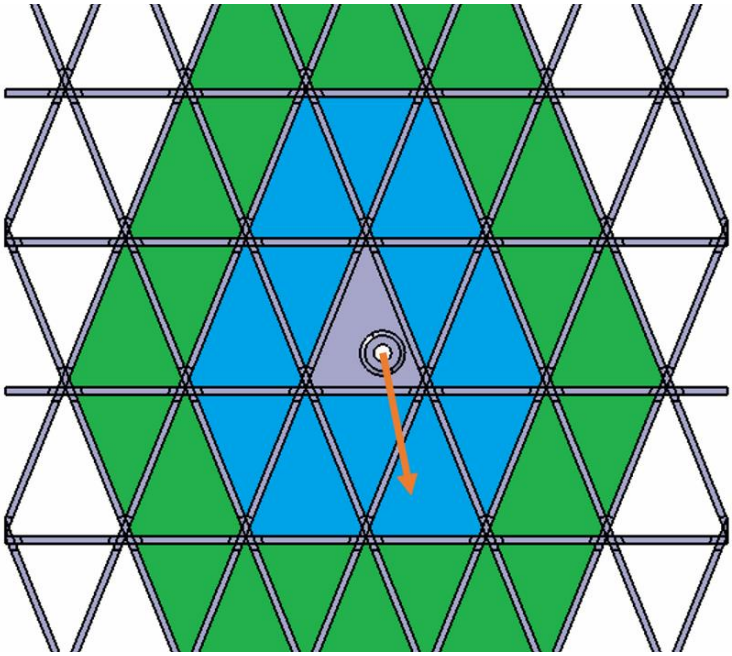

Figure 4-1 Design case lattice configuration, with attachment laminate patch and aluminium insert, point load direction indicated by arrow

The design case was defined with the attachment point located off-centre from the cell in order to test a more general optimisation problem and avoid special case results that could be symmetric, as shown in Figure 4-1. The blue highlighted inner ring of cells represents the optimisation space where local modification can occur.

Furthermore, it was defined that optimised solutions must have a continuous lattice structure. The resulting designs should represent modifications to the lattice, and not a separate structure within the lattice that would undermine a layout suggested for global lattice loads. This suggests that basic rib elements, although modified in direction or dimensions, must be continuous through the modified region. Ribs connected to the regular lattice structure should not terminate and begin again at any point. However, additional ribs may be added which do not align with the principle positive, negative or horizontal directions of the regular lattice. The results of the FEM analysis of the design case are presented in Figure 4-2.

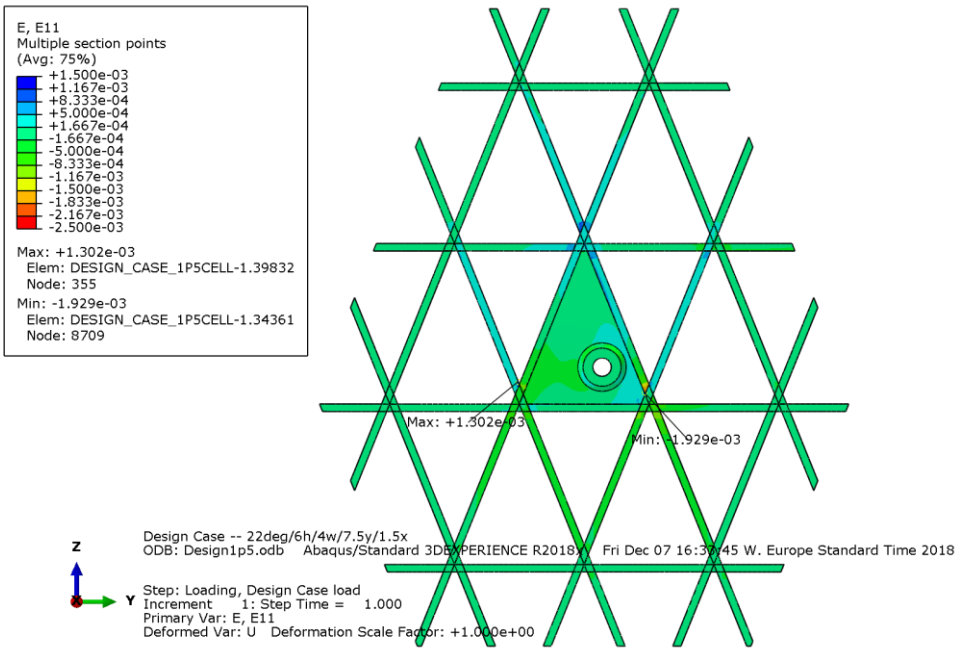

Figure 4-2 FEM results for the design case, displaying strain in the fibre direction

The boundary conditions of this model are fixed, being applied at the protruding rib elements on the perimeter. The fibre strain results of the design case show a typical response for a composite lattice structure. The load is distributed from the attachment point to the surrounding lattice elements, with the nodes above and to the right of the attachment point showing regions of higher strain in tension and compression. These strains are further distributed into the surrounding elements. The clear regions of high strain are due to the modelling approach taken, whereby the rib-node transition is modelled with reduced stiffness. This approach is one taken in previous testing and correlation campaigns to account for areas of fibre misalignment and resin rich pockets at the rib-node transition, and has been shown to correlate with test results in previous testing.

In composite lattice structures, composed primarily of uni-directional ribs, the key failure criteria is maximum strain and has been found to represent the lattice failure reasonably well. The results of the design case show peak strain values of **+1302** με and -**1929** με, which is within the material allowable. Therefore it is expected that that design case will not fail. Optimisation efforts will aim to increase the efficiency of the layout within the design area to reduce peak strain values. The addition of material should be justifiable.

4.1.2 Topology Optimisation

Topology optimisation with traditional composites is complicated by the anisotropic nature of composite materials. However composite lattice structures utilize uni-directional ribs that are loaded along their axis, in the direction of the fibre. The results of an optimisation could be valid for interpretation as a composite lattice structure in the case that the topology results in material that is loaded in tension and compression, with negligible shearing or bending. The topology layout could be approximated with uni-directional material aligned to the topology member's axis such that the material is loaded in the fibre direction.

With the above in mind, the optimisation was carried out using the topology optimisation package available in ABAQUS. The approach was to fill the design area with an isotropic

material with elasticity equal to the fibre direction to approximate the stiffness of a uni-directional rib element. Clearly this approximation is unrealistic but served as a starting point for the optimisation efforts since the optimisation package does not support anisotropic material. The sensitivity optimisation method was selected, with minimum strain energy as the objective function. Volume was selected as the optimisation constraint. 8 elements were used in the thickness direction of the optimisation area.

Several geometric restrictions were necessary to obtain results that resembled lattice structures and satisfy the requirements described previously. Firstly, the thickness envelope constraint was activated to reject thin truss-like structures from the optimisation result. The constraint means that the resulting topology should have a thickness with an upper and lower bound, and that the structures should maintain a minimum gap to surrounding material in the optimisation area. It was foreseen that truss structures within a cell would result in manufacturing complexities, if at all feasible.

Another required constraint was to freeze the material that makes up the base lattice structure. Since no global compression load was applied, many parts of the base lattice show very low strain. The base lattice structure was rather inefficient in supporting point loads. This led the optimisation to completely remove the base structure and directly connect the load introduction point to the boundaries of the design area. This is a logical result for a single attachment load case but is unsuitable for adaptation to a lattice structure because horizontal and helical ribs were entirely absent. As discussed above, the lattice elements are the primary load members and should remain continuous, removing them will likely have a significant effect on the global behaviour i.e. global buckling. Freezing the base structure to allows the optimisation algorithm to consider additive solutions that build on the existing structure and result in feasible lattice modifications that are foreseen to have a lesser effect on global behaviour. The result of an optimisation is shown in Figure 4-3.

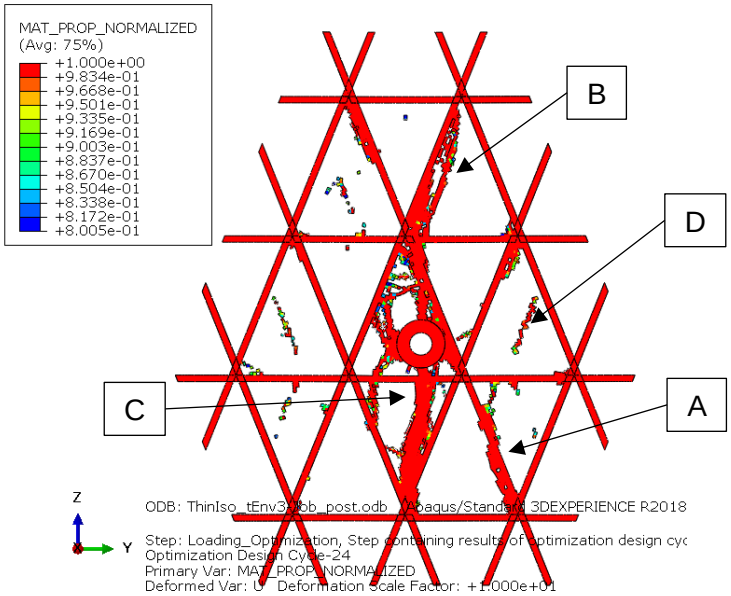

Figure 4-3 Topology optimisation result showing kept material, with members identified and discussed below.

The results are displaying the remaining elements with a density (and so elastic stiffness) greater than 0.8 of the nominal material. This provides a good representation of the topology that results in the minimum strain energy of the design area [24]. The volume of material remaining in this optimisation case is 15% of the original volume, as defined by the optimisation constraints.

Inspection of the maximum principle strain in the elements remaining show that the direction of maximum strain is aligned to the longitudinal axis of the remaining members. This indicates that the topology could be reasonable approximated with uni-directional ribs in the respect that the anisotropic material will be aligned with the loading direction.

Clearly, some artefacts remain from the optimisation process such as the isolated elements that were connected with very low density elements (Label *D*), and the generally rough boundary of the remaining structure. The suitability of this topology to be produced as a lattice structure without further processing and interpretation is questionable. Interpreting the optimisation results as modifications to the existing lattice structure provides three modification concepts.

First, some members show increased width, as indicated by *A*. The topology shows that material is added to existing rib members suggesting that if the existing lattice cannot be eliminated, it may be beneficial to increase the cross-section area of some members such that the member can support load with lower strain.

Second, some members show material added asymmetrically to the width of a member, as indicated by *B*. This asymmetric addition of material shifts the central axis of the member, which could be realised by changing the angle of the member with respect to the regular lattice. Such an angle change could provide a load path more favourably aligned to support the load, minimising bending strain and loading the rib equally.

Lastly, the results show added material that does not relate to any of the existing members, as indicated by *C*. This represents a new load path and could be accomplished by integrating a new lattice member that is not be aligned or parallel to the principle lattice directions. Of the modification concepts presented here, this is one most closely resembles work done concerning irregular lattice designs and so has some precedent [9].

The potential for these three modifications to improve the performance of a lattice design was explored with FEM analysis, as presented below.

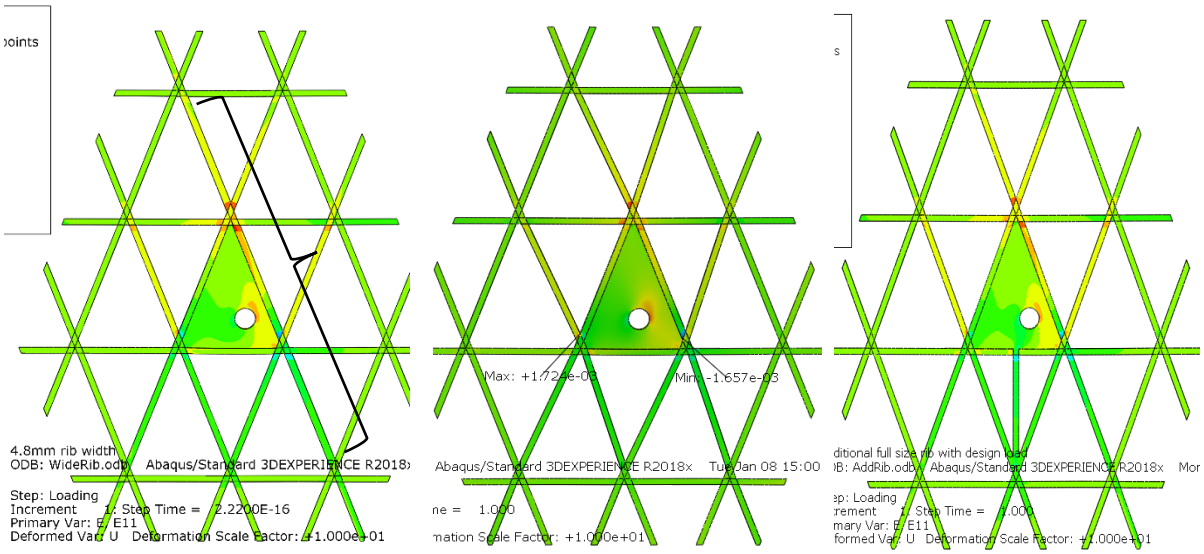

Figure 4-4 FEM results for modified geometries, (left) increased 4.8 mm rib-width as marked, (centre) attachment cell shifted to the right 6 mm, (right) additional rib member of nominal dimensions.

Each of the modification concepts showed a reduction in the peak strain values for a modest increase in mass. The reduction in strain was 14-22% while the increase in mass in the design area was 0.1-3.7%.

For the additional rib width modification, there was an 22% reduction in peak compresive strain. Given that the modification increased the cross-sectional area of the highly loaded members by 20%, this result is unsurprising.

The angle modification was acomplished by shifting the three nodes surrounding the attachment to the right by 6 mm. This changes the angle of the helical members in the design region and results in the load point being closer to the centre of the patch. This change seems to promote the balanced distrbution of load among the connected helical ribs as the peak compression strain is reduced by 14%.

Lastly, the additional rib placed below the load introduction patch improved the peak compression strain by 21%. The additional rib provides a load path that connects the load introduction patch to a lightly loaded node, reliving a portion of the load concentration elsewhere.

The results support the idea that simple modifications can improve the performance of the lattice surrounding an attachment point. Furthermore, it suggests that an isotropic topology optimisation can provide guidance for composite lattice structures. In the following section a trend study will be performed to investigate the sensitivity of each modification or combinations thereof to the improvement in structural performance.

4.2 Evaluation of Lattice Modifications

This section will evaluate the performance of the lattice modifications for the design load with FEM analysis and present conclusions.

4.2.1 Trend study

Based on the previously identified lattice modifications, a trend study was designed to test the effect of a modification on the strength performance of the resulting structural configuration. For each of the three modification concepts, configurations were

developed with various degrees of change to observe the sensitivity of the performance to the modification. Furthermore, some configurations were tested that included multiple modification concepts.

The results were compared to an unmodified design case model on the basis of maximum compressive strain values. In order to do this consistently, a mesh size of 1 mm was used for all models to minimise the sensitivity of the result to mesh effects as much as possible. Therefore a new model was set up such that CAD geometry could be generated and exported to ABAQUS for meshing and analysis in a semi-automated process. This new mesh resulted in an approximate 8% reduction in peak strain values for the unmodified design case compared to the previous analysis model. Part of the reduction could be due to the removal of the aluminium insert that was done to simplify the model. However the observed reduction in peak strain values demonstrates the mesh sensitivity of the model.

Based on previous work, it is known that the micro-structural effects in the rib node transition, such as resin pockets and fibre waviness, leads to a reduction in the mechanical properties in this region. To account for this reduction and make reasonable predictions about the failure strength of the lattice, it is necessary to model the transition regions with a reduced material stiffness. Given that the failure criteria adopted is based on maximum strain, the reduced stiffness directly affects the failure strength of the lattice structure. At the time the trend study was conducted, it was not known how the lattice modifications would influence the transition region micro-structure. Therefore the assumption was made that the modelling approach for the rib-node transition region would be applicable for all modified members.

A trend study with 21 cases was conducted with the breakdown presented in Table 4, and a comparison was made to the base case in terms of peak compressive strain:

Table 4 Lattice modification trend study trials

Modification	Number of Trials	Best	Worst
Width	10	-9%	+1%
Angle	7	-12%	+19%
Addition Ribs	3	-7%	+22%
Combination	1	-22%	

The comparison by compressive strain is not a complete description of the performance of the lattice configuration, however it was the simplest comparison to make. Evaluating other parts of the structure with lower strain found that the difference in strain or stress values was marginal, meaning that most structures are performing equally. Only the peak strain values separated different configurations significantly, thus the comparison is made with peak values.

The width modification was the simplest to implement by reinforcing the highly loaded members. With the implemented modelling and analysis method, the increase in width was proportional to the decrease in peak strain values, so greater rib widths reduced the peak strain value. The best performing configuration was found to be the same as the one presented at the left of Figure 4-4, with the increased width along the 3 highlighted members.

The angle modifications explored do show potential to improve the performance, but there is probably equal potential to compromise it, given the results presented above. In this case, the best performing configuration is also shown in the centre of Figure 4-4.

The worst performing angle modification is show at the left of Figure 4-6, where rib angles were adjusted to reduce the size of the attachment patch. This seemed to compromise the node interfaces of the structure by exaggerating stiffness discontinuities, resulting in greater peak strain values.

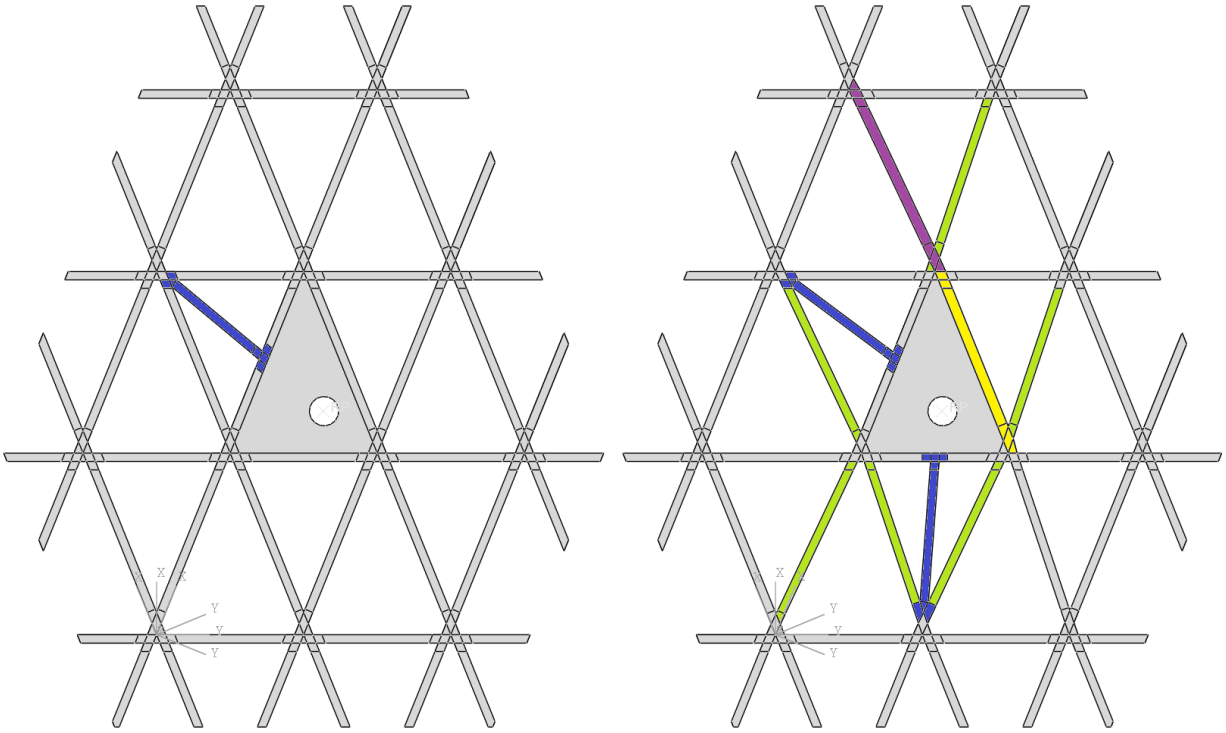

Figure 4-5 Best performing lattice designs in terms of peak compressive strain, where colours represent modifications to the base lattice (left) an additional member, (right) combination of lattice modifications

Additional ribs modifications were investigated in two locations, either with the nominal lattice height or a rib height equal to the laminate thickness. In this case, the best performing modification was an additional member on the left side of the attachment patch that provided a load path favourably aligned to the loading direction that relieved strain at the critical node region (lower right of the patch), shown in Figure 4-5. The worst performing design was an additional rib below the attachment patch, shown in Figure 4-6. Since the additional member was close to the load introduction point and nearly aligned to the load direction, the additional member did attract a portion of the load. This resulted in highly localised peaks where the additional member terminated into a node due to the modelled stiffness mismatch. The sharp transition, which in reality would be a softer interleaving of fibres, resulted in an exaggerated peak compressive strain. Therefore this design may have been over penalised on the basis of peak compressive strains alone.

The combination design looked at taking the best performing modifications and superimposing them. As presented in Figure 4-5, the lattice included modified rib widths, rib angles and additional members. Overall this design showed the lowest peak strain value.

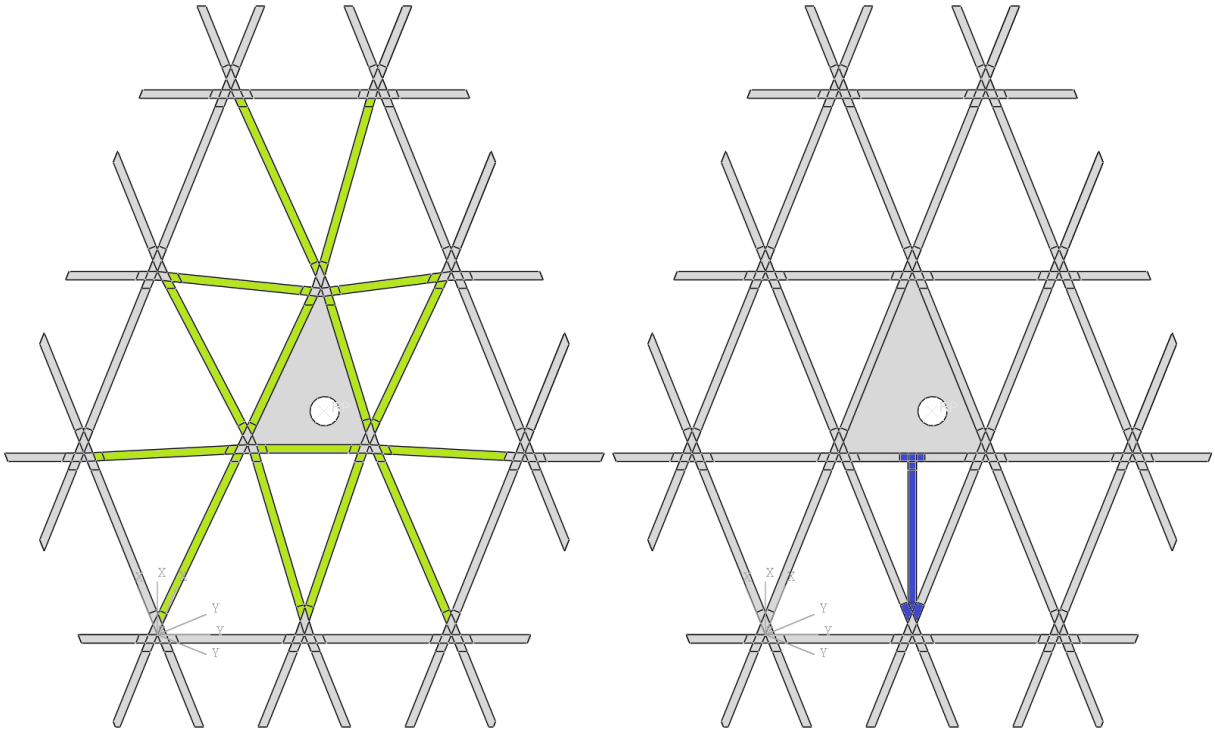

Figure 4-6 Worst performing lattice modifications in terms of peak compressive strain

4.2.2 Discussion

The trend study shows that lattice modification can reduce the peak strain values in the region around a load introduction point. The best improvement suggested a 22% reduction, while even a modest change of rib width for a few members reduced the peak strain by 9%. Interpretation of the topology optimisation result using the three modification techniques explored in the trend study can therefore lead to performance improvement. Besides the identified modifications, other lattice modifications are possible (e.g. varied rib heights, sub-cell trusses, curved members etc.) but the manufacturability of such modifications is not known. Only one load case has been considered, while practical lattice designs must be suitable for a multitude of load cases and requirements. It is questionable how a design that suggests a radical departure from a regular lattice could also satisfy other load cases and requirements.

For the trend study considered, the additional weight of the modifications compared to the base lattice structure is less than 5%, or in the order of a few grams. This is rather small in the scale of a satellite structure that weighs tens of kilograms. A more relevant aspect to consider would be the manufacturing complexity increase. Some lattice modifications could be more difficult to implement than others due to having additional members, whereas implementing a grid angle change has not been found in literature. In considering a lattice modification, a trade-off would be made for the simplest modification that results in the greatest performance benefit. The manufacturing complexity of the identified modification concepts will be explored in the following section.

Another point to consider is that the modelling method adopted for the modified structures is not validated by mechanical testing. For example, the details of how rib width changes will be physically implemented are not known. The effect of such modifications on the structure in terms of micro-structural quality is also not known. In the case of additional members, the integration of a member into a regular node as presented, is an uncertain detail with critical implications. In the previous research on

attachment point patches, a laminate was integrated into a node by overlapping a small portion of the plies into the node region [4]. However, an additional member will potentially increase the number of plies in a node region by 50%, and so the previous experience might not be extrapolated to include additional ribs. Such changes could mean that the standard modelling approach cannot be directly applied to the additional members, and that the results of the trend study may be invalid.

4.2.3 Conclusion

The short investigation shows that lattice modification by rib width changes, angle changes and additional members could produce strength performance improvement for point load introductions. Mass increase associated with the 3 modifications is minimal. These findings are based on a modelling technique that treats the modified rib-node transitions as regular lattice transitions.

The mechanism of this performance improvement can be described by 3 aspects:

- Reinforcement: increase the volume of material in the highly strained regions.
- Geometric efficiency: adjust the geometry of the surrounding structure to align the uni-directional ribs to the load direction.
- Additional load path: provide a new load path for the point load to be distributed into the surrounding structure

In the following sections, manufacturing trials will investigate the modifications presented in this trend study and determine how they relate to the quality of the lattice structure.

5. Manufacturing & Evaluation

This chapter will describe the manufacturing process of fibre placed pre-preg lattice structures through a manufacturing campaign consisting of two irregular lattice panels measuring 680x355 mm. The investigation will explore the differences of the manufactured lattice with the designed layout. The geometry and dimensions of the rib elements and their dependence on the layout of the lattice structure will be examined. Destructive and non-destructive methods of inspection will be evaluated for their suitability for characterising the quality of composite lattice structures. Finally, the particular features of the rib-node transition region will be examined and characterised for a regular lattice structure. The effect of the various modifications proposed in section 4 on the quality of the lattice structure will be evaluated and commented on.

This discussion will relate to the quality of the manufactured lattice structure. In this sense, quality refers to the observed and measurable deviation of the manufactured composite from the ideal design, where greater deviation corresponds to lower quality. Deviations such as fibre disorientations, resin rich pockets or voids constitute a degradation of quality that can be expected to reduce the mechanical performance of the structure compared to a pristine design with nominal material properties. The precise correlation of quality to mechanical performance reduction for lattice structures is outside the scope of this research.

Reference will be made to the terms consolidation and compaction, which are familiar to traditional composite processing where they are sometimes used interchangeably. In the context of the composite lattice manufacturing process, these terms will refer to specific actions that form the lattice rib sections. This reference is described in Figure 5-1 that shows a before/after comparison of the process of forming composite lattice ribs from uni-directional tows. The left of the figure illustrates the tows as they are laid up and shows the compressive *consolidation* and *compaction* forces that form the tows to the desired rib dimensions. The right of the figure illustrates the idealised design of the lattice, showing the designed *rib height* and *rib width* dimensions. The intersection of the rib elements forms a *node*.

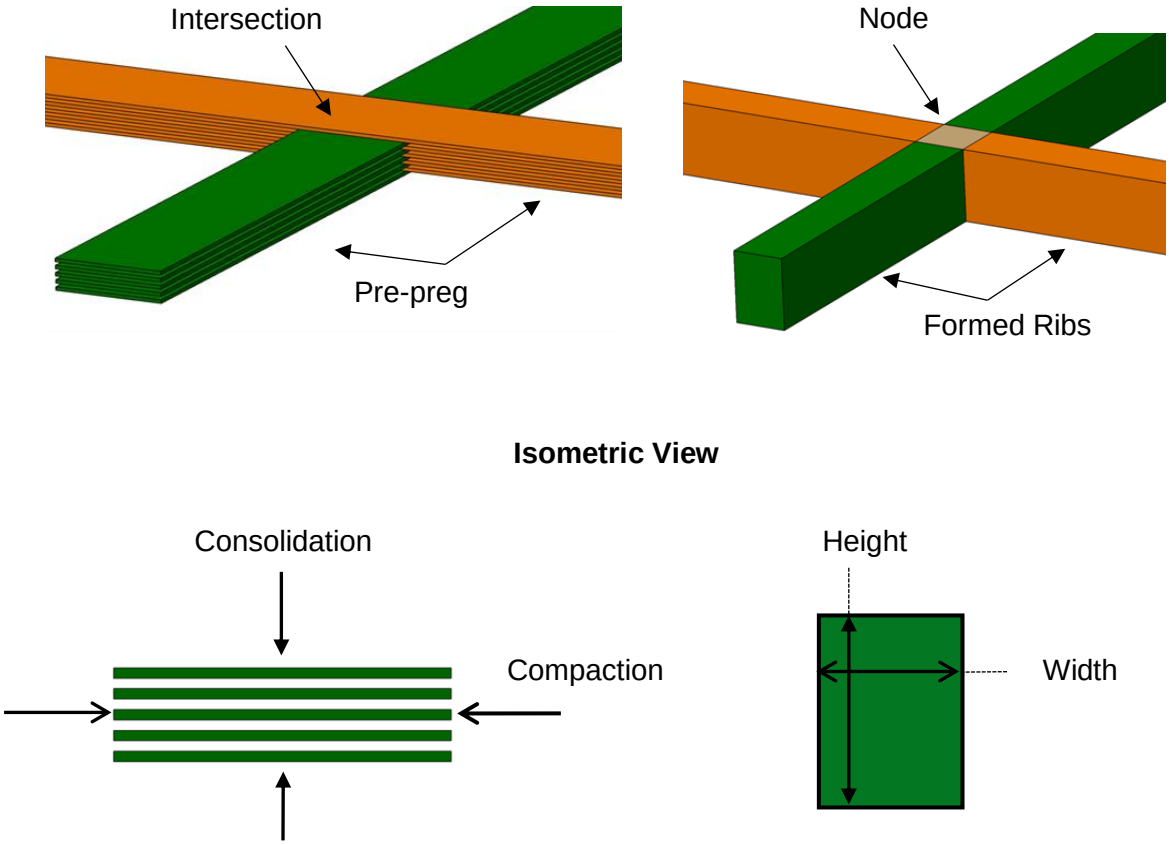

Figure 5-1 Illustration of lattice conventions and dimensions showing layup tows and formed elements

The schematic shows the primary compressive forces acting on the lattice during cure and the key rib dimensions:

- *Consolidation* is the **out-of-plane** response of the composite to the action of the caul plate and autoclave pressure. The autoclave process forces the caul plate to compress the composite part through the thickness of the layup. The effect of the consolidation is most significant at the node, where the pre-preg tows intersect and build-up, but is also responsible for forming the upper and lower surfaces of rib elements.
- *Compaction* is the **in-plane** response of the composite to the in-plane compression. The compression results from the expansion of silicone tooling (not shown above) and is most significant in compressing the tows to form the rib elements between nodes. Thus all rib elements experience the compaction along their length. The node region also experiences a compaction force.
- *Height* is the lattice dimension in the **out-of-plane** direction, that is the direction of the ply build up. The height of ribs and nodes is equal and interchangeable for the lattices discussed in this research as the height is constant.
- *Width* is the lattice dimension in the **in-plane** direction, that is the in the plane of the fibres. The ideal design considers the width of a rib element to be constant between node points.

5.1 Method

One panel was designed and manufactured based on a judgement of what was thought to be possible with the pre-preg fibre placement process, and aimed to incorporate the design modifications that were indicated to be beneficial to irregular lattice designs described in the previous section. Based on the analysis of the first panel, the objective of the second panel was to incorporate lattice modifications with a method that resulted in the best lattice quality. The lattice layout and details of the manufacturing choices are presented in this sub-section.

5.1.1 Metal Tooling

The composite layup and expansion tooling are surrounded by an aluminium dam and plates that from an enclosed space for the processing of the composite, as shown in Figure 5-2.

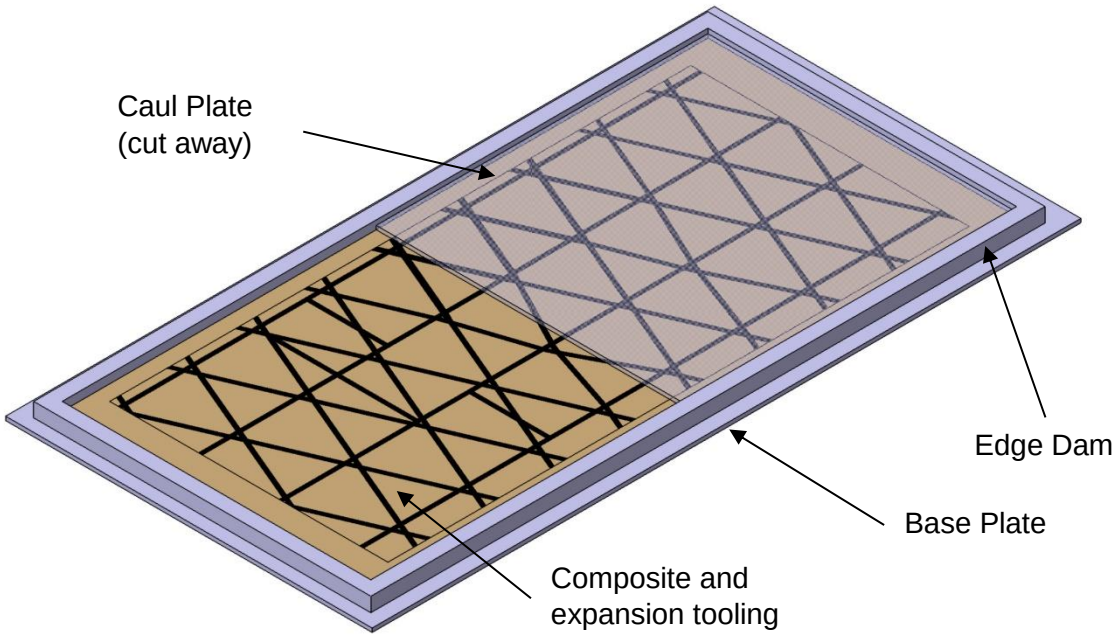

Figure 5-2 Diagram of metal tooling used for lattice manufacture

Aluminium base plate and caul plate have a thickness of 4mm. Since these parts are a mould face, they have been polished to remove any light scratches and improve the surface finish of the composite. The aluminium edge dams are fabricated from solid square sections of 15mm edge length but do not require polishing. All the metallic tooling is covered with release film.

5.1.2 Layup

The layup of both panels was done manually using pre-slit tows. The tows are pre-slit to a specified width of 6.35 mm and wound onto reels of approximately 60 m. From the reels, the tows are manually cut to length depending on the position in the panel. The material used is M55J fibre with RS-36 modified epoxy resin system manufactured by *TenCate* ®. The tows had a specified thickness of 0.195 mm that reduces the number of plies required to reach the desired build-up compared to a thinner tow.

In total, the first panel used 556 tows which required approximately 20 work-hours to lay-up. The second panel used 684 tows and required approximately 25 work-hours to lay-

up. The number of tows required depends on the designed rib dimensions, as described in [11] with the relevant calculation presented below:

$$T_n = \frac{R_W R_H}{T_A}$$

Where:

T_n is the number of tows required
R_W is the design rib width, as measured in Figure 5-1
R_H is the design rib height, as measured in Figure 5-1
T_A is the cross-section area of the tow, the tow width multiplied by the average tow thickness, i.e. 6.35 x 0.195 mm in this case

Essentially, the cross-section area of the designed rib is equal to the area of the laid up tows, which is the area of one tow multiplied by the number of tows. For a greater rib width, more tows will be required, while a narrower rib width requires less tows. This design parameter, together with the silicone tooling design determines the final rib geometry.

Layup is carried out manually and free standing using a printed template calibrated to the correct size. The layup progresses layer by layer, working by rib elements i.e. hoop ribs, helical positive, helical negative and then any additional rib elements. The tows are mildly consolidated with finger-tip pressure where the tows reach an intersection, as illustrated in Figure 5-3. This results in fibre bridging between the node points as shown in Figure 5-4. Fibre bridging is desirable as it prevents the additional length of material being included in the part, as would occur if the tow followed the contours of the build-up. Additional lengths of material could result in waviness in the cured panel as the length of fibres is forced into a shorter space.

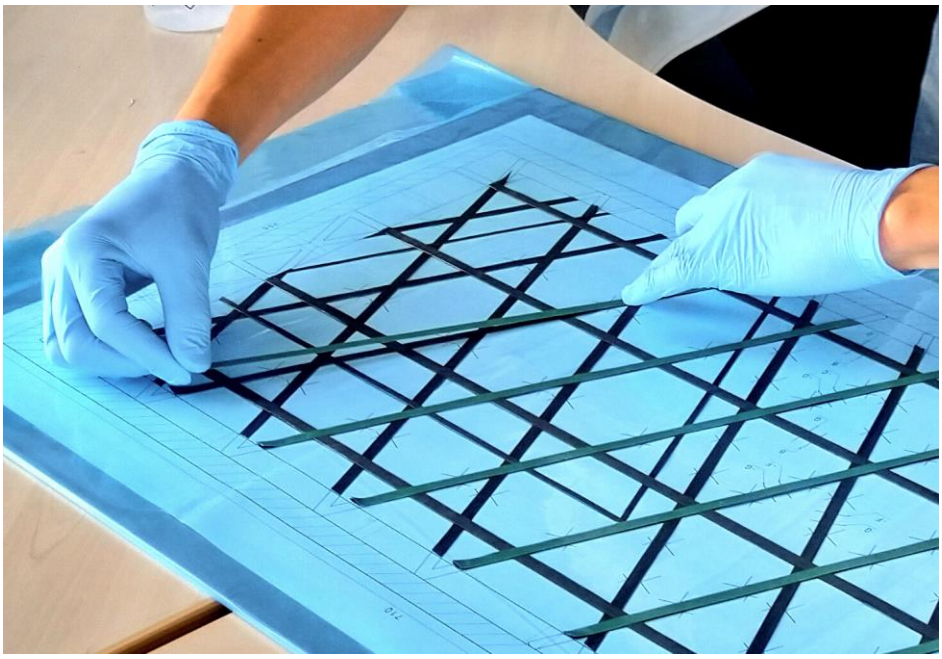

Figure 5-3 Manual tow layup showing light consolidation at tow intersections and layup template

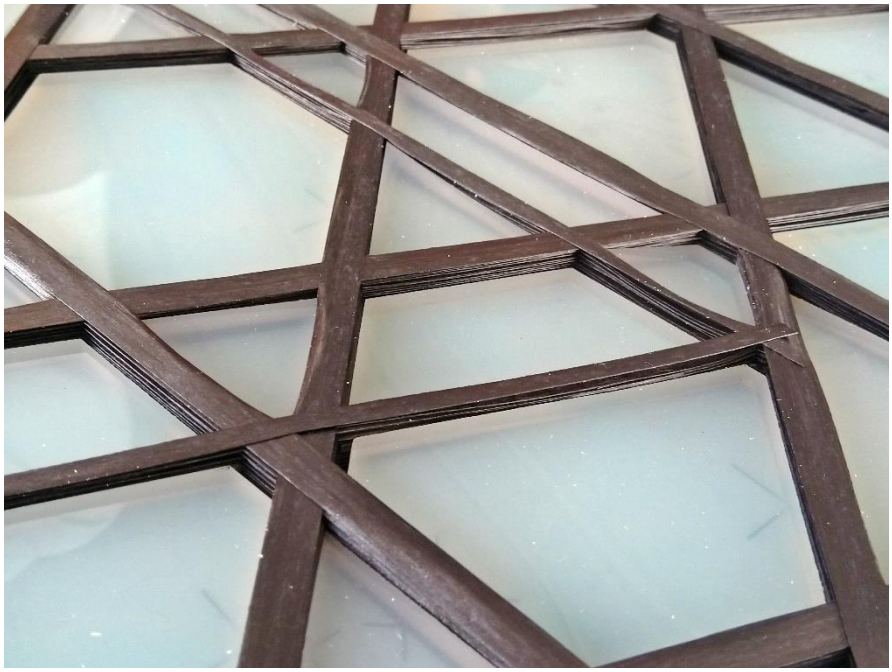

Figure 5-4 Layup showing fibre bridging between nodes with silicone expansion tooling

No intermediate de-bulking is carried out. After all the tows are laid, the silicone tooling is inserted into the cells, also visible in Figure 5-4. Following the insertion of the silicone tooling, the caul plate is placed over the composite and the whole assembly is vacuum bagged.

The part is placed under vacuum and de-bulked for several hours. The initial height of the layup can be calculated as the number of plies at a node multiplied by the average tow thickness. After de-bulking, the lattice height is near the designed height.

5.1.3 Autoclave Cure

Both panels were cured at the Delft Aerospace Structures and Materials Laboratory. No thermocouple was included in the layup. The cure cycle used was modified from the manufactures specification to include several temperature dwells. Briefly, the cure cycle is:

1. Apply vacuum to 25 inHg at ambient temperature and pressurise autoclave to 6 Bar (gauge). These pressure conditions are maintained.
2. Ramp temperature to 110°C at rate less than 3°C per minute. Hold for 60 minutes.
3. Ramp temperature to 140°C at rate less than 3°C per minute. Hold for 60 minutes.
4. Ramp temperature to 180°C at rate less than 3°C per minute. Hold for 120 minutes.
5. Depressurise autoclave, release vacuum to 0.5 Bar.
6. Cooldown at less than 3°C per minute.

This modification was implemented to improve the resin flow of the composite during cure. The data from the cycle used to cure the first panel is presented in Figure 5-5.

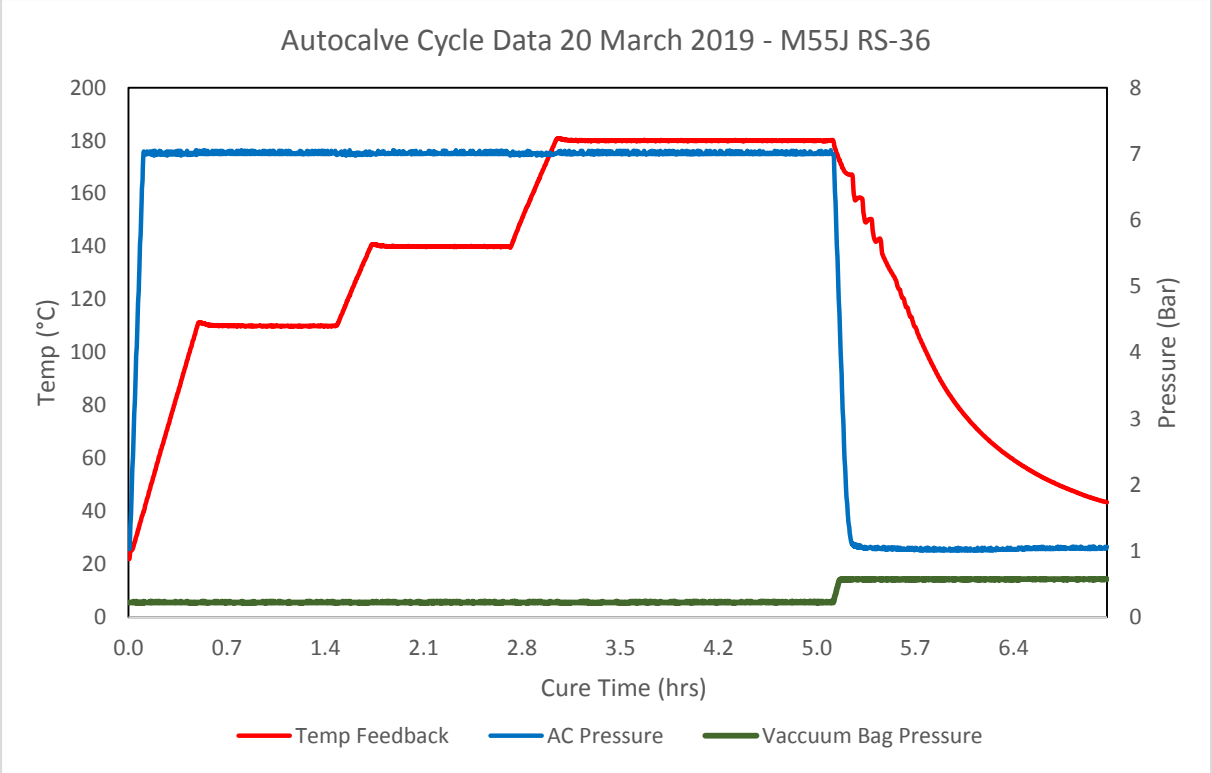

Figure 5-5 Cure cycle data for the first manufactured panel

Overall the cure cycle was carried out as desired. During the cooldown, the temperature ramp did lag the desired input, but this is to be expected and should have no impact on the composite part.

5.1.4 Sample Panels' Layout

The first panel incorporated rib width variations, rib angle variation and additional rib members, including several increments of variation detailed below.

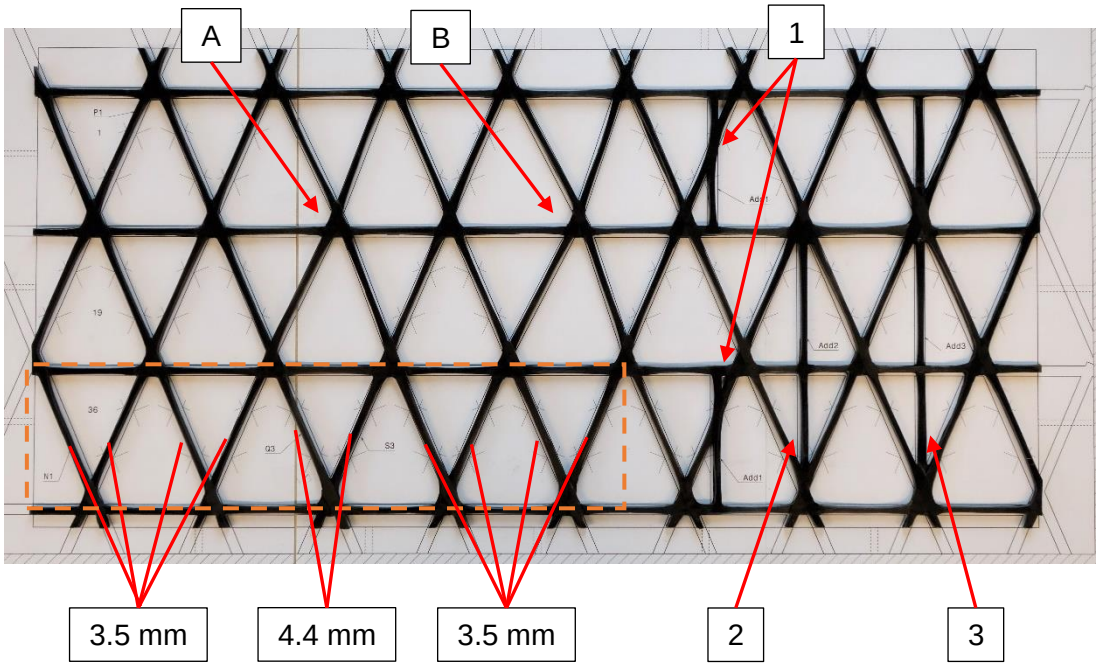

Figure 5-6 Manufactured first panel with layup template

The irregular lattice is a modified regular lattice with the geometry described in Table 5. The cell geometry refers to the conventions presented in Figure 3-3. Note that helical spacing is the horizontal distance between helical rib elements and is equal to the cell width.

Table 5 First panel base lattice geometry parameters

Lattice Geometry	Value
Grid Angle	23°
Rib Width	4.0 mm
Rib Height	6.0 mm
Helical Spacing	72.0 mm

The modifications to the base geometry are shown in Figure 5-6 and briefly presented here. They are discussed in more detail later in this section.

- Rib angle changes are incorporated by shifting the nodes at *A* and *B* by 4 and 6mm to the right respectively. This corresponds to a 2.5° and 5° angle change for the rib elements joining the nodes, and approximately double the degree of angle change for the rib angles at the nodes *A* and *B.*
- Rib width changes are incorporated on the helical ribs of the lowest row on the left side marked with a white outline. The rib widths designed are 3.5, 4.8 & 5.2 mm, representing a change of -10% to +20% from the nominal 4.0 mm rib width and are labelled respectively. Between two and four helical ribs were manufactured at each design width.
- Lastly, the right side of the panel incorporates four examples of additional rib elements. The upper and lower rows have short additional ribs which do not terminate at nodes. This results in a divided cell. To the right is an implementation where the additional members terminate at nodes. At the extreme right is an additional rib of half the height of the nominal ribs as shown in Figure 5-7 below.

Each of the modifications is a novel concept.

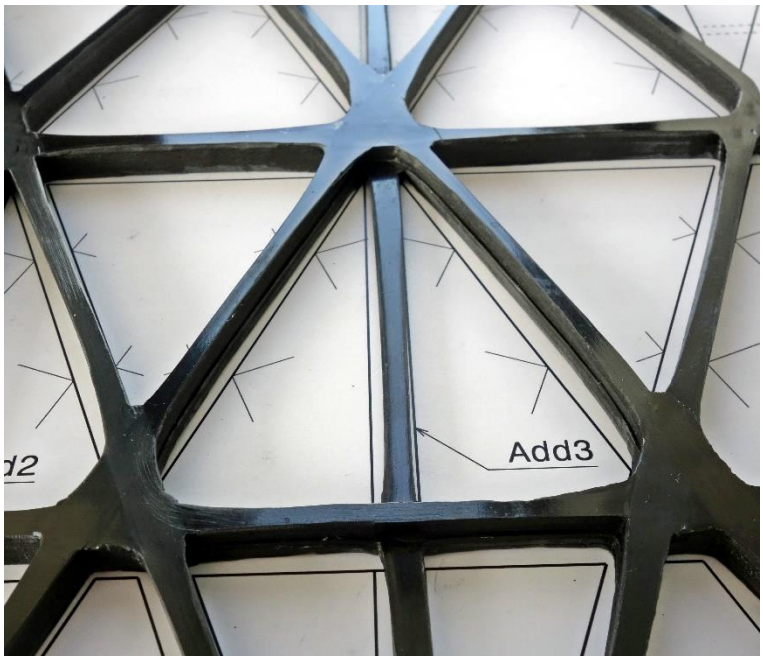

Figure 5-7 Detail of additional rib with half nominal height

A second panel was manufactured, shown in Figure 5-8 below. The objective of the second panel was to correlate a process model described in section 0This panel incorporated lattice modifications with an improved implementation that was predicted to result in higher quality. The modifications are detailed below.

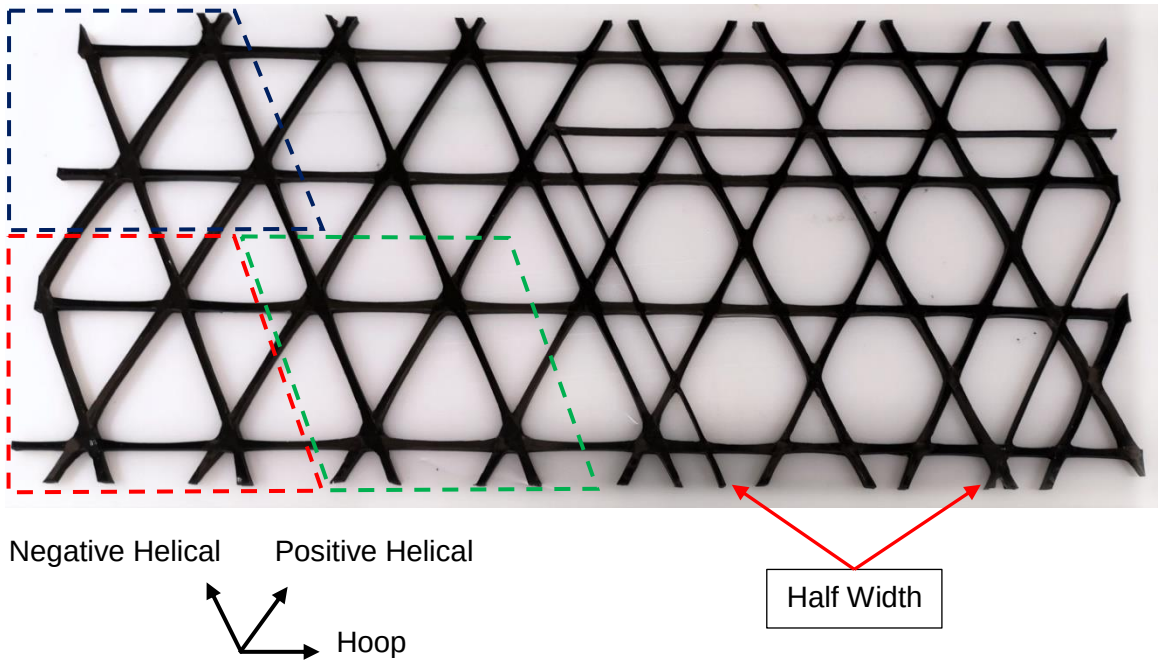

Figure 5-8 Manufactured second panel with lattice orientation and modifications indicated

The base lattice geometry has two parts: on the left the lattice forms *collected node* regions whereas on the right the lattice is comprised of *binary intersections*, these terms are defined here in the context of this research.

A collected node is where 3 or more rib elements intersect at a point, forming a region in the centre where all sides are surrounded by tows. Conversely, a binary node is where only two rib elements are intersecting. Besides the region of overlapping tows, all parts of the elements intersecting are compacted by silicone tooling from both sides. A comparison is presented in Figure 5-9.

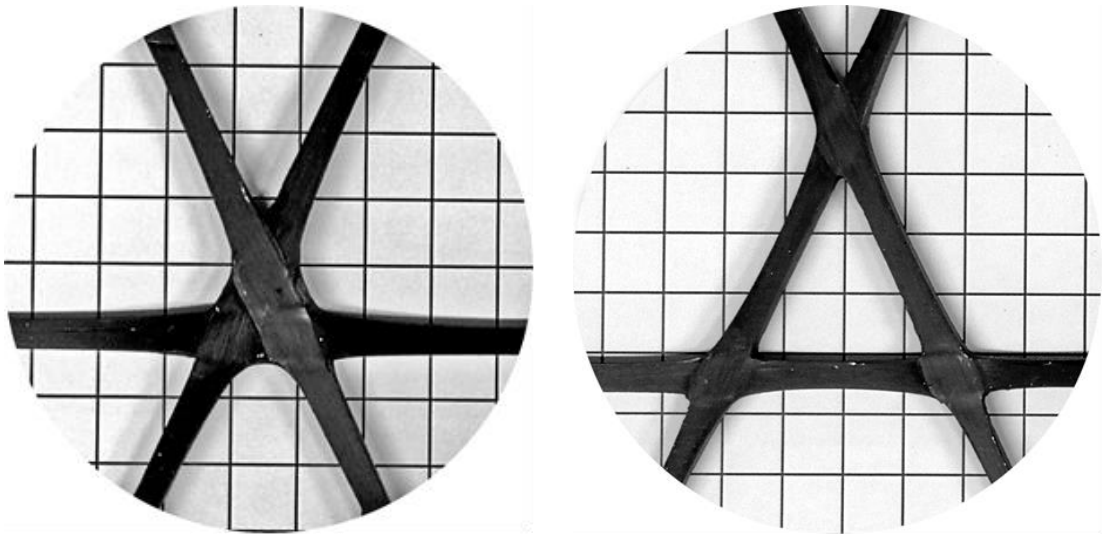

Figure 5-9 Comparison of a "collected node" (left) and 3 'binary nodes" (right)

The nominal lattice dimensions for the second manufactured panel are presented in Table 6.

Table 6 Second panel base lattice geometry parameters

Lattice Geometry	Value
Grid Angle	25°
Rib Width	4.8 mm
Rib Height	6.9 mm
Helical Spacing	76.6 mm

The modifications to the base geometry are as follows:

- The left side of the lattice is divided into three regions: *Red, Green & Blue*. In the *red* region, all rib widths are 4.4 mm. To the right in the *green* region, the lattice transitions to 5.2 mm rib widths. Above these two areas is the *blue* region where the nominal rib width is 4.8 mm, so the third section is an area with mixed rib width intersections. This provides several rib elements for each increment of design width, and several examples of intersections with ribs of different width.
- The right side of the panel maintains the hoop rib and positive helical spacing, with the nominal rib dimensions stated above. However, the negative helical spacing (cell width) is shifted by half a step such that it is out of phase with the positive ribs, resulting in the helical ribs intersecting at the mid-point between hoop ribs[1]. With this layout each intersection is comprised of only two ribs, a binary node.
- The right side of the lattice also includes additional ribs with half the design width as noted.

5.1.5 Design details

This section will explain in some depth the details of the design modifications and the reasoning for the choices made.

Rib Angle Modification

Rib angle changes were accomplished by manually manipulating the tow during layup. By pressing the tow at a node and moving the free end to reach the shifted node, the tow angle could be altered. This results in a “corner” in the tow path, a curve with a small radius. It was apparent during the layup phase that this would result in the buckling of some fibres as the tows would not stay flat, as shown in Figure 5-10. The left side of the figure shows a diagram of the angle change that results from shifting the node horizontally. The dashed lines represent the base lattice structure with the nominal grid angle, while the solid lines show the angle modification. Essentially, the location where the positive and negative helical plies intersect has been translated horizontally. The image on the right of the figure shows that the buckling of plies is concentrated at the inner radius of the angle change, as indicated.

Buckling of tows is undesirable, and occurs when a minimum steering radius is violated. This minimum radius is related to the tow width as shown by Smith [25]. Using ¼” tows, the minimum radius was found to be approximately 1350 mm, suggesting that the angle modification presented in Figure 5-10 is theoretically possible. However, the research conducted by Smith utilised an automated fibre placement (AFP) machine which is able to smoothly steer a tow on a flat base with a precise and repeatable radius. With the lattice structures, the tow only contacts the built up node regions (as described in section 5.1.2), so a smooth steering of tows is more complicated and may not be possible. The manual placement of tow is closer to a “connect the dots” method and results in a much

[1] For grid nomenclature, refer to Figure 3-3

smaller inner radius with the associated buckling defects. However this method was thought to be the most repeatable for a manual layup process. AFP techniques could possibly utilise a smooth angle change with good repeatability between layup courses that may reduce the tendency of the tows to buckle for a given angle change.

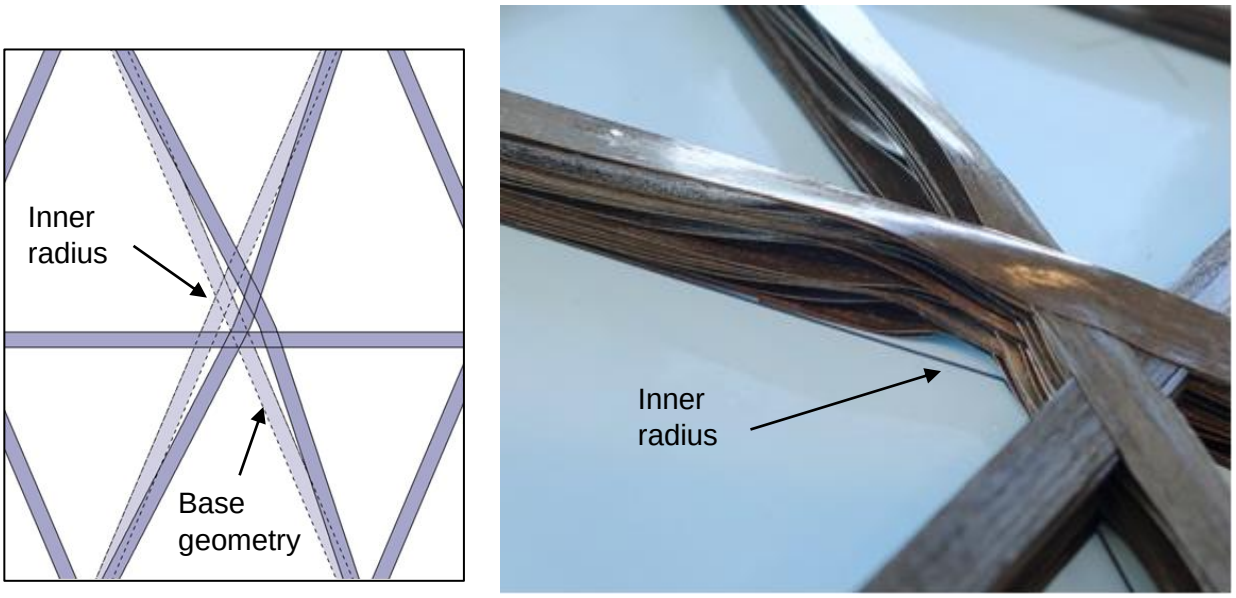

Figure 5-10 Node layup with an angle modification showing the buckling of tows

Rib Width Modification

Rib width modifications were accomplished using three methods. As previously presented, rib widths are altered by changing the volume of material laid up for each rib member. The simplest method is a step change in rib width that is realised by removing or adding tows. Wider ribs will be have more layers of tows, while narrower ribs will have fewer. For the first manufactured panel the number of plies required are presented in Table 7.

Table 7 Required tows for design rib widths in the first manufactured panel

Design Rib Width [mm]	Required Plies
3.5	18
4.0	20
4.8	24
5.2	26

The simplest method for adding or dropping the tows was to do so at a node, leaving the free end in the centre of a node, as shown in Figure 5-11. This method has advantages in manufacture because the termination is at a natural build-up point, meaning the tow can be pressed securely onto the node. This method generally results in a biased interleave transition as discussed in section *5.4.3*.

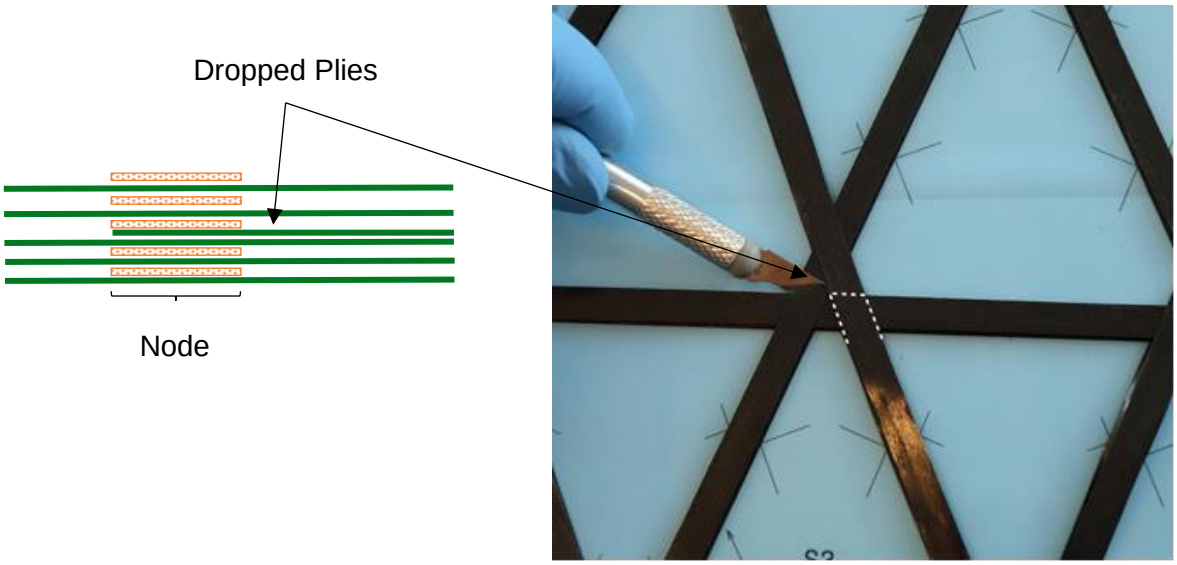

Figure 5-11 Biased node build up with a ply drop (highlighted) occurring at the node

A different rib width modification can maintain an equal interleave at the node by moving the ply drops to the mid-rib section. The interleave refers to the tows overlapping at the node, with equal being defined as an alternate stacking of the intersecting tows, one after another. With ply drops in the rib section rather than the node, a transition can be made between two lattice regions of different rib widths (and therefore different ply counts), as shown in Figure 5-12. The length of the rib provides ample distance to terminate additional tows gradually. From the perspective of traditional laminate ply drops the ratio is generous. The second panel drops one ply in 8 mm, thus the drop ratio is approximately 40.

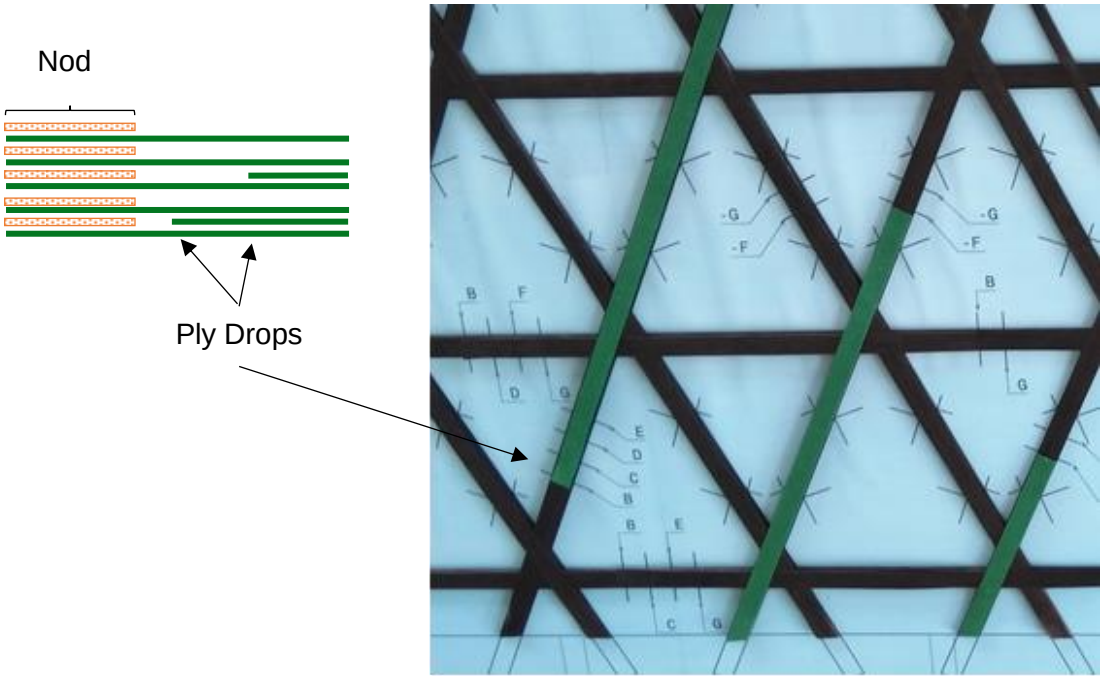

Figure 5-12 Rib width transitions using a gradual build up, where ply drops occur at the mid rib

From a manufacturing perspective, this method presents more challenges compared to the step change method as it is undesirable to consolidate or press the tows at points

between the nodes, meaning that the tow end is free during the layup, being supported by the tackiness of the layup material at a node. This method was possible with experienced technicians in the manual layup process, but may have issues with an automated process.

Another method to produce rib width changes while maintaining equal interleave at nodes or intersection utilises tows of different width. Simply, narrow tows to produce narrow ribs, wide tows to produce wide ribs. Given that interleave is equal, the particular tow width required to produce the desired rib must have the same compaction ratio as other ribs at the intersection or node. Rib compaction ratio is described in Appendix D.

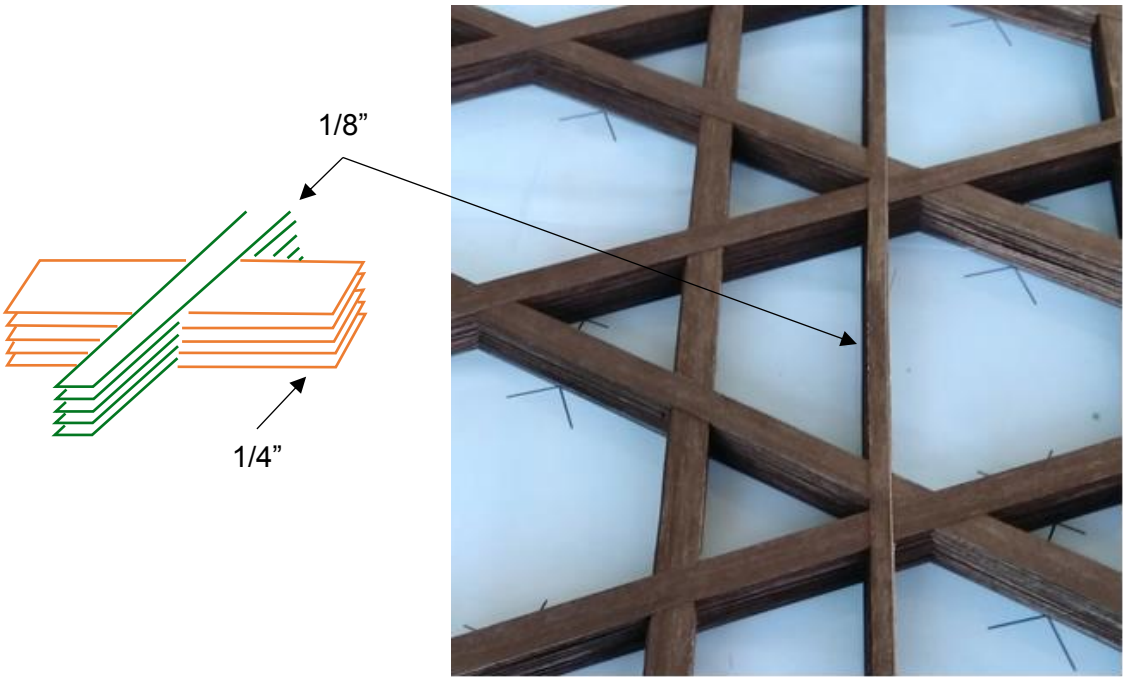

Figure 5-13 Schematic representation of mixed tow widths (1/8" and 1/4") before compaction used to produce ribs of varying width and image of the layup

This method is complicated by the requirement to have tows of different widths to produce rib width variations, increasing complexity with designs that may incorporate several different widths.

Tapered tow widths were not investigated regarding rib width changes. This was thought to be difficult to manufacture with a manual slitting operation. Furthermore, it could result in more free fibres on the outer edge of the rib element. Combinations of the above method were also not investigated as it was thought that correlation would be difficult.

Additional Rib Elements

Additional rib members incorporated into the base lattice structure terminated either at nodes or at other rib members. In regular lattice designs, the elements are continuous and the tows only terminate at end-zone interfaces where particular attention is paid to the transition. This has been the subject of earlier analysis, manufacture and testing research by te Kloeze [26]. Other terminations occur at attachment point patches, where a laminate is incorporated into the UD rib elements and nodes surrounding the attachment point cell. The particular details of this interface in composite lattices structures have been the subject of a more recent research campaign by Smeets [4].

For the additional rib elements that terminate at other ribs, one aspect to consider was how the additional ribs would be integrated. It was decided that the simplest manufacturing approach would be adopted for the purposes of the trial. This meant that the overlap would not include a tapered drop off, all tows would be the same length. The length selected was chosen such that the tow would overlap the full width of the ideal compacted rib, in other words, being just a few millimetres shorter than the distance between the edge of the un-compacted tows.

For the additional rib elements that terminated at the nodes, an initial concern was that the extra rib element would cause a significant build-up at the node, where there could be areas with 3 tows overlapping instead of the regular 2 tows. It was thought that this could lead to undesirable consolidation behaviour at those nodes, and it would be beneficial to limit the size of regions with additional build-up. For this reason, node terminations mainly included an overlap with the other rib elements, and a minimal area where 3 tows are present. This is illustrated below:

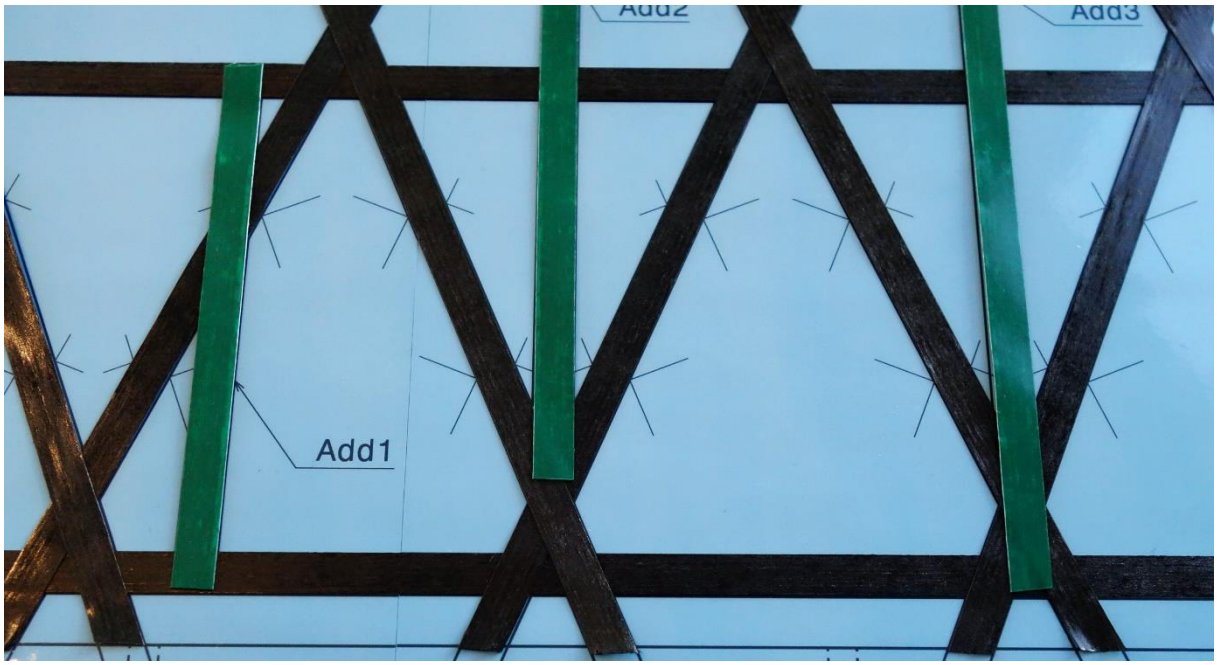

Figure 5-14 Position of additional members during layup showing the overlap principle adopted.

At the right of Figure 5-14, the additional member is designed to have half the height of the nominal lattice design. This was accomplished by only placing tows in the first half of the layup, such that the additional member only had half the nominal number of tows. For this reason, it was thought that the full overlap at the termination node would be acceptable.

5.1.6 Expansion tooling manufacture

Two methods were explored to produce silicone expansion tools: individual moulding and waterjet cutting. Both methods are suitable for producing the required expansion tools.

The required tooling shape and dimensions depends on the designed cell shape, rib dimensions and processing parameters. Since the panel is processed as one part, it is assumed that the processing conditions are the same for each part of the lattice and each expansion tool. Therefore, the ideal size of the expansion tools depends only on the cell shape and rib dimensions. Clearly, the cell shape changes for each of the

various lattice modifications described above, resulting in a range of required silicone tooling shapes. Since the thickness of the expansion tools is proportional to the designed rib height, and rib height modifications were not explored, the ideal expansion tools for each panel had the same thickness.

Regarding the individual moulding process, the various cell shapes would each require a unique mould. In the waterjet cutting process, a series of large silicone plates can be produced with the desired thickness. The individual and unique cell shapes are cut from this sheet.

One difference that resulted from the manufacturing method was the surface finish of the rib elements. Since the silicone tooling is in direct contact with the resin during the cure cycle, an imprint is made on the surface of the composite part. The moulded silicone shows the horizontal layers of the 3D printed mould that are approximately 0.1 mm in thickness. The waterjet cut expansion tooling produces very fine vertical cut marks that appears as a roughness similar to 400 grit sandpaper. Overall, the waterjet finish appears to be the smoother, as shown in Figure 5-15. While Huybrechts mentions that imprinting is undesired, no elaboration is made on what the effect is or what is allowable [11]. It is not known what effect imprinting has on the composite performance as both tools produce a minimal resin layer compared to the rib width.

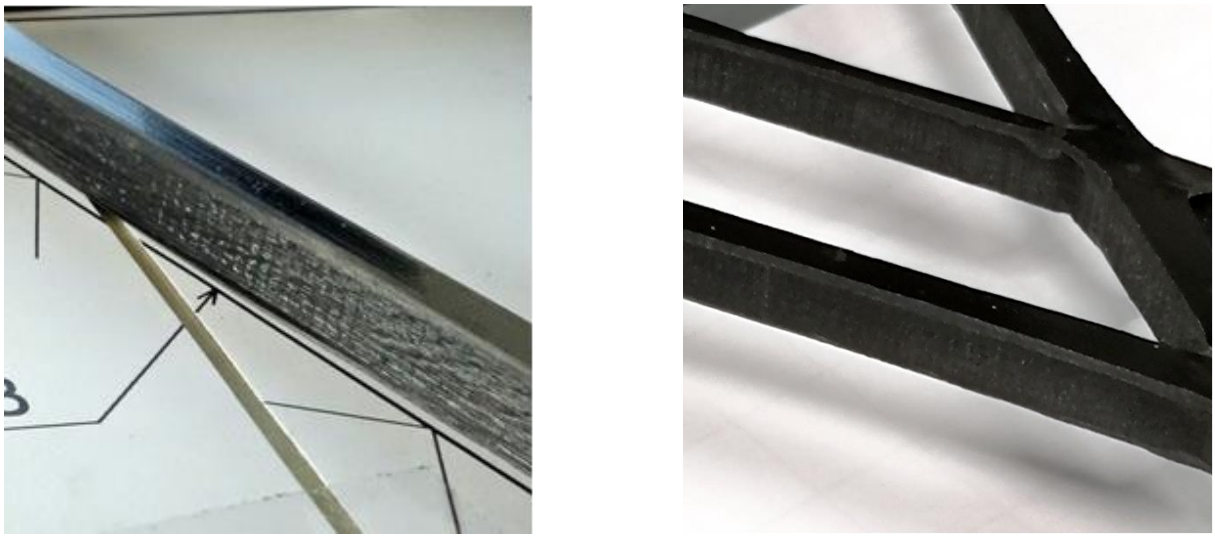

Figure 5-15 Comparison of surface finish from moulded (left) and waterjet cut (right) expansion tools

In practice, although the rib height was constant for each of the panels, tooling of different thickness was produced to work around small cells. For tooling that is scaled down in all directions, point scaling, cells with a boundary area smaller than ~15 cm^2 present a challenge as the tooling at room temperature will interfere with un-compacted tows. However, if the tooling is only scaled in the in-plane direction, and not in the thickness direction, the room temperature footprint of the expansion tool will be smaller, allowing the tools to fit into the un-compacted layup of smaller cells.

Using in-plane scaling, expansion tools with the same mass/volume of silicone material are placed with less interference to the un-compacted tows. Practically, the difference in dimensions for the two scaling methods is 0.1 – 0.2 mm in the thickness direction, and 0.3 - 0.5 mm for the in-plane dimensions, or approximately 1.5%. This small margin provided more freedom in manufacturing cells with bounded areas smaller than 10 cm^2.

This deviation in dimensions from a point scaling approach to an in-plane scaling while maintaining mass/volume was thought to be acceptable given the other tolerances applied. These tolerances are detailed in the following section. Furthermore, using the point scaling approach there is a measurable difference in manufactured cell volume compared to the ideal design cell volume. Typical manufactured volumes are 1 - 3% larger than the designed, demonstrating that the process is imprecise. Furthermore, the almost incompressible nature of silicone rubber was thought to be insensitive to the marginal deviations.

The tolerance of the expansion tooling used to manufacture the sample panels was measured on a mass basis. Given that the compaction is provided by material expansion, and that the shape of the tooling closely matched the desired cell shape, mass was thought to be the most accurate and convenient determination of tooling volume. The measured mass is compared to an ideal design value that is the product of the ideal shape volume and a measured density value.

The tolerance for the tooling used in the manufacture of the sample panels had a mass tolerance of 2%, although in the case of the second panel, some tools exceeded the tolerance. For an average expansion tool, this tolerance amounts to ±0.30 g.

This tolerance is thought to be suitable given the other approximations made in the modelling and manufacturing calculations, discussed in the following section. Though the expansion tooling accounts for approximately 88% of the material by volume, the process is thought to be determined by equilibrium conditions. Small deviations in tooling volume from the ideal value may result in small deviations in local lattice geometry and other effects in neighbouring cells. Again, given the other approximations, it may not be possible to detect these differences. Furthermore, this investigation is focused on the general effect and feasibility of larger lattice modifications and design. In order to precisely study the effect of small tooling deviations, a more controlled study might be required.

Another point to note is that during the post curing operation performed with the silicone tooling, approximately 2% of the mass is lost. This is thought to be due to volatile oils or other substances escaping from the solid silicone. The effect of this is thought to be negligible and no adjustment is made during design.

5.2 Lattice Dimensions

The dimensions of the manufactured lattice differ from the ideal design values. This is due in a small part to the approximations in the manufacturing calculations, in the design method and clean-up operations post cure. The *maximum* estimated effect of these is tabulated below:

Table 8 Maximum estimated effect of design approximations

Source	Difference Manufactured vs design width
Rounding of ply count	+ 3%
Modelling	+ 2%
Slit tow dimensions	± 2%
Flash removal	-3%
Resin squeeze out	<-1%

The number of plies required to produce a rib of a given cross-section is calculated by dividing the cross-section area by the slit tow dimensions, discussed in section 5.1.2. This value is generally rounded up to an integer number of plies. When using thicker plies that are preferred for manual layup, this rounding could account for up to +3% deviation for typical rib dimensions, meaning the quantity of material is more than required for the designed rib dimension.

For the typical modelling method used, some approximations are made around the node region where some regions are not filled, and the overlapping of material is not accounted for. This deviation systematically contributes an additional 2% to the composite dimensions.

Regarding slit tow dimensions, the tolerance of the tow is approximately 0.127 mm based on manufacturer specifications. This equates to 2.0% of random variation in material quantity that relates directly to the compacted rib dimensions.

After the curing of the panel, it is observed that some plies are not compacted by the expansion tooling. This is due to the tooling having a smaller thickness than the un-consolidated layup such that during consolidation, some tows may become trapped between the tooling and the caul plate. Before the panel can be handled safely, these thin plies that have a burr like feather edge should be removed. Comparing the weight of the first manufactured panel before and after flash removal showed that the removed material accounts for approximately 3% of the total (314 vs 324 g). The flash removed for the second panel was not measured but is estimated to be less due to the in-plane scaling method adopted for the expansion tooling design that reduced the tendency for plies to become trapped.

Another deviation that is noted should be the quantity of resin that escapes from the composite during cure that is absorbed by the breather material. Generally this is a small amount that is less than 1% by mass.

With the above sources of error identified, it should be noted that measurement of rib widths show systematic deviations from the design geometry of approximately -10%. Essentially, the rib width, measured at the mid-point is consistently smaller than the design width. Such deviations cannot be explained by the above sources of error and are explored in the following sections.

5.2.1 Rib width

Inspecting the manufactured lattices, it was noted that the rib widths measured around the mid-point between nodes were consistently less than the design value. Furthermore, the deviation was generally larger for hoop ribs. From previous work it is known that the fibre volume fraction (FvF) in the ribs is higher than the nominal value for the pre-preg,

with typical values of around 65% versus 60% nominal. Measurements made at the node, where plies are overlapping, found the FvF to be 62%. However, in the region next to nodes the FvF was found to be approximately 56%. This indicates that there is resin migration occurring in the rib sections, since little to no resin in found to be squeezed out post-cure at locations far from the edge. Given that the fibres are not displaced and that the rib height is close to nominal, it is not surprising that the measured reduction in rib width corresponds to the measured increase in FvF. The nominal rib dimensions are calculated assuming the nominal FvF.

In this case, resin is migrating away from the mid-rib regions and node, towards the region just outside the node. Resin migration should occur when a pressure gradient exists in the resin of the composite. The origin of this pressure gradient was not clear in the case of composite lattices.

It was thought that the expansion tooling might be a cause. However, FEM simulations of the expansion tooling interacting with the cured cell geometry showed that at cure temperatures, the contact pressure of the tooling on the composite interface resulted in a pressure gradient in the opposite direction i.e. lower pressure at the mid-point of the rib and higher at node, described in Appendix A. This result is consistent with the deviation of the cured composite from the design geometry, where the rib geometry is “over compacted” at the mid-point, and “under compacted” near the nodes as shown in Figure 5-16.

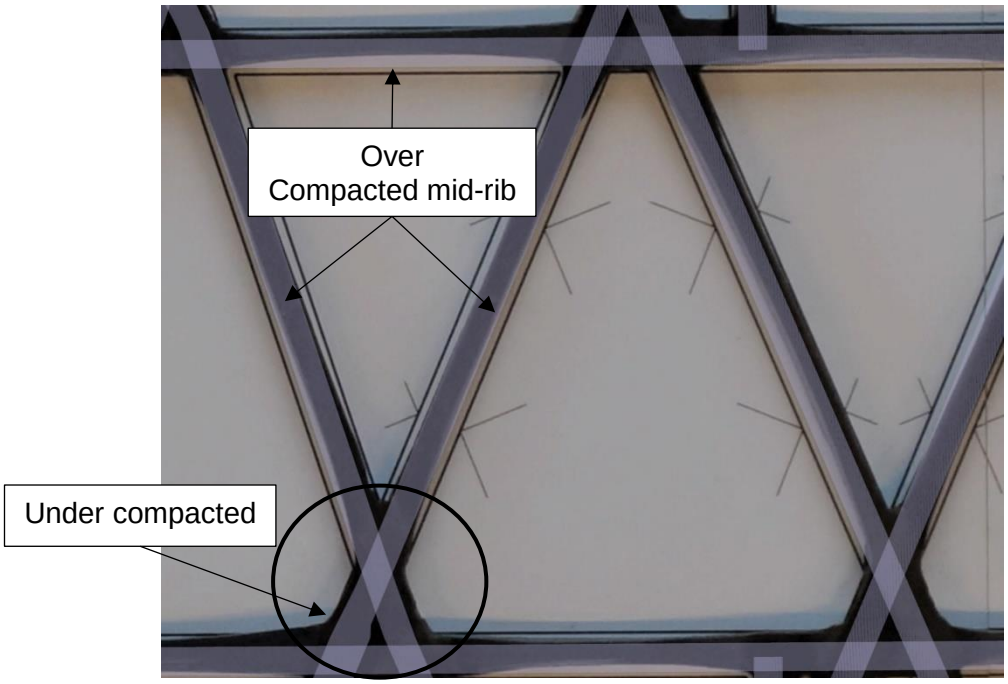

Figure 5-16 Manufactured part with design geometry over-lay with showing rib width deviations

The pressure gradient must only exist in the resin phase of the composite. Based on the effective pressure principle of porous media consolidation, the fluid phase of a material only experiences the applied pressure less the elastic response of the solid phase. In this case, the fibre network provides the elastic response.

At the mid-rib, the UD fibres are well aligned and can be easily compacted, thus providing a low elastic response and resulting in high resin pressure despite the lower applied pressure. In comparison, at the transition to the node, the fibres are forced to spread out by the consolidation of the caul plate such that they become thin enough to

pass through the node. This spreading out opposes the compaction pressure of the expansion tooling, resulting in a significantly higher elastic response of the fibre network at the node transition. In this small transition region outside the node the resin will have a lower applied pressure, despite the higher applied pressure from the silicone tooling. Due to the difference in resin pressure in the transition region compared to the rib sections, the transition region becomes a resin sink where resin from the rib and node area will migrate to. The migration of resin is represented in Figure 5-17.

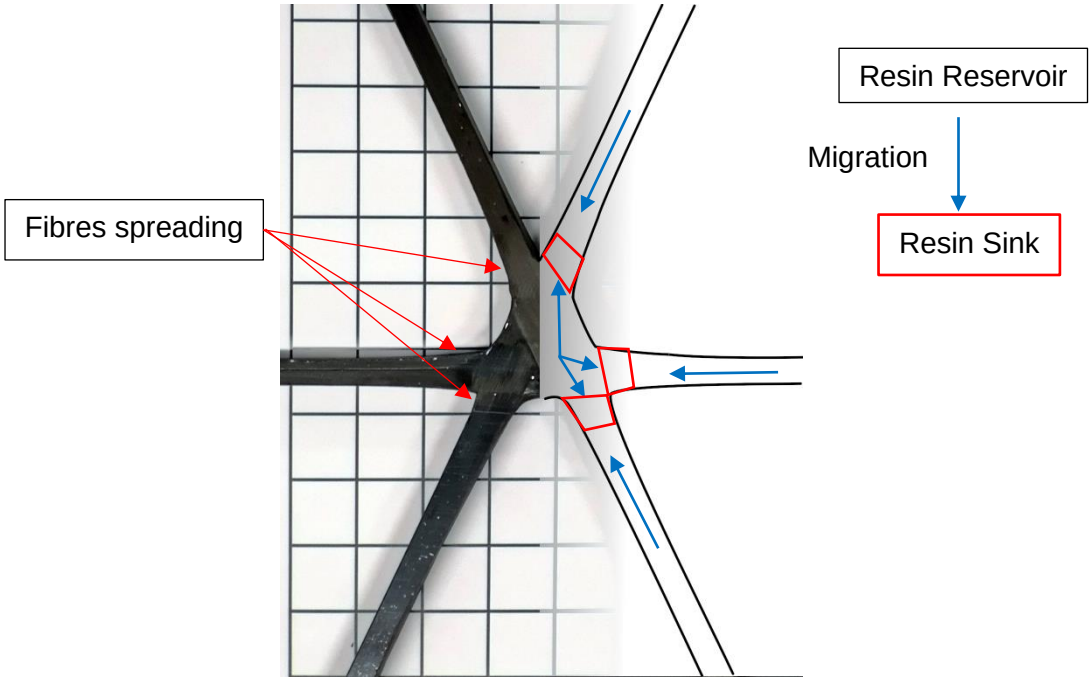

Figure 5-17 Resin migration at node and surrounding ribs

The propensity for resin migration to occur under given processing conditions should depend on the size of the rib members (that act as the resin reservoir) and the size of the transition regions where fibres spread out or cannot be compacted (and therefore become a resin sink). With the assumption that the resin cure occurs at equilibrium conditions, that is, where the expansion tooling expansion is balanced by the fibre and resin parts of the composite, we expect shorter rib members to be compacted more than longer rib members for similar transitions. One further assumption is that the void content is negligible. This measurement is shown in the table below:

Table 9 Measured rib widths compared to design value for various node types

Panel	Rib Type	Length [mm]	Node Type	Relative Rib Width
1st	Helical	77	Collected	**0.93**
1st	Hoop	60	Collected	**0.90**
2nd	Helical	73	Collected	**0.85**
2nd	Hoop	61	Collected	**0.83**
2nd	Helical	39	Binary	**0.90**
2nd	Hoop	33	Binary	**0.91**

Relative rib width is defined as the measured rib width compared to the design rib width. The table shows a trend that supports the above explanation. Considering the first and second panels had different geometry, it can be seen that the longer rib elements experienced marginally less compaction for the collected node type. The difference in

lattice geometry, collected vs. binary nodes as presented in Figure 5-9, together with other manufacturing approximations, could explain the disparity in relative rib dimension between the two panels.

Considering the comparison of the binary nodes to the collected nodes in the second panel, the rib lengths are significantly shorter. However, the relative rib dimensions are greater, meaning that the ribs are produced closer to the design dimensions. Again, this could be related to approximations in the design, but also suggests that the binary node transition is a smaller resin sink compared to the collected node. Considering the complexity of a collected node, where there are several short sections between overlaps that also act as resin sinks, the binary node is simpler.

Taking to an extreme, if the length of rib section in relation to the node is short enough, there will not be a sufficient quantity of resin available to migrate to the sink regions. This results in a resin starvation situation, where the volume of resin available is less than required to fill the space between fibres. In this case the resin pressure is minimum and the formation of voids is maximised. The first manufactured panel included sections with short ribs (<10 mm). The observations were that the surrounding ribs had smaller rib widths, while micro-sections of the transition regions revealed several small voids. This is the expected result based on the process explanation.

Practically speaking, the small variations in rib width do not have a significant effect on the performance of the lattice since the changes are determined by resin flow while the performance of the structure is dominated by the fibres. Furthermore, the global bucking performance that generally drives lattice design is more sensitive to the rib height, the out-of-plane thickness. However, the measurement of rib geometry is a useful tool to determine if the manufacturing process has produced a consistent part quality. Isolated and significant variations in rib geometry indicate issues in the compaction and consolidation process.

5.2.2 Node Height

The node height is a measure of how much the lattice has been consolidated in the thickness direction. For flat panel lattices, such as the two manufactured panels, the node and ribs have equal height due to the flat base plate and caul plate. Options for panels with varying lattice height have not been explored, and while possible for flat samples, might lead to additional manufacturing issues with cylindrical lattices.

In general, while the rib width shows some deviation from the design values, the node height measurements are closer and shows less variation compared to the nominal. An explanation of this is based on the assumption that at the point when the composite is cured, the state of the autoclave pressure, expansion tooling and laminate response is in equilibrium. It is believed that this equilibrium is stable around the design height.

Above the design height, the consolidation of the caul plate is not resisted by the expansion tooling by design but only by the node build ups that represent a small area of the panel. Given that the tooling is not restrained in the out-of-plane direction, it can provide limited compaction to the tows. Therefore the consolidation of the node should be relatively free above the design height. Indeed, the nodes are consolidated to near the design height by vacuum pressure alone.

Below the design height, the consolidation force is resisted by the volume of nearly incompressible expansion tooling. Nearly incompressible materials, such as silicone rubber, strongly resist compression. For the correct volume of expansion tooling and

composite plies, consolidation below the design height is expected to require a significant increase in consolidation pressure.

Based on this explanation, consolidation above the design height has low resistance, while further consolidation below the design height is strongly resisted. Measurements of the panels show that the average design height is indeed close to the design values, presented in the table below.

Table 10 Average node heights compared to design value

Panel	Relative Node Height
1st	**1.01**
2nd	**0.98**

The deviation compared to design values is significantly less than the rib width dimensions while the variation across the panel is also very small. The difference between the first and second panels is within the manufacturing tolerance of the silicone tools.

5.2.3 Discussion

Given the variety of geometry explored in the first and second panels, it can be said that the node height is not sensitive to the lattice geometry. This is reasonable given that the mechanism that determines the node height is a global one which should not be affected by local variation in lattice geometry. In comparison the mechanism that contributes to the final dimension of the rib width, the migration of resin, is a local phenomenon. It depends on the relationship between the reservoir and sink, and this is largely determined by element lengths and node type. Therefore, in qualifying and evaluating the manufacturing process is important to consider the meaning of each lattice measurement.

Measurements of lattice dimension should be taken in the context of the process, of the lattice design and of the surrounding cells. Isolated or inconsistent measurements could indicated issues with the manufacturing process or inherent sensitivities in the lattice design. Observing a manufactured dimension close to the design value does not necessarily indicate that the process was successful or desirable, just as a systematic deviation does not represent a failure. For example, if a cure cycle is used that does not permit adequate flow of resin, parts of the lattice may experience resin starvation that results in the formation of voids. In this case the ribs do not lose any resin, they will appear closer to the design dimension that is based on the nominal FvF. Without a physical understanding of the process specific to lattice structures, this result might indicate a successful cure process, while the manufactured part is in-fact compromised by high void content in locations already weakened by fibre alignment deviations.

The process explanation suggests there is a relationship between minimum rib lengths and node regions. If the rib length is short enough compared to the node type, it may result in a resin starvation situation. If a given node type has a certain requirement in terms of resin volume, there should be a corresponding minimum rib element volume that is able to satisfy this resin requirement. Such a relationship limits the geometry that is can be manufactured with low void content. Specific manufacturing trials would be necessary to accurately quantify these small changes, since they are likely smaller than the design and manufacturing approximations discussed previously.

It is difficult to make a judgement on the effect of a different fibre type or resin system. Higher viscosity resin will certainly have less freedom to migrate within the lattice. However, a high viscosity resin may also result in different consolidation and compaction behaviour that reduces the requirement for resin migration to occur. Thus it is possible that one effect is mitigated by another.

5.2.4 Conclusions

- Approximations in modelling and manufacture account for a small portion of deviations in lattice dimensions.
- Resin migration is responsible for larger systematic variations in lattice dimensions, particularly rib width.
- Resin migration is thought to be caused by a pressure gradient that arises due to the disparity in compaction response between ribs/nodes and transition regions.
- Rib widths are sensitive to local lattice geometry, element lengths and node types.
- Rib and node heights are determined by a global equilibrium that is stable about the design height, thus are not sensitive to local lattice geometry.
- Measurements of lattice dimensions should be evaluated within the context of the lattice design, process and in comparison to local cells.
- A requirement for void free manufacturing could determine limits for lattice design with regard to minimum rib element length for a given node type.
- Measurements of rib geometry and noted void locations for the manufactured panels are consistent with an equilibrium model of compaction and consolidation as described.

5.3 Quality Evaluation Tools

This section will review the quality evaluation tools used for the two lattice panels. The review will explain what is shown by the various techniques and how results may be interpreted.

5.3.1 C-Scan

C-scan techniques are commonly used to assess the quality of composite laminates, for example to locate areas of delamination. With lattice structures, there is a systematic variation in quality between the rib and node sections due to resin rich regions and fibre alignment deviations. This produces a c-scan result as shown for the first manufactured panel.

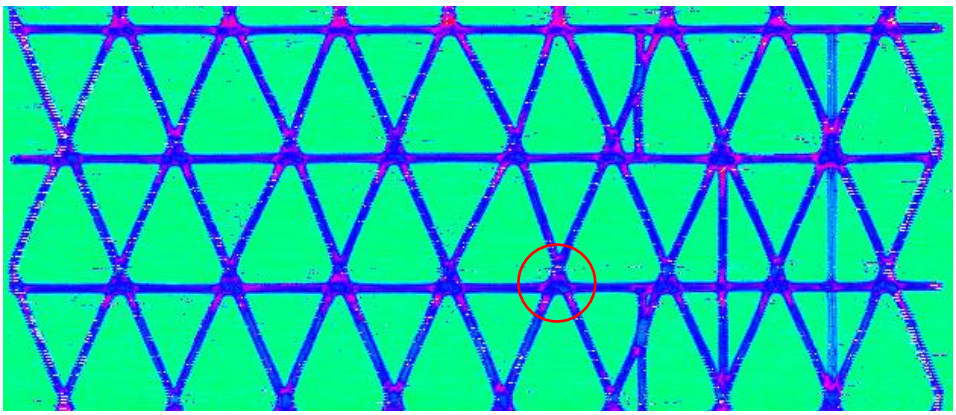

Figure 5-18 C-scan result for the first manufactured lattice panel, circled node indicates the CT-scan sample

The results show the intensity of the ultrasonic signal that propagates through the sample. In the free space, the signal is unimpeded and shows green. As the transducer scans over the composite, the signal is attenuated to varying degrees and shows a blue to pink colour as the signal intensity diminishes. Generally the results show that the rib sections and centre of nodes provide a good signal that corresponds to measurements that the composite is well consolidated at these points with a high FvF and low void content. The pink highlights appear at the transition zones outside the node area.

One issue with the c-scan is that the results alone cannot distinguish if the highlighted regions are due to resin pockets, fibre waviness or voids. Each of these features could reduce the strength of the signal and all of them typically occur in the transition region of the node. Comparison with the micro-section results and understanding of the typical transition features is needed to interpret the results.

A transition with low-waviness appears with the following c-scan result:

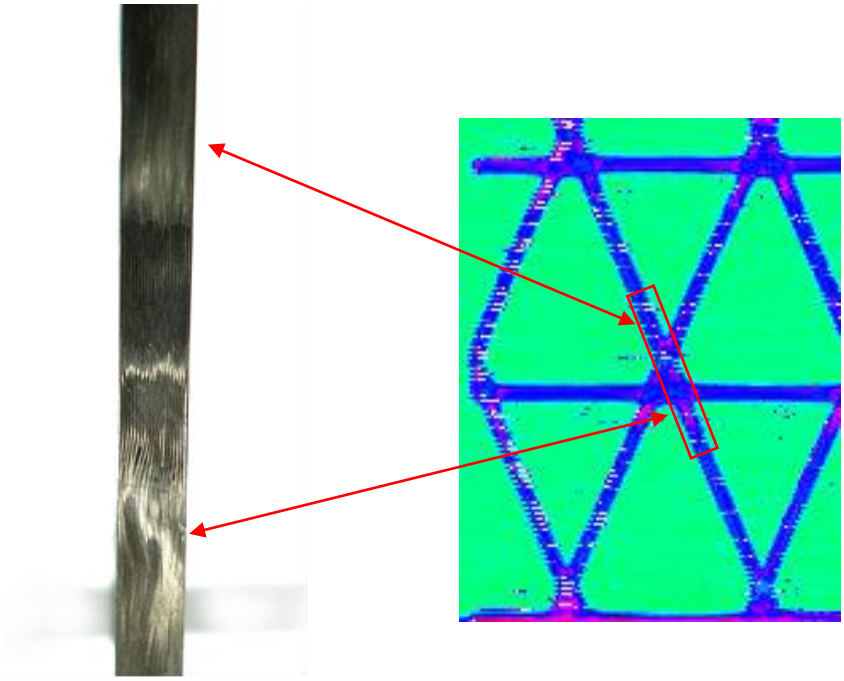

Figure 5-19 Comparison of micro-section and c-scan results for a helical rib

This comparison shows a helical rib transition through a node and the corresponding c-scan image. The features of note are the extended waviness in the lower transition (indicated by the lower arrow) as well as the relatively uniform transition region above the node (upper arrow). Examination of the section shows that both transitions show resin pockets at the point where the tows interleave, whereas the obvious difference is the severity and extent of the ply waviness.

In the lower transition, the waviness extends for approximately 20 mm before diminishing and aligning with the straight fibres of the mid-rib. The highlighted region on the c-scan is approximately 15 mm in length, corresponding to the majority of the wavy region. At the upper transition, little waviness is visible in the section while the highlighted region is just 5 mm in length. This suggests that the size of the highlighted region may indicate transitions with significant waviness if it extends beyond approximately 5 mm. Another example is presented below.

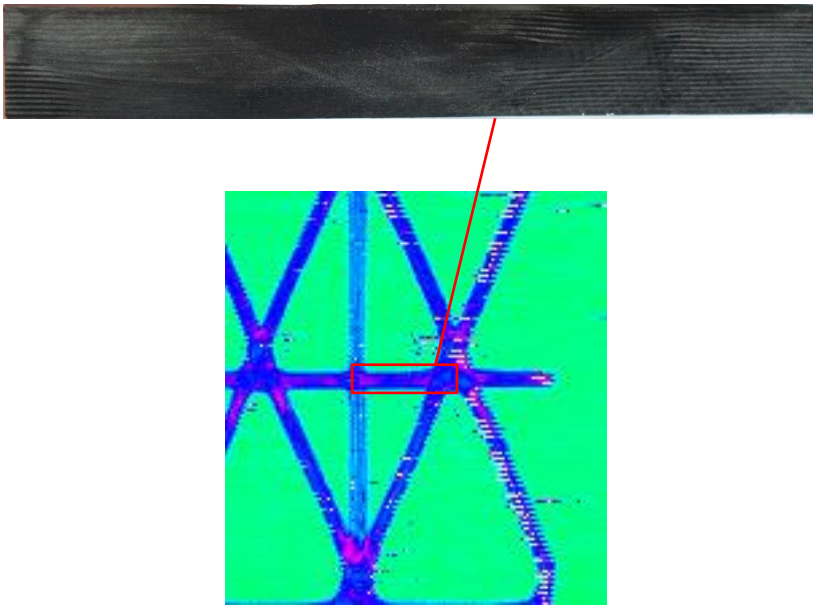

Figure 5-20 Comparison of micro-section and c-scan for a hoop rib

This comparison shows a hoop rib with an intersection (with a vertical additional rib) and a node region. The left side intersects with a half-height rib while the right side enters a node region. Overall the section shows low waviness with the plies transitioning smoothly and with minimal deviation. Again, this corresponds with the c-scan that shows two regions that extend approximately 5 mm into the rib.

A c-scan was also made of the second lattice panel:

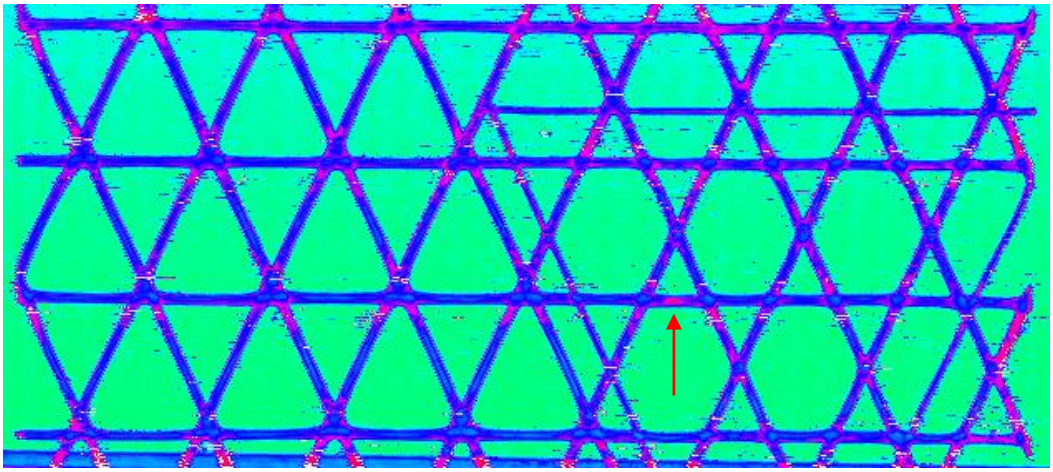

Figure 5-21 C-Scan result of second lattice panel, arrow indicating the presence of voids

One aspect that remains unclear is the determination of voids. In the first example there was not a clear indication in the c-scan results that would suggest the presence of voids. However, in some micro-sections small voids (<0.5 mm^3) were visible. These typically appeared in the hoop-helical node transitions. Compared to the c-scan results, the hoop-helical transitions appear as a small highlighted region with unremarkable intensity.

In comparison to the CT-scan, the voids are clearly visible in a plane montage:

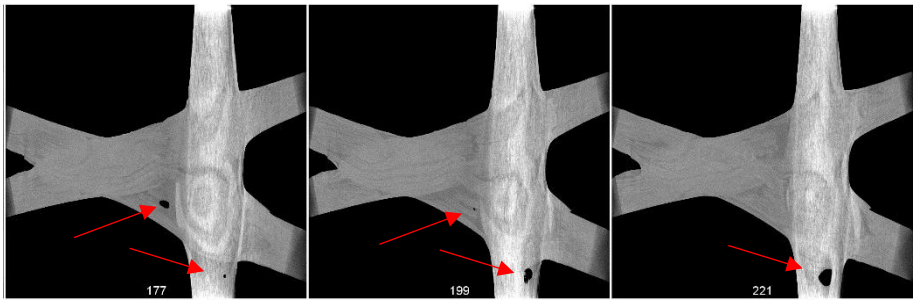

Figure 5-22 Selection of CT-scan images with void locations indicated

The images show a series of sections through the height of the sample node. This is discussed in detail in section *5.3.3* and presented here for comparison to the C-scan results. The void visible in the left image is comparatively small with an estimated area 1.0 mm^2 and thickness of 0.5 mm, resulting in a volume of 0.5 mm^3. The void visible on the right side has an area of 2.8 mm^2 and a thickness of 0.45 mm, resulting in a volume of 1.26 mm^3. Again, since they appear in the transition region, it is not possible to differentiate them from the other effects with the c-scan results alone.

On the other hand, an unusual C-scan result showed an attenuated signal in the mid-rib section, indicated by an arrow in Figure 5-21. This is remarkable because the fibres in the mid-rib section are generally well aligned and compacted, resulting in good signal propagation. This also means that it is unlikely for there to be significant fibre waviness. In this case, micro-sections revealed that there were indeed significant voids. The conclusion is supported by rib width measurements that show the rib was not compacted to the design width.

Overall the C-scan is a useful check to perform to correlate the expected lattice quality in transition regions. The results may highlight significant deviations from the nominal results as described above that could also be flagged by rib dimensional checks. The C-scan is not able to clearly determine the presence of voids in transition regions or the areas around the node.

5.3.2 Micro-section analysis

Sections were made in the thickness plane along the axis of the rib elements in order to observe the rib-node transition. The locations for micro-section analysis were selected to obtain information about how lattice geometry and lattice modifications effected the transition regions. The position of the section plane is illustrated in Figure 5-23.

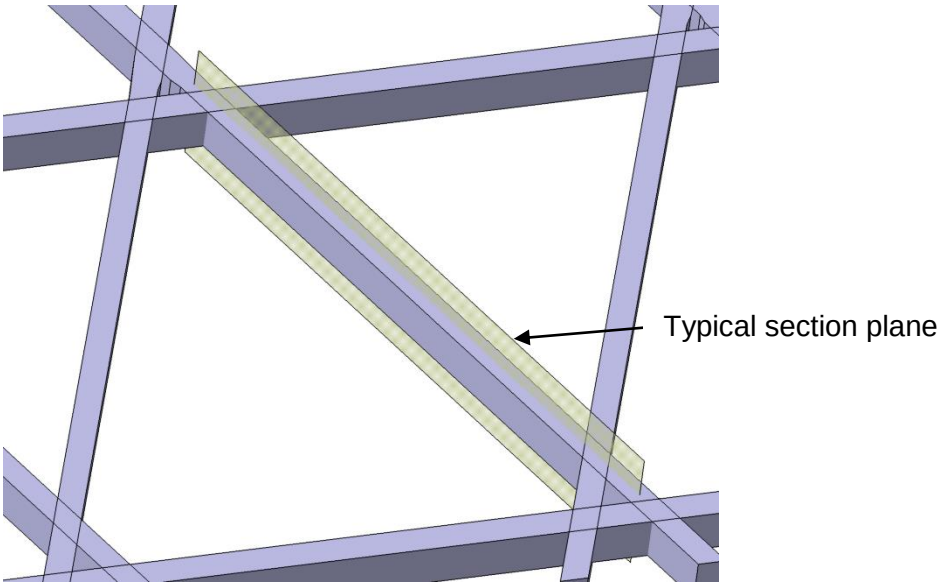

Figure 5-23 Example of section plane location

The section plane is ideally along the centre line of the rib axis. This location is thought to be representative of the rib quality through the width direction of the rib element as discussed in section *5.3.3*. In practice the cutting disc has a thickness of approximately 1.7 mm and the cutting plane needs to be offset to account for the lost material.

For high resolution microscopy analysis it is necessary to polish away the cutting marks. However, this analysis was principally focused on the mesoscopic behaviour of the plies in the transition region, and it was thought that the surface quality of the cut parts was acceptable for this purpose without further polishing. An example of a sectioned rib element is shown in Figure 5-24.

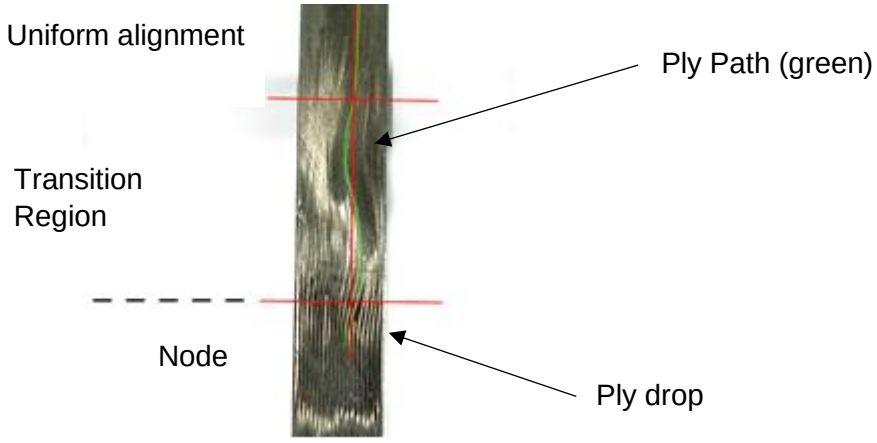

Figure 5-24 Typical micro-section view of a rib-node transition with the ply path highlighted

The plies in the node region, consisting of alternating layers of UD plies with different arrangement angles, are clearly visible as lamina. For nodes with a biased build-up, the ply drops are also visible as indicated above. In the transition region, the plies exiting the node are briefly separated by small resin pockets that are visible with low (10x) magnification, and appear as darker areas compared to the fibres that tend to reflect incident light. Moving further away from the node, the plies orientation may become distorted. This is clearly visible for distortions in the layup direction, and has been highlighted in the above figure by the green trace. The region that the distortion is clearly

visible by inspection is indicated by red horizontal lines, while the vertical red line indicates that axis of the rib element. It is possible to measure and quantify the extent and severity of these distortions using low magnification and simple measurement devices such as Vernier callipers.

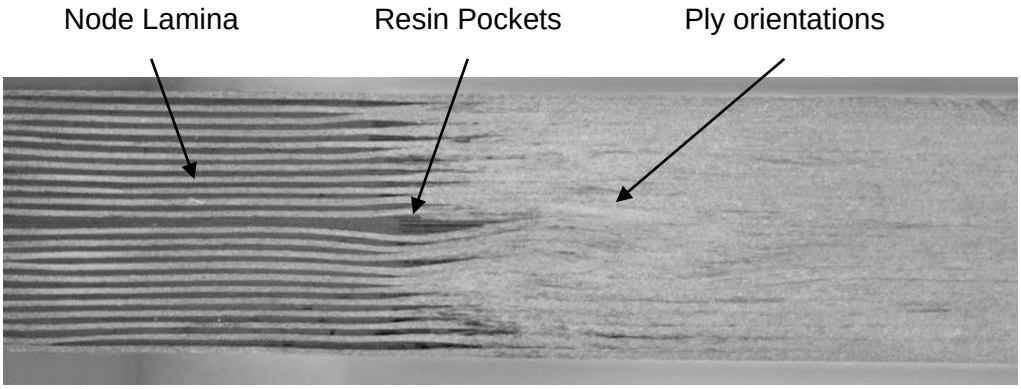

Figure 5-25 High resolution image of a node transition showing low ply waviness

Distortions in the width direction (i.e. out of the page for the section shown above or in the plane of the plies), are also visible, though they were more apparent in locations where the ply waviness is also significant. The in-plane waviness is difficult to measure with these sections without advanced techniques based on the observation that a plane section of a circular cylinder (the fibres in this case) becomes an ellipse, as described by [27]. However this technique may only be applicable for fibre misalignments up to 10°, whereas observations of the in-plane ply waviness on the surface of the composite suggest the fibre misalignment w.r.t to the rib axis is approximately 10-20°. In the typical sections this corresponds to an angle of 70-80° which is clearly outside the range for the method described.

For the majority of the rib sections made, the location of the section is not thought to have a significant impact on the observed transition behaviour. The section produces two surfaces separated by the thickness of the cutting disc, it was generally found that these surfaces were complementary and showed the same characteristics for a given node-rib intersection. No significant variation was observed for sections made near the centre line of the rib samples. CT-analysis supports this observation and is discussed in the next section. The exceptions to this, as will be discussed in following sections, are node transitions for ribs with an angle modification as they have shown to exhibit significantly different transition characteristics.

5.3.3 CT-Scan

Computed (micro-) Tomography is a technique available for composite analysis that offers a significant improvement in resolution compared to the above techniques. This facilitates detailed observations of the fibre directionality at node transitions and quantification of the void content given the sub-micron resolution available. Advanced techniques are able to reconstruct the microstructure of composite parts [22], as well as provide other composite quality assessment parameters. Such advanced techniques could be used to further quantify the characteristics of rib node transitions, and could be the subject of future research.

For the purposes of this investigation, one node was selected from the first manufactured sample. This node, and the six constituent rib members, included a hoop rib, a thickness

change helical rib, an angle change helical rib and two nominal size helical ribs. This represents a selection of lattice modification techniques and regular lattice geometry. The selection was limited to a single sample due to the cost of performing a CT scan, as well as the considerable resources required to post-process the results. Details of the equipment and software used to conduct the scan are presented in the appendix. The selected sample is presented in Figure 5-26.

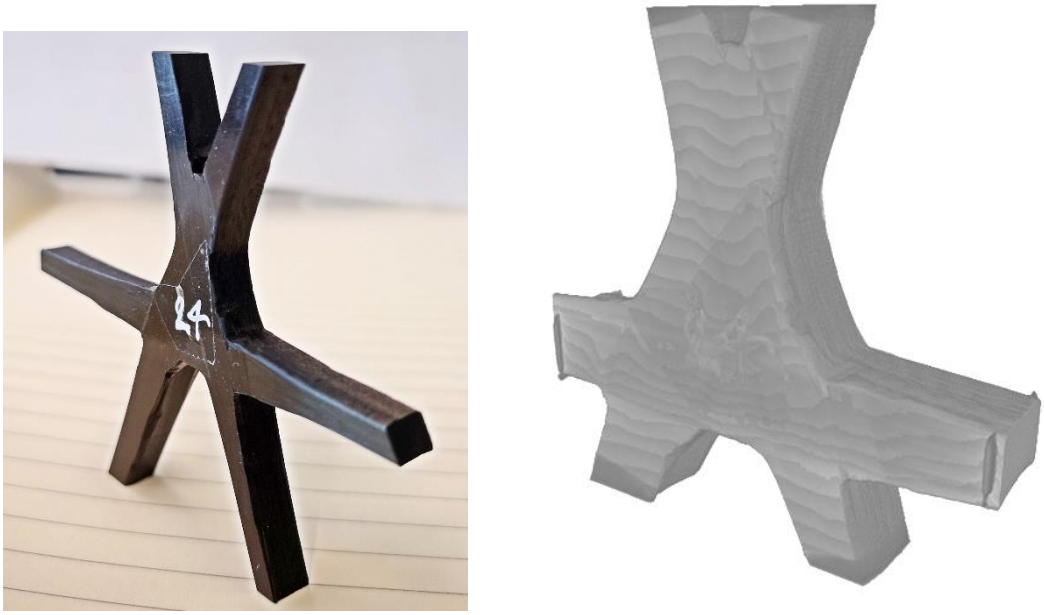

Figure 5-26 Selected node sample and 3D view of CT scan result

A point of interest related to the micro-section analysis was to investigate the sensitivity of the cutting location to the observed transition characteristics. This is possible with a CT scan by observing microstructure at sections progressing through the width of the rib at the node transition. The position of the section planes are represented in Figure 5-27

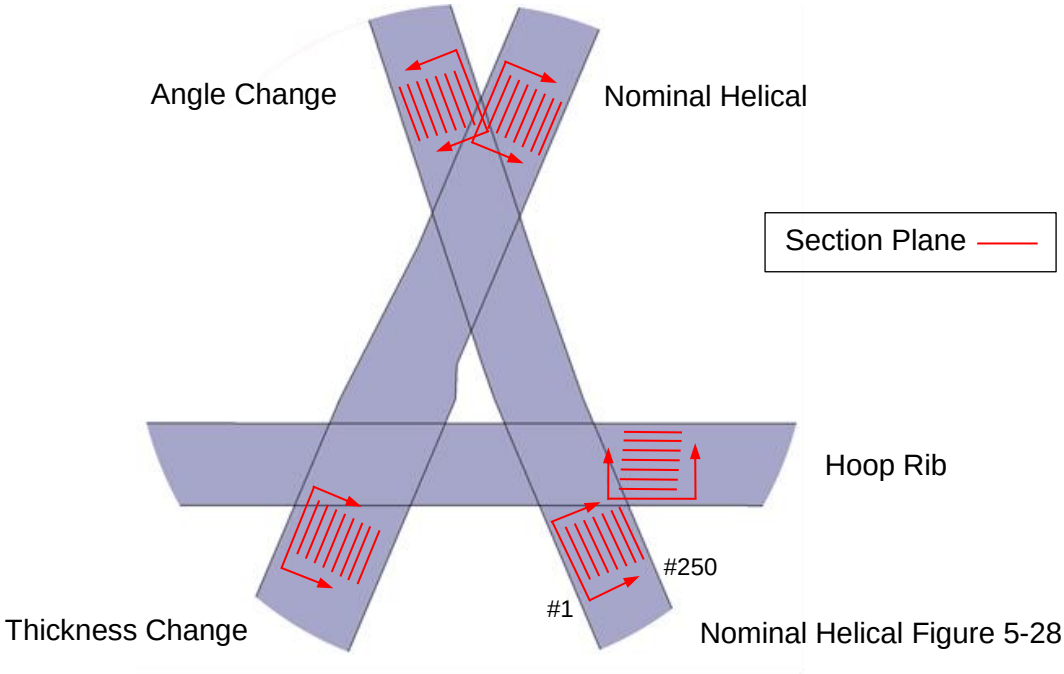

Figure 5-27 Section planes analysed using the results from CT-scan

This results in a series of images through the width of the rib (approximately 250 images over the width of 3.8 mm). A montage of the images for a nominal helical rib is presented in Figure 5-28, beginning with the slice #1 close to the surface on the left side, and progressing in the direction indicated by the arrows.

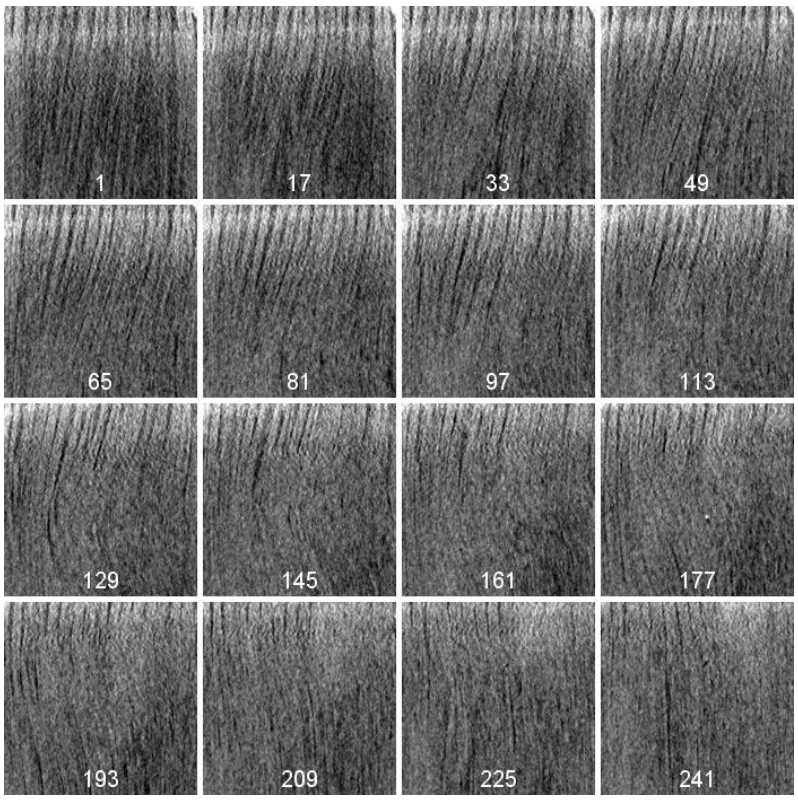

Figure 5-28 Montage of section images though the rib width showing the transition region ply waviness

In this montage, each slice represents a thickness of 0.015 mm. The initial slices near the inner surface of the rib show well aligned plies. Progressing through the width of the rib shows that ply waviness develops within the first 50 slices or approximately 0.75 mm. Visual assessment of the centre section of the rib shows that the waviness direction changes, but it is unclear if the intensity changes. At the far edge of the rib, the ply waviness diminishes in the final images.

The lower observed ply waviness close to the edge of the rib corresponds to observations of increased in-plane waviness. It is observed that at the node transition there is smooth increase in the rib width as the fibres spread out. Although the plies show lower waviness at the edge of the ribs, it is possible that they have more in-plane deviation.

Waviness development in the other ribs of the sample and the corresponding montages are presented in the appendix. These ribs show the same development trend as the example presented above, although the intensity of the observed waviness varies. One exception is the angle change rib, where the observed waviness is skewed to the rib surface on the inside radius of the curve. The surface of the rib element on the outer radius of the cure shows significantly less ply waviness. CT images and measurements of the angle change rib are presented in Appendix B. This correlates with the observations made during the layup which showed the tow wrinkling on the inside corner and flat tows on the outside curve, visible in Figure 5-10.

In relation to the micro-sectioning analysis discussed in the previous section, the montage shows that the developed ply waviness in centre section of the rib, which is more than 0.75mm from the edge, does not vary significantly. Therefore it should be reasonable to measure the waviness characteristics from sections made in the centre of the rib to quantify the rib transition.

Image analysis tools are available to quantify the directionality and distribution of an image, a description of the method is presented in Appendix B. Applied to the montage of images this shows the average alignment and deviation of tows that could help to characterise the rib transition. The results of the image analysis are presented in Figure 5-29 where 0° is aligned to the longitudinal ply axis.

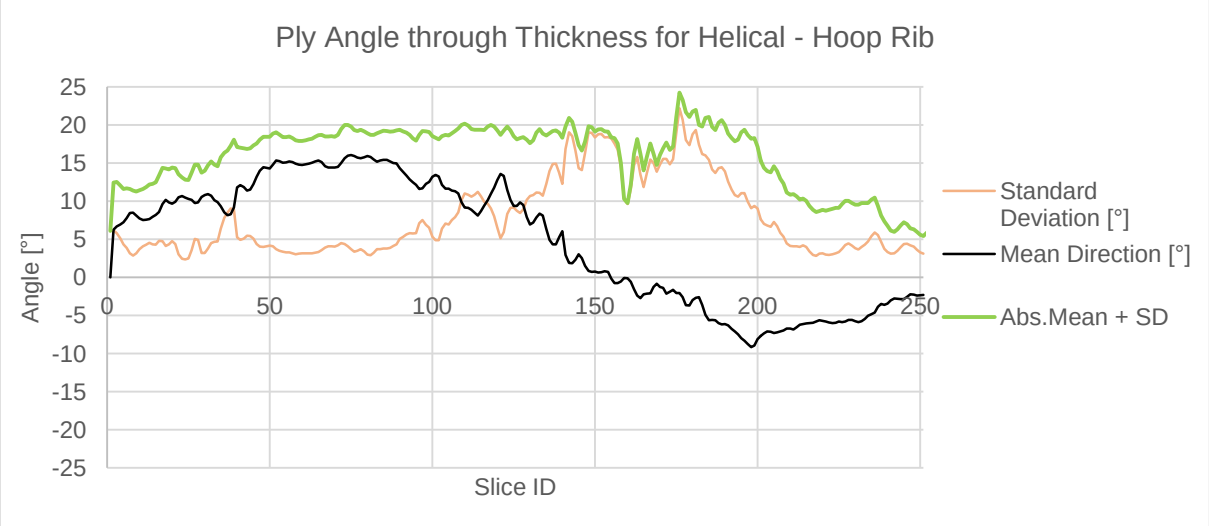

Figure 5-29 Image directionality analysis of slices through rib width

The image analysis shows the mean directionality and the standard deviation. In the case that the mean direction is close to 0° with a low standard deviation, the plies should be well aligned. This is visible in at slice 241. In the case that the mean direction deviates, but the standard deviation is low, the plies should be parallel to one another but shifted from the 0° orientation. This situation is shown in slice 49. In the case that the mean direction is close to 0° but the standard deviation is high, it is the situation where the ply deviations are aligned in a +/- symmetric direction. This situation is demonstrated in slice 145.

The addition of the absolute mean and the standard deviation gives a value that can be used as an approximate quantification of the ply waviness present in the transition region. Using this index a low value indicates the majority of plies are aligned to the 0° direction. A high value indicates ply deviations. The full ply directionality charts for the other node transitions are presented in the appendix. The average values of the analysed slices are summarised below together with the index value:

Table 11 Ply directionality in the transition region for various ribs types

Rib Type	Mean Direction Misalignment [°]	Mean Standard Deviation [°]	Absolute Sum
Helical – Helical	1	3	4
Hoop	0	5	5
Helical – Hoop	5	8	13
Rib Width Change	-4	5	9
Angle Change	-4	6	10

The summarised data shows there is a significant difference in the characteristics of the rib transitions. The helical-helical and hoop rib transitions both show good ply alignment with low misalignment values. Due to the complex ply distortions of the helical-hoop and rib width change rib, the misalignment values are significantly higher and also show a higher standard deviation.

5.3.4 Conclusion

- There is a qualitative correlation between the c-scan results and micro-sections in terms of waviness.
- C-scans are not able to distinguish voids in the transition regions from other effects.
- Micro-section analysis seems to be a valid method for assessing transition quality in ribs (excluding angle change ribs).
- High magnification and advanced techniques image analysis techniques may provide more information about fibre directionality from micro-sections.
- CT scans provides an extremely detailed view of the node and transition regions, including fibre directionality and void presence.
- Image analysis techniques can quantify the directionality in CT scan images.
- All of the above can be used to support direct measurements of lattice dimensions.

5.4 Transition Quality

This section will describe how the lattice quality changes for the various rib intersections observed in the two manufacturing trials. The two panels were evaluated using micro-section analysis to determine the waviness at the centreline of each rib. The transition region is of interest because there is an observed difference in ply waviness

characteristics and quality for each intersection type, whereas the microstructure at the nodes and mid-rib sections had consistent quality.

This section will present a method to quantitatively characterise ply waviness in the transition region. The typical waviness observed for various intersections will be presented. The effect of various lattice modifications on the observed ply waviness will be presented. Lastly, a general discussion on the impact of the measured waviness on the overall quality of the lattice will be made.

5.4.1 Waviness characterization

The observed ply waviness at rib-node transitions is complex. The ply deviation angle varies with distance from the node as well as height and width position in the rib. It is useful to describe the complex behaviour with as few parameters as possible in order to make comparisons of transition quality. The proposed method to characterise lattice transitions is adapted from the ply waviness approximation for traditional composite laminates, where waviness defects are modelled with a sine curve approximation [20]. The key values are the wavelength and amplitude. This is demonstrated with an example rib transition shown in Figure 5-30.

Figure 5-30 Micro-section of a helical rib joining a hoop rib, showing typical ply waviness

The micro-section shows how the waviness is distributed in the height. It is maximum at the approximate centre line, and practically 0 at the upper and lower boundaries. Moving away from the node, the amplitude decreases until the plies are more or less parallel. The paths of the plies are traced in Figure 5-31 to present them clearly.

This behaviour of each ply i can be approximated by a decaying sine wave of the form:

$$y_i(x) = A_i e^{-\lambda x} \sin(\omega x) + 2 \cdot i \cdot t_{avg}$$

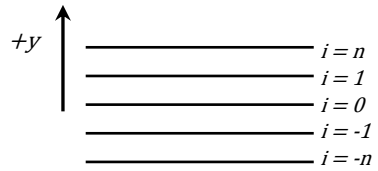

Where:

$\boldsymbol{A_i = a \cos(\frac{\pi i}{2n})}$ is the amplitude, maximum value $\boldsymbol{a}$ at the centreline and 0 at the upper and lower plies

$\boldsymbol{\lambda}$ is the decay/damping constant

ω is the wavelength parameter i.e. $\frac{2\pi}{L}$

$\mathbf{t_{avg}}$ is used to separate the individual plots based on the average ply thickness

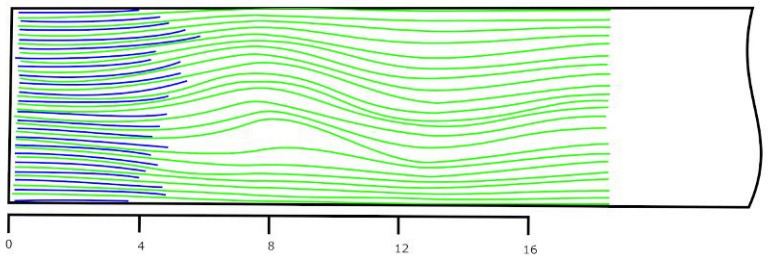

Figure 5-31 Trace of plies showing their path moving away from the node

Plotting the decaying sine function shows the visual correlation to the observed ply behaviour.

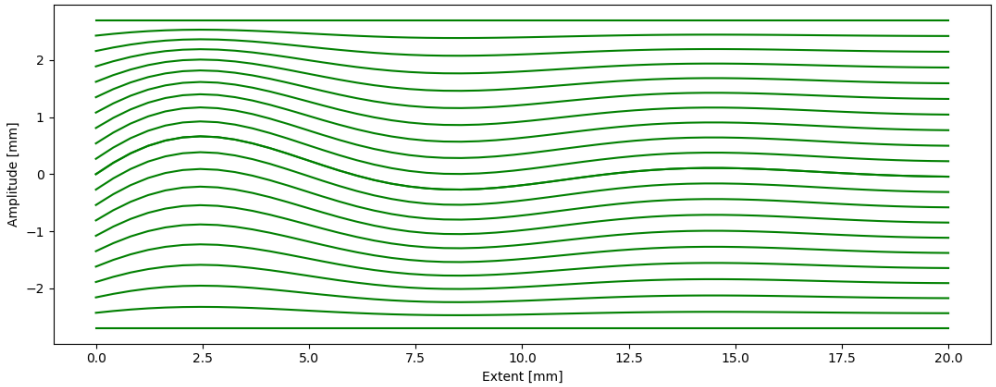

Figure 5-32 Idealised ply waviness for a typical node transition with 2a = 0.75, L = 12, W_s = 3.1%

The main features of the waviness are expressed by the ideal function. By selecting the values of **a**, **λ** and **L**, the ply path can be idealised. These values express the maximum ply deviation at the centre of the rib and the degree that the amplitude of the deviation is attenuated as the ply progress away from the node.

Additional features of the waviness could be related to three-dimensional nature of the rib compaction. Similar to the plies at the upper and lower surface experiencing less deviation, plies at the edge of the rib (in the in-plane direction) also experience less deviation as discussed in section *5.3.3*. Thus this model is valid for sections made at or near the centre line of the rib where it is expected to see the maximum waviness severity.

Using this method, the ply waviness in the transition can be characterised by measuring the approximate wavelength, peak amplitude and extent in a micro-section at the approximate centre of a rib element. The extent describes the distance from the node where the ply waviness has decayed such that deviations are scarcely perceivable, that is when the deviations are much smaller than the thickness of a ply. Using the values of wavelength and amplitude, the waviness severity can be calculated as follows:

$$W_s = \frac{a}{L}$$

The waviness severity expresses the maximum intensity of ply waviness as the ratio of *a* to *L*. In traditional composites, the waviness severity is linked to mechanical performance knock down. To correlate the waviness severity of a node transition region would be useful starting point to estimate the performance degradation of a lattice structure node transitions.

The waviness severity was measured for the micro-sections made on each of the manufactured panels. In total 95 measurements were recorded, the results are presented in Appendix E.

5.4.2 Base Lattice geometry

This section will explore how the regular lattice geometry relates to the measured waviness severity in transition regions. For regular lattice geometry, each transition type is presented with the transition region circled. Average values of measured waviness severity will be reported.

Transition type	Location	Waviness Severity	Notes
Hoop to Helical	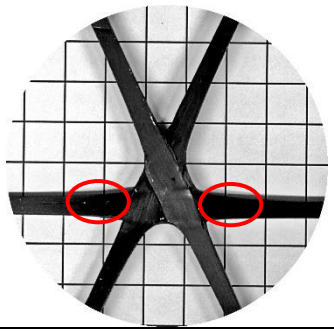	1.3 %	13 measurements from panel 1
Helical to Helical	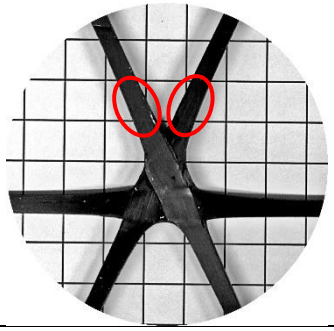	1.9 %	10 measurements from panel 1
Helical to Hoop	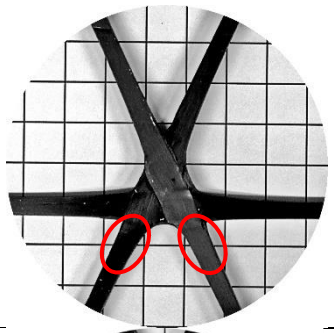	2.8 %	6 measurements from panel 1
Binary Node	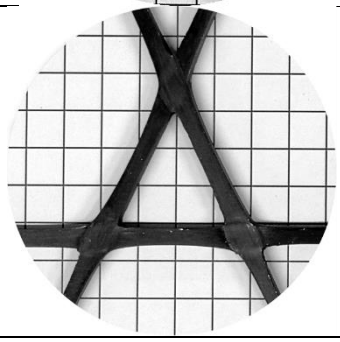	1.8 %	11 measurements from panel 2

In terms of waviness severity, there is a visible and measurable difference in the transition type for the studied geometries. Considering the lattice geometry with collected node, the transitions of a hoop rib to a helical rib consistently showed the lowest ply waviness. Helical to helical rib transitions showed slightly higher ply waviness, while the helical to hoop transitions had consistently higher ply waviness. Regarding the binary node samples, the transitions generally showed similar waviness across all of the transitions, thus they have not been segmented.

5.4.3 Effect of rib width transitions

At least 3 methods are available for manufacturing ribs with varying widths as described in section *5.1.5*. A comparison of these modifications to the quality of the node transition is described in this section. Wherever possible a like-to-like comparison is made by

comparing transitions with the same geometry to isolate the change to the rib width transition. The comparison is made based on measured waviness severity from micro-sections. Since waviness severity is measured as a percentage, the comparison is made by percentage points (p.p.). The increased waviness at a node transition associated with a modification is presented as p.p. increase in measured waviness severity over a similar unmodified node transition.

Interleave	Schematic	Waviness Severity Change	Comments
Tapered	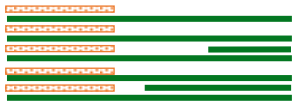	No measurable change	4 measurements compared. C-scan comparison shows no differences. Rib width changes: 4.4 to 5.2 mm 4.4 to 4.8 mm 4.8 to 5.2 mm
Biased		+1.3 p.p average +3.5 p.p maximum	6 measurements compared. C-scan shows significant differences. Rib width changes: 3.5 to 4 mm 4.8 to 4 mm 5.2 to 4 mm
Tow Width	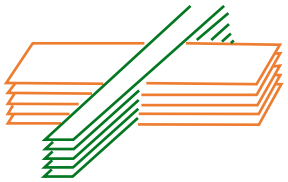	+0.6 p.p	2 measurement compared to similar rib. C-scan comparison shows minor differences in similar ribs.

Regarding the tapered rib width change, it is not surprising that there is no measureable change meaning that the measured values show the expected variation within the tolerance of the manufacturing process. There is no statistical change in measured quality related to this feature. An explanation could be that the ply drop is occurring outside the transition region in the rib section where the plies are generally well aligned. Given the generous 40:1 ply drop ratio, it is probable that the effect on the mechanical performance of the rib section is minor, and no effect is observable in the transition region for the geometries studied.

The biased interleave generally showed an increase in the measured waviness. This was proportional to the magnitude of the rib width change. Larger rib width changes increased the measured severity more than smaller changes. The rib elements investigated are all helical ribs from the first panel, thus the measurements are reported for the helical-hoop transitions that have the highest base values of waviness severity in general. Although not reported above, it should be noted that the complementary hoop ribs, that typically show very low waviness, did not show a measureable change in waviness severity. In other words, the biased node interleave increased the waviness severity of the helical-hoop ribs, while the hoop ribs were unaffected. This demonstrates that the consolidation and compactions process at a node is asymmetric and unbalanced.

In the case of the tow width modification, it was difficult to make micro-sections due to the thin rib widths, hence the scarcity of measurements. For the observable sections, there was a minor increase in waviness severity compared to a similar rib geometry. However, the measured value was just around 2%, meaning that the quality was average-to-good. Differences in rib geometry could explain a portion of the disparity in measured quality. Comparing the c-scan result of other modified ribs shows that the transition characteristics are similar to the measured regions. Based on this assessment, the tow width modification does not seem to significantly reduce transition quality, and this method would certainly be preferable to biased node transitions from the perspective of manufacturing high quality transitions.

5.4.4 Effect of additional members

Several examples of additional members were investigated in the first manufactured panel. The waviness severity was measured at the node transition. This is presented in Figure 5-33.

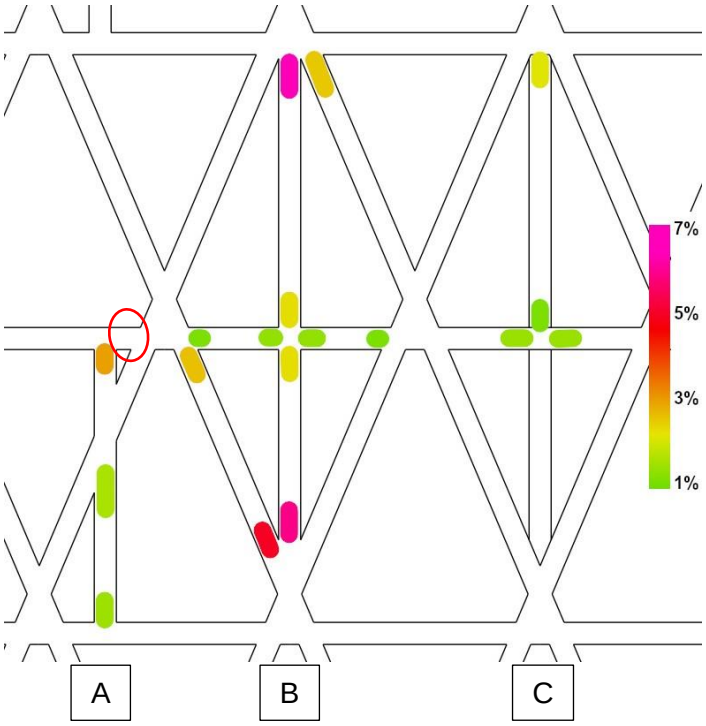

Figure 5-33 Observed waviness severity for various additional ribs, circled region indicates observed void location

Several points of interest:

- There is a measureable effect of the additional ribs on the surrounding rib elements in the case that an additional rib meets a node (ribs B & C). The observed waviness is slightly higher (~0.5 p.p.) compared to a regular rib when an additional member is present at the node.
- Additional ribs crossing a hoop rib do not have a significant effect on the ply waviness of the hoop rib. The quality observed in the hoop rib is similar to that of a hoop rib at a regular node, in other words it is very good.
- The additional rib B has very poor quality where it meets the nodes. It is among the worst measured in the panel and significantly worse than the regular lattice geometry.

- The additional rib C has the same layout as rib B, but the rib height is only half. The quality observed is slightly higher. This suggests that there is a dependence on the rib height for the observed waviness.
- Above additional rib A in the circled region, voids were observed in the hoop ribs. This is thought to be related to the under compaction of the ribs that results in a paucity of resin.

Overall, it can be concluded that the investigated methods of incorporating additional ribs result in quality well below that of an unmodified structure. In some cases the additional ribs cross the base structure with minimal disturbance, but when crossing a node (as in B & C) the quality is severely reduced. In the case that the additional rib crosses close to a node (as in A), the small size of the split cell could result in insufficient compaction that leads to the formation of voids, as discussed in section *5.2* .

5.4.5 Effect of angle changes

Two angle changes were investigated by offsetting the node position, resulting in rib angle changes between 2.5° and 10°. Overall, the angle change ribs are associated with a reduction in quality due to fibre waviness that is present during the layup phase. Clearly, the complex ply distortions introduced during layup are not improved during the curing process.

Investigating the transition quality, 11 waviness severity measurements were recorded. Measurements suggest a 2.5 to 3.0 p.p. increase for angle changes less than 5°. For the ribs with angle changes of 10°, the quality change was a 3.5-5.0 p.p. increase. In both cases, this represents a significant increase in measured waviness, with a 7.7% value among the highest measured. This poor transition quality is correlated with the results from the c-scan. Angle change ribs show extended regions where signal intensity is diminished, indicating that the ply waviness is more severe and extends further from the node.

An observation was made during analysis of some micro-sections that the complementary section surfaces did not result in the same waviness measurement, particularly for ribs with higher angle deviations. In this case, one section surface resulted in a higher measurement. This observation is supported by the CT-scan analysis that showed the ply distortion through the width of the rib was not symmetric but biased to surface of the rib on the inside radius of the rib angle change. Sections made in different positions in the rib would therefore result in different observed quality.

This more complex transition characteristic and dependence on section location provides some explanation for the wide range of the measured values, but also suggests that meaningful comparisons could be difficult. Overall the trend is that larger angle modifications result in greater reductions in transition quality, but the quantification of this phenomenon is significantly more complicated compared to other lattice modifications.

5.4.6 Conclusions

Qualitative conclusions regarding the transition quality are:

- Ply waviness can be characterised by an approximation with a decaying sine function.
- Analysis of micro-sections can determine the amplitude and wavelength to characterise the peak waviness severity for a node transition.
- An idealised model based on the peak measured values can reasonably represent the plies in the transition region.

- There is a visual and measurable difference in ply waviness in transitions at collected nodes. Binary nodes show a smaller variation.
- Biased interleave width changes reduce the quality of the node transitions.
- Tapered width changes explored in the second panel did not reduce transition quality.
- Width changes based on different tow widths explored in the second panel had a relatively small impact on transition quality.
- Additional rib modifications that terminate at nodes had the lowest observed quality, far less than a regular lattice.
- Angle changes are difficult to quantify and characterise given the different ply waviness pattern observed.

6. Compaction & Consolidation Model

This chapter presents a discussion of the process that describes cause of the observed ply waviness at node transitions. The lattice geometry factors thought to influence this process are identified and described. These factors are used to form a quantitative model of the transition quality. This quality model is calibrated based on measurements from the first manufactured panel. With the insight provided by the model, the second panel is designed with the goal of incorporating lattice modifications without compromising node transition quality. Measurements of the second panel transition quality are compared to the values predicted by the quality model. A discussion is made of the model correlation before conclusions are presented.

The process description deals with the intersection of tows from two rib elements, for which we are considering the transition region in the one of the rib elements. To minimize confusion, the rib elements will be referred to as the *principle* tows/elements and the *complement* tows/elements, illustrated in Figure 6-1. The transition region of interest always refers to the principle rib element.

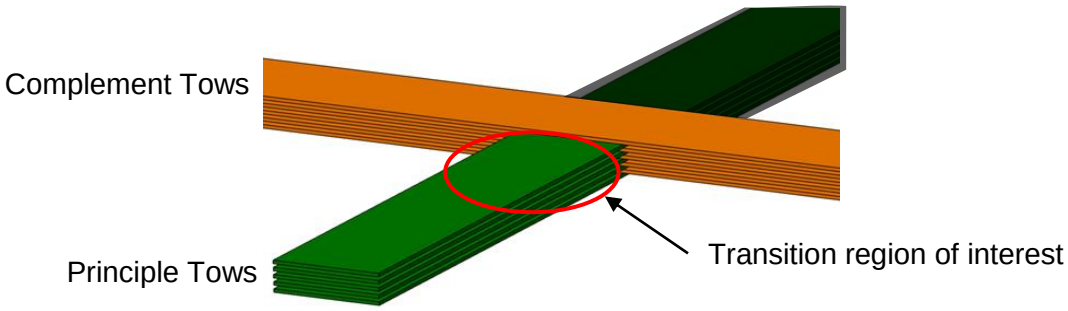

Figure 6-1 Convention for *principle* and *complement* rib elements, green and orange respectively, with transition region highlighted

6.1 Process Discussion

Ply waviness in the transition region is due to the change the tows need to make to enter a node. It has been shown that the severity of the waviness depends on the particular arrangement of the node, where members exhibit clear differences in quality. For a given node arrangement, the transition may be smooth and result in low waviness severity for one rib element, whereas a different rib element of the same node may have high waviness severity. To understand this process, the out-of-plane consolidation and in-plane compaction must be considered.

An explanation for this imbalance is based on how much the piles are spread out by the consolidation force compared to how this is resisted by the compaction force in the region around a node. First, consider the composite alone without any silicone tooling. The out-of-plane consolidation tends to reduce the thickness of the tow bundles in the overlapping areas. Since the compression of the fibres is negligible, this consolidation results in the physical spreading out of the tow bundles to accommodate the reduction of the stack height, as required by conservation of volume. Therefore in the region around a node, the ply thickness decreases which results in a local width increase, as shown in Figure 6-2.

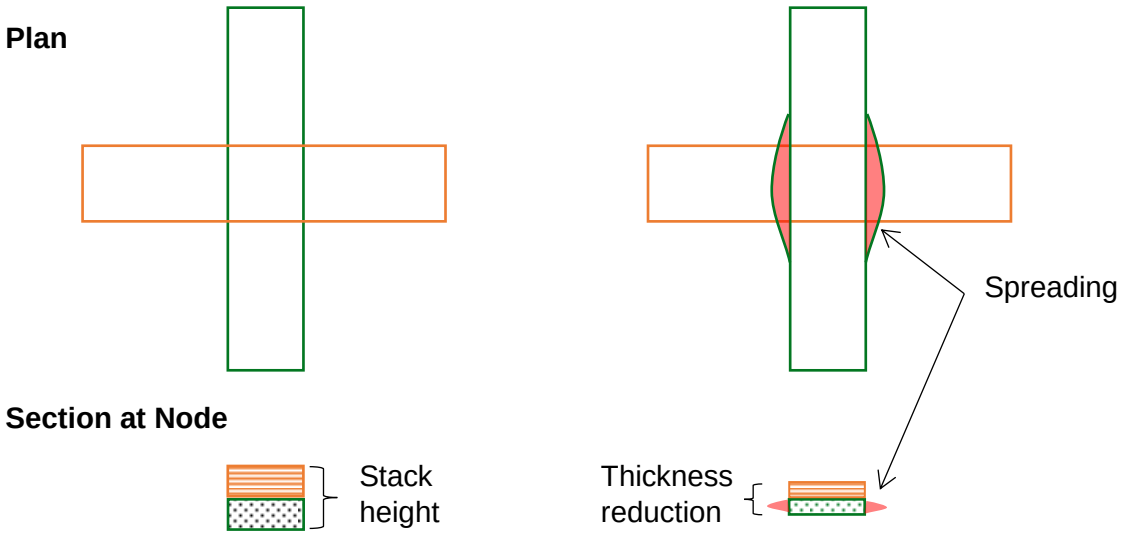

Figure 6-2 (a) Plan and section views of principle and complement tows (green and orange respectively) at an intersection, (b) consolidation resulting in spreading/thinning of tows at the overlap

Now consider the additional effect of the compaction force from the silicone tooling. Firstly, this in-plane force opposes the spreading out of tows near the node. Secondly, the silicone expansion will compact the tows to the design rib width at some distance away from the node. This process is shown in Figure 6-3 (a). The tow width is represented with a dashed green line and the design rib width is represented by a solid green line. The compaction of the tows to the design rib width appears to exaggerate the spreading of tows at the node, an observation that corresponds to manufactured parts. In this idealised situation the resistance provided by the expansion tooling is balanced for the principle and complement elements. Therefore the spreading of tows at the node occurs equally for both elements, and so the thicknesses of the tows at the node are reduced equally. This situation is balanced and equal for the primary and complement elements. Considering the thickness of the tows, there are twice the number of tows at the node intersection compared to the rib sections. Therefore the thickness of plies in the rib is *2x* the thickness of plies in the node, given the rib and node height is equal.

Consider now the case where the resistance provided by the silicone tooling is not equal and balanced for both intersecting elements. Figure 6-3 (b) shows a case where the compaction force acting on the complement plies is greater than the force acting on the principle plies. This doesn't change the thickness of the plies in the ribs far from the node, at sufficient distance the rib is not affected by the node transition. As consolidation tends to spread out the tows at the node, the spreading does not happen equally due to the unbalanced compaction. The restrained complement tows will spread out less compared to the principle tows because the principle tows are lightly restrained. This means that the thickness of the plies at the node will be unequal. Since the complement tows spread out less, the thickness reduction is than the nominal *2x* reduction in the balanced case. While the principle tows spread out more, the thickness reduction is greater than the nominal *2x* reduction of the balanced case. Therefore the situation of unequal compaction leads to a node where the principle element plies are thin and wide while the complement element tows are narrow and thick.

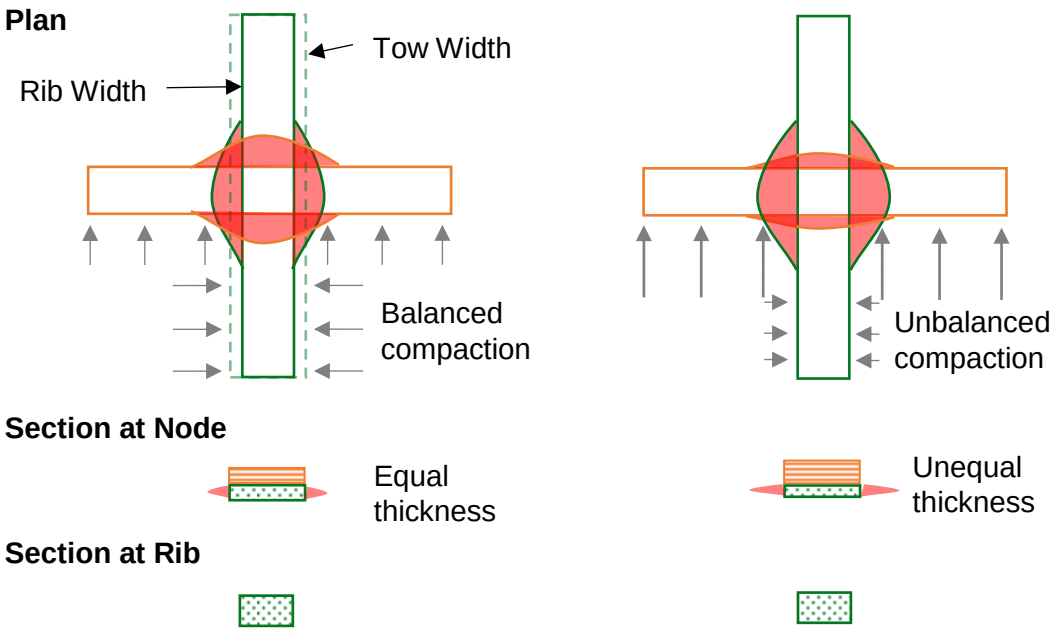

Figure 6-3 (a) balanced compaction force at the node transition, ply thicknesses are equal, (b) un-balanced compaction force means uneven ply spreading and results in thicker complement plies

A mismatch of ply thickness at the intersection point results in different node transition conditions for the principle and complement tows. This is illustrated below in Figure 6-4 by section views of a node with unbalanced compaction, one view along the principle rib and one view along the complement rib. As noted, there is a difference in ply thickness at the node where the plies have been consolidated. Far from the node the plies are compacted together by the silicone tooling, and the thickness must be (on average) equal to the number of plies divided by the rib height. This is true for both the principle and complement tows as the rib height is found it be constant in manufactured samples, discussed previously section 5.2.2.

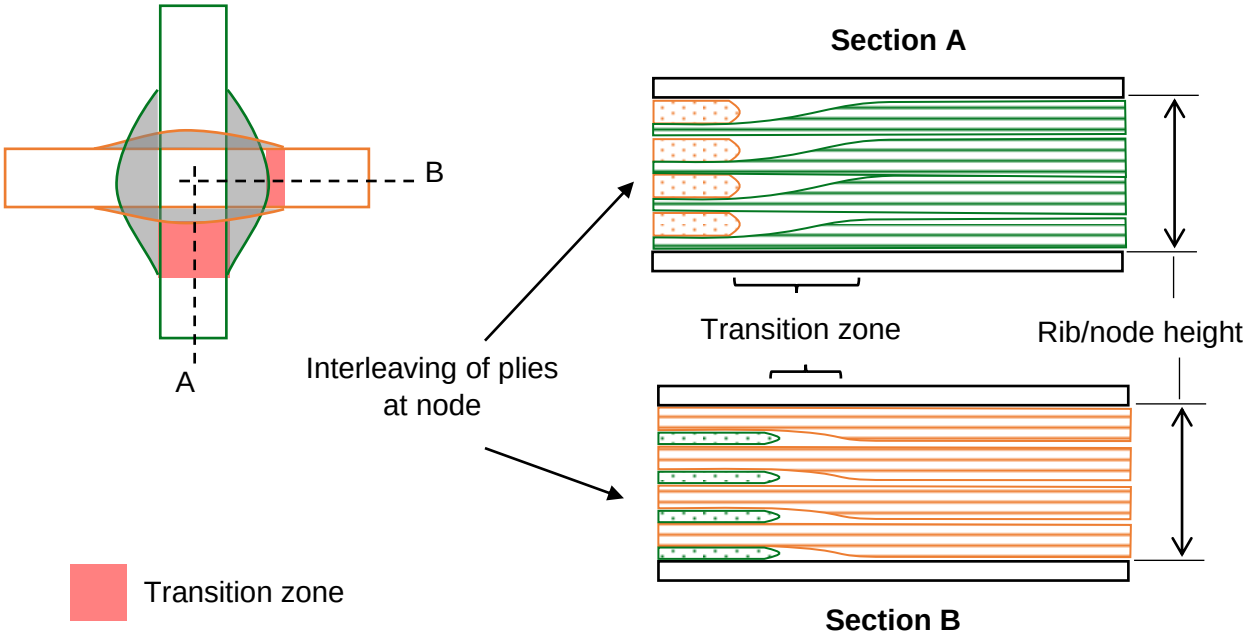

Figure 6-4 Section views of a node with mismatched ply thickness

The key difference to note is the *Transition zone*, indicated in Figure 6-4 on the plan view by the red shading and marked in the section views. The transition zone begins where plies exit the interleaving area and ends where the plies have been compacted (in the in-plane direction) to the full height of the rib.

Section A shows that the transition between the node and the rib area is a large. For these principle element tows marked in green, the plies have spread out further at the node and so they are thinner. There is a greater distance from the point the plies exit the interleaved area at the node to the point that the spread out fibres can be compacted and the thickness can increase to reach the nominal rib height, thus the transition zone is longer. The difference in ply thickness between the principle tows at the node and principle tows that form the rib sections is more than a factor 2.

Section B in comparison shows same transition from the perspective of the complement tows. These tows have spread out less at the node and so the thickness reduction is less in comparison. Therefore the transition region is relatively smaller. The difference in ply thickness between the node and rib sections is less than a factor 2.

The transition zone is a critical region for the plies because there is a step reduction in the consolidation force compared to the node region or the rib section. As discussed, due to the build-up of tows at the node, there is a high consolidation force that compresses and spreads the tows. The fibres of initially separate tows are in physical contact as a result of the consolidating force. In the rib section, the plies are well compacted and consolidated, and the rib section is well formed. Again, fibres from initially separate tows are physically in contact meaning there is no measurable resin layer separating the tows. However in the transition zone, the sum of the ply thicknesses is less than the rib height. There can be no applied force to consolidate the plies in the out-of-plane direction as the fibres are not in contact.

Low out-of-plane consolidation force can result in ply waviness because the plies are not restricted from moving in the out-of-plane direction. Therefore the size of the transition zone as discussed above can be related to observations of ply waviness in the region where a rib meets at node. Asymmetric compaction leads to a mismatch in ply thicknesses and results in large transition zones that promote ply waviness. Small transition zones may be less likely to result in ply waviness because of the short length that is not restricted.

The special situation is that the spreading out and thinning of tows at a node is equal. As discussed previously, this means that there is equal thickness for both element plies at the node, as presented on the left of Figure 6-3. The balanced ply thickness at the node means that the thickness change required is equal for both rib elements. The size of the transition zone for both rib elements is equal, as presented in Figure 6-5.

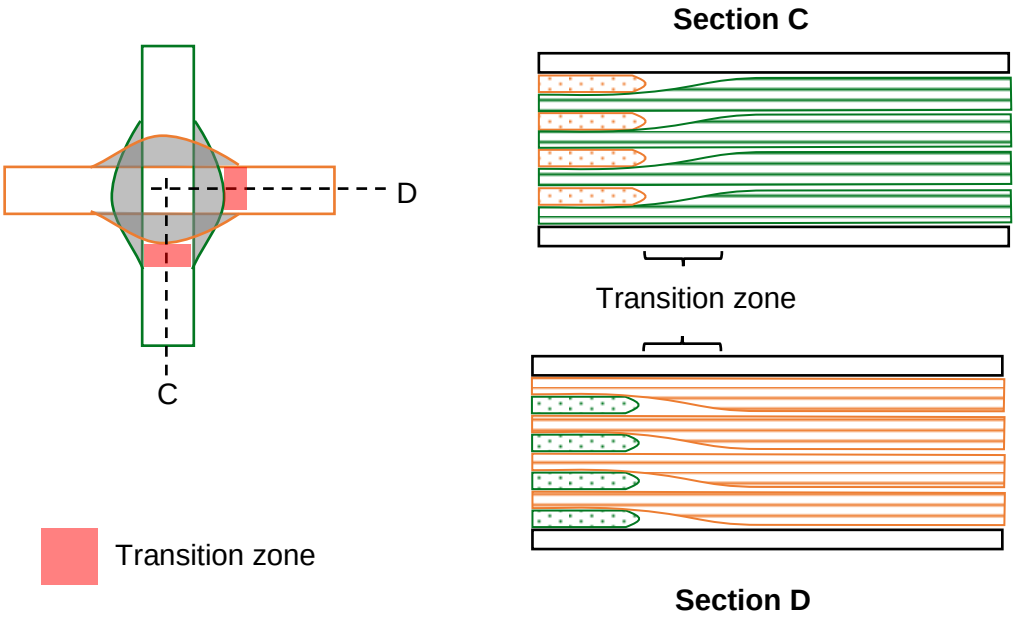

Figure 6-5 Section views of a node with equal ply thicknesses

It should be noted that the above examples are exaggerated to demonstrate the process in the simplest form. Measured ply thickness at the centre of an overlap area suggest that the difference in thickness between principle tows and complement tows is the order of 15-20%, which amounts to a difference of just 0.02 – 0.03 mm between thick and thin plies.

In practical lattice designs, the uneven compaction force around a node is likely the result of the geometry and the behaviour of expansion tooling. Clearly the above examples use the same geometry for demonstration. Furthermore, the compaction and ply thickness may vary from one side of the transition to the other, resulting in a wedge shaped ply cross-section that adds additional complexity. However the general explanation, that unbalanced compaction can lead to large transition zones where out-of-plane consolidation force is reduced correlates to observations and measurements of distinct differences in ply waviness characteristics at node transitions.

The process description proposed provides a framework to understand how different node types result in particular ply waviness characteristics. For example, the biased interleave nodes that are associated with increased ply waviness as discussed in section 5.4.3. The process described provides an explanation for the increased ply waviness associated with biased interleave nodes compared to an unmodified node. Consider the case that a biased interleave node with equal compaction, as presented in Figure 6-6.

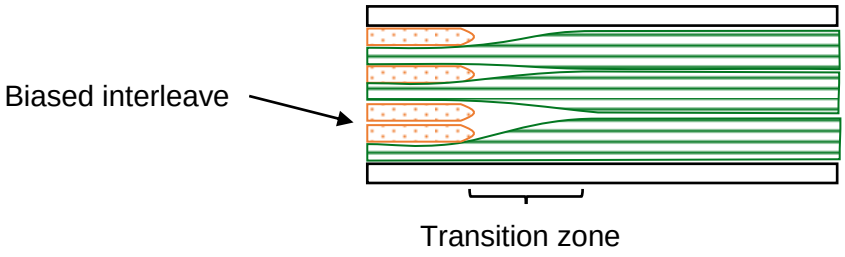

Figure 6-6 Transition zone for a biased interleave node

In the case that the node compaction is balanced, the individual ply thicknesses are equal for the principle and complement tows. However, considering the principle tows (in green), there is a smaller fraction represented at the node interleave, whereas they must transition to the full height in the rib section. In this example, at the node the ply thickness is 1/7 of the node height while in the rib section it is 1/3 of the rib height. Thus the thickness change from node to rib is greater than a factor 2 (i.e. 7/3 = 2.33…). This contributes to a longer transition zone that should be associated with greater ply waviness.

This process description is qualitative. The following section will aim to use lattice geometry to quantify the node compaction and consolidation process to provide a numerical characterisation of the node transition zone.

6.2 Geometry Factors Identified

This section describes three geometric factors identified that quantify the process discussion above. These factors are based on the ideal lattice geometry and rib dimensions, thus the factors can be calculated *a priori* and do not rely on manufacturing observations. Each factor is presented in a generalised form and its relationship to the process discussion of the previous section is explained.

Interleave Ratio

The interleave ratio describes how the principle and complementary plies interleave, presented in Figure 6-7. This is necessary to describe the situation at biased interleave nodes that are shown to have different transition characteristics.

Figure 6-7 Schematic showing different interleave ratios

The left side shows a typical node intersection, where equal numbers of plies are present such that the interleave ratio is unity. The right side shows a biased node, as with some rib width modifications, with unequal numbers of plies. The interleave ratio is simply the number of plies in the principle rib divided by the number in the complementary rib.

Physically, the interleave ratio is a factor that attempts to account for part of the imbalance at an intersection. Higher interleave ratios indicate greater imbalance that is associated with increased ply waviness.

Practical interleave ratios from lattice modifications explored in the first manufactured panel range from 1.0 to 1.3.

Node Consolidation Ratio

The node consolidation ratio describes the degree of consolidation required at the node to reach the design node height, as shown in Figure 6-8.

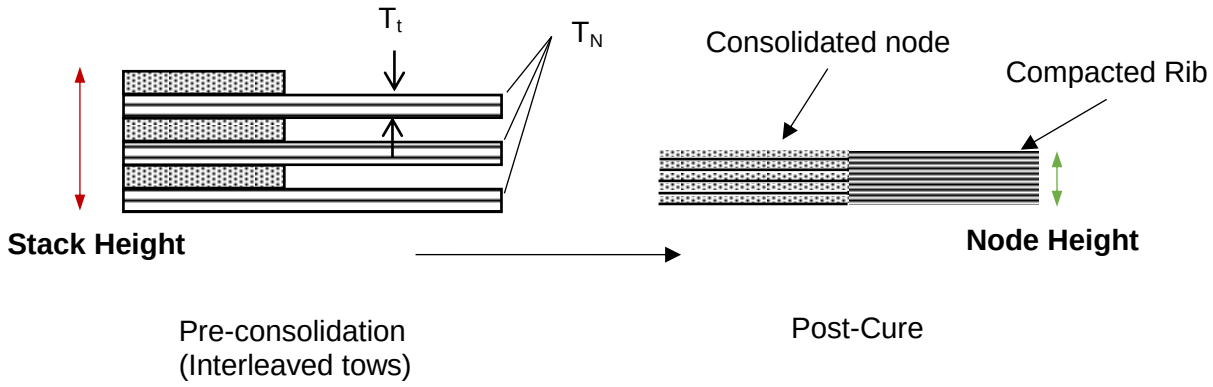

Figure 6-8 Node consolidation - as laid up and after curing

The left side shows the node build up with un-compacted tows, as would be observed after layup. The right is the consolidated and cured node and rib, with a node height that is equal to the design height as discussed in section 5.2 . The stack height can be calculated as the product of the number of tows at an intersection and the tow thickness. For regular lattice designs node regions, the number of tows at an intersection is twice the nominal number of plies. Therefore the node consolidation ratio for a regular node is as follows:

$$C_n = \frac{Stack\ Height}{Node\ Height} = \frac{2 \cdot T_N T_t}{R_H}$$

Where:

T_n is the number of tows in a nominal rib element
R_H is the resign rib height, as measured in Figure 5-1
T_t is the thickness of a the pre-preg tows

A node region may have more than two elements intersecting in the case of additional members. The node consolidation ratio will also describe this situation by summing the number of tows that overlap instead of simply taking a factor 2 as in the above equation. The node height is a basic design parameter, equal to the rib height for the lattice designs considered in this research.

Physically, the node consolidation ratio describes the factor by which each tow is compressed in thickness during the cure to reach the design height. Higher ratios mean each tow becomes thinner with more consolidation, and therefore spreads out more by the process discussed in section 6.1 . Node consolidation, by definition, is also a measure that describes the compaction process in the rib sections. If the rib-width compaction can be expressed a ratio of the design rib-width divided to the pre-preg tow-width, then the node consolidation ratio is to twice the rib-width compaction ratio. This point of information is not essential to understanding the compaction and consolidation process, and is therefore explained in Appendix D.

Node consolidation ratios for typical rib widths manufactured with ¼” (6.35 mm) wide tows are presented in Table 12 to show a representative range.

Table 12 Node consolidation and rib compaction ratios for ¼” tows

Design rib width	Node Consolidation Ratio	Rib Compaction Ratio
4.0	1.25	0.63
4.8	1.51	0.76
6.35	2.00	1.00
3.18	1.00	0.50

Designs with rib widths of 3.18 to 6.35 mm would have node consolidation ratios of 1.0 and 2.0 respectively. This seems to be a logical limit for the use of ¼” tows, but no manufacturing trials have been conducted.

Compaction Ratio

The compaction ratio describes the interaction of expansion tooling with the tows in the region near the node. Specifically, it attempts to describe how the expansion tooling interacts with the principle tows compared to the complementary tows. This relates to the process description because it is thought that unbalanced compaction behaviour results in lower quality. The geometric measure used is the ratio of principle and complement member lengths as shown in Figure 6-9.

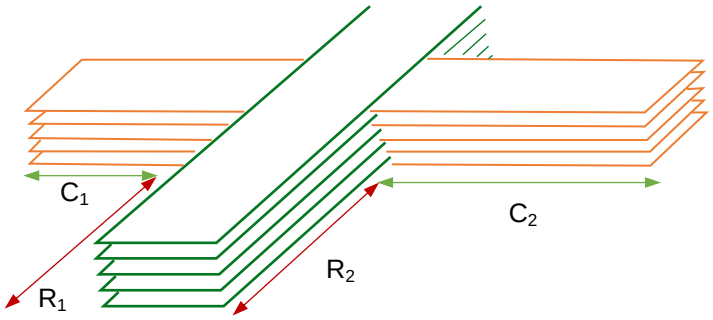

Figure 6-9 Schematic of Compaction Ratio

Essentially, the compaction ratio compares the lengths of the principle and complementary rib elements on each side of the intersection. In more detail, the C measure is the average length of C_1 & C_2 along the complementary rib elements, looking at each side of the principle rib. Similarly, the R measure is the average of R_1 & R_2 along the principle direction, on the same side of the intersection as the transition region of interest. Each length is measured from the point of intersection, along the respective rib to the next intersection of lattice elements, thus describing the length of the lattice elements. The compaction ratio is simply ratio of average lengths R_{avg}/C_{avg}.

In the above example, it seems that R_1 & R_2 have the same length. However applied to a practical lattice design it becomes necessary to have individual measures as shown in Figure 6-10.

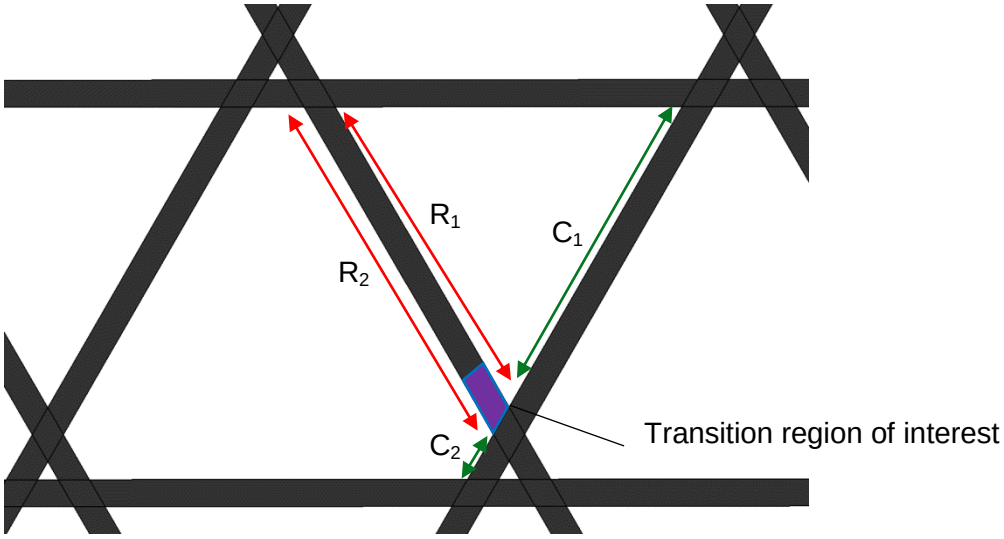

Figure 6-10 Example of RC ratio measures on a practical lattice design

The diagram shows that for practical lattice designs there can be significant differences in member lengths. The member length depends on the particular geometry of the lattice, so taking the average of the applicable member lengths provides a flexible and robust method to characterise a node transition.

High RC ratios indicate that the length of the principle rib is greater than the average length of the complementary ribs. This relates to the compaction behaviour of the principle and complementary tows that reduces the quality of the manufactured lattice because it represents an imbalance in the quantity of silicone tooling that compresses each rib element.

The compaction ratio associated with each of the transitions around a collected node depends on the lattice angle. It is insensitive to the helical rib spacing because the hoop rib spacing is a derived parameter, meaning the compaction ratio is unchanged for different helical spacings. The compaction ratio is marginally affected by the rib width since these parameters are small compared to the rib element lengths. The relationship of compaction ratio to lattice angle is presented in Figure 6-11.

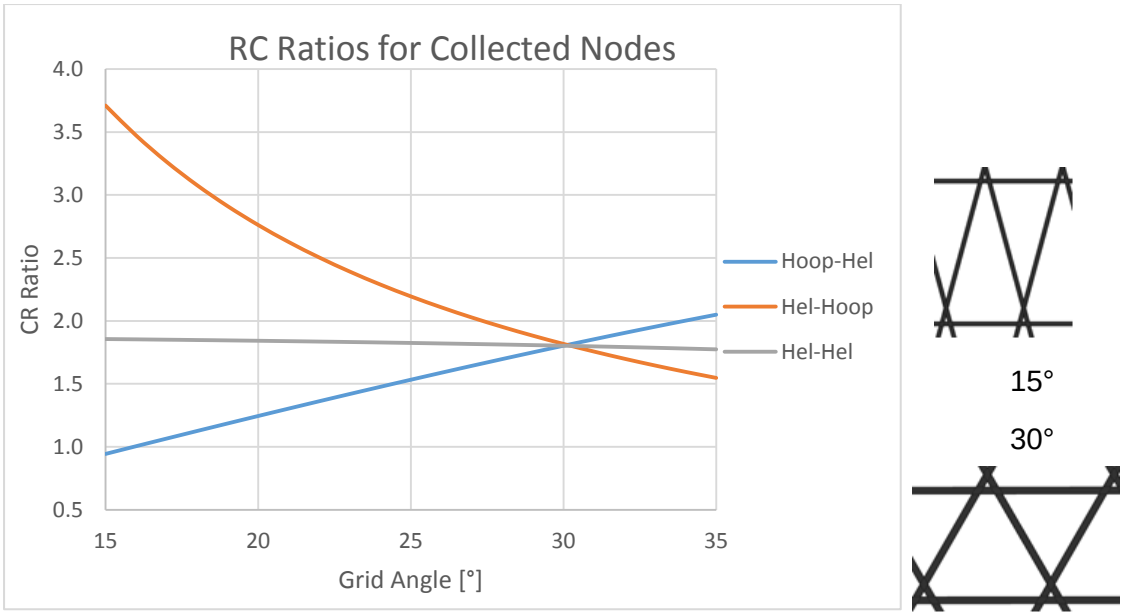

Figure 6-11 Compaction ratio for each transition in a collected node with associated lattice geometry

For practical grid angles, the RC ratio varies between 1.0 and 3.5. The chart shows there is a clear difference between the transition types at low grid angles, with the helical-hoop having a high compaction ratio compared to the other transition types. At 30° the ratios become equal as the lattice shape approaches equilateral triangles. Initial inspection shows that the ratios correlate with the average waviness severity measurements for the first manufactured sample with a 23° grid angle, with the ratio being proportional to waviness severity.

Irregular lattice designs may have higher ratios than those indicated on the chart. Additional elements that intersect with a node can significantly increase the ratio since the R_{avg} can become very small. Practically, R_{avg} should have a minimum values of 5 mm to prevent the ratio becoming unstable.

6.3 Correlation to Measurements from first panel

The manufactured panel was sectioned and 63 ply waviness measurements were taken. The lattice geometry was used to determine values for the three geometry factors for each measurement. The product of the factors is used to create an index that should be proportional to the measured waviness severity. The fit of the index can then be adjusted with coefficients. A fitted index is presented in Figure 6-12.

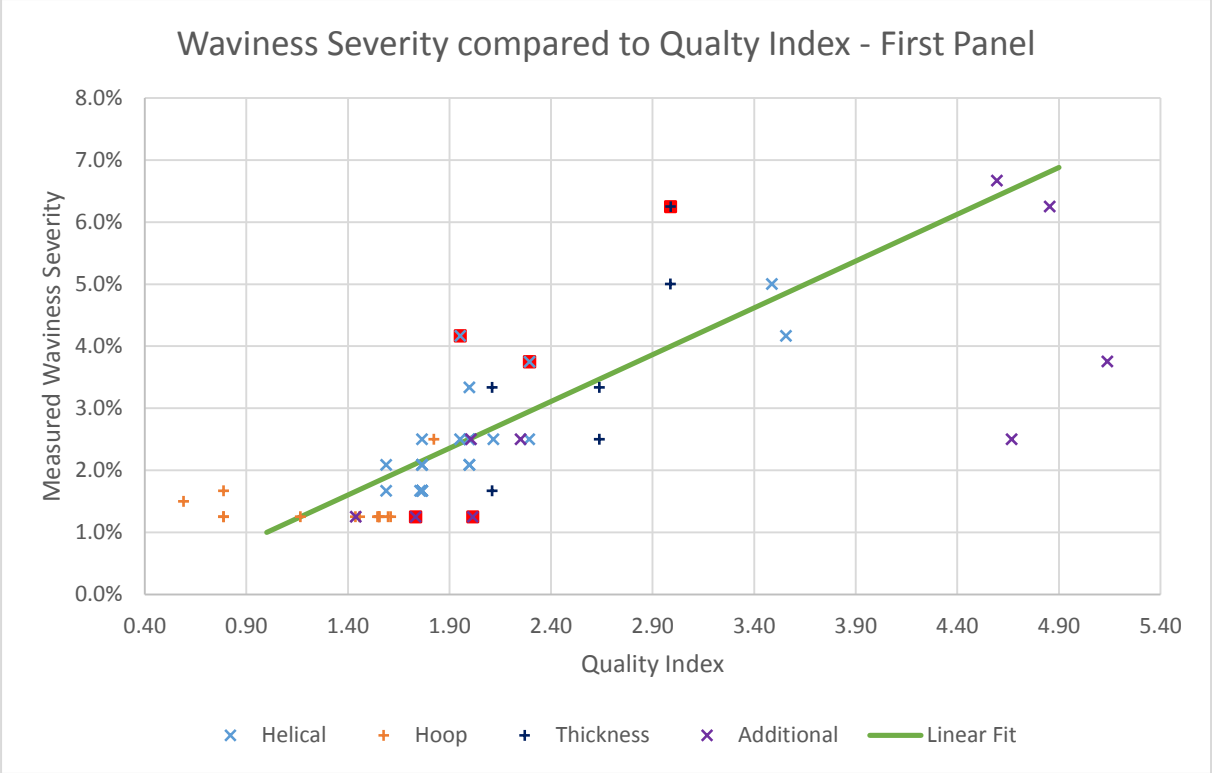

Figure 6-12 Fitted quality index with measured waviness for the first manufactured panel

The quality index is calculated as follows:

$$Quality = I \times N \times R^{0.5}$$

Where:

I is the Interleave Ratio
N is Node Ratio
R is the RC Compaction Ratio

Overall the index correlates to the measured ply waviness between index values of 1 and 5. If the index value is below 1, the transition quality tends to be good (less than 1.5%), though these points do not fit the linear regression. As discussed previously the *Helical* and *Hoop* ribs exhibit different waviness characteristics and this is largely described by the quality index. The thickness change ribs reduced the quality of transitions to varying degrees. This is less well described by the index but the measured waviness severity showed more scatter. This could be related to the higher waviness values associated with thickness change ribs. Additional ribs accounted for the greatest variation in measured waviness severity and most fit very well, showing less than 0.5 percentage points difference to the regression line.

Several outliers warrant discussion. Three points above the fit line (under predicted waviness severity) are highlighted red. These three points are noted because they have the same geometry as another part of the panel that had a different measured waviness severity. In other words, there is another point with the same index value that has a better linear fit. These points could represent the variations in manufacturing and measurement.

Below the fit line there are two points from the *Additional* set with high index values but low measured waviness. These relate to the half-height rib. It is thought that these are under predicted since the waviness severity is not normalised for the rib height. Adjustments are discussed in the following sections.

Two other points from the *Additional* set with low index values are highlighted red. These points relate to the additional ribs that did not terminate at nodes and produced very small cells. It was known that the silicone tooling in these cells was undersized due to interference with the un-compacted tows. The volume of silicone was approximately 2/3 of the ideal design volume. It is an interesting result that the transitions were measured with remarkably low waviness, in comparison to the general results as well as the predicted index value.

Clearly, the quality model presented does not quantitatively describe the case where silicone tooling is undersized, and these points should not be considered for the overall fit. However, qualitatively it is less surprising that the transition should have low waviness. With undersized tooling the transition behaviour is dominated by the consolidation force with other geometry effects being minimised. The node is simply compressed and the plies are less restricted in spreading out, resulting in balanced ply behaviour and low waviness. It should be noted that the node height was as designed, most likely because the rigidity of the caul plate did not permit additional consolidation. Further, these members also resulted in the formation of undesirable voids around the transition region that is also likely due to the insufficient compaction.

It has been discussed in section 5.4.5 that the angle change modifications resulted in different ply waviness characteristics. Furthermore it was decided that angle change modifications would not be explored further in this research. In order to maintain the clarity of the chart, angle modifications waviness measurements are presented and discussed in the appendix.

6.4 Design changes for second panel

Based on the lessons learned from the quality model, design changes that could realise lattice modifications without compromising the quality of the structure were investigated for the second manufactured panel.

Furthermore, it was decided to investigate methods that could improve the quality of a regular lattice structure, particularly for the helical-hoop transition that is predicted and found to have the highest waviness severity. If the model is found to be accurate, it could help to determine which lattice configurations can be manufactured with high quality.

This led to the lattice design described in section 5.1.4. As discussed, the tapered rib transitions maintain a balanced interleave ratio, that should contribute to minimal waviness. The tow width variation was included to investigate rib width changes that also maintained a unity interleave ratio. This line of thought was extended to include thin tows to produce thin ribs. Again, this should result in higher quality because it avoids an un-equal interleave.

The biased rib width transitions were included to provide data points to verify the correlation of interleave ratio at different values. Including discrete regions of different rib widths was done to investigate the effect of the node consolidation ratio.

Lastly the binary node geometry was included to investigate the accuracy of the RC ratio in describing significantly different geometries. This would help to characterise

generalised lattice designs if found to be accurate. Binary nodes are predicated to have a favourable RC ratio as shown in Figure 6-13.

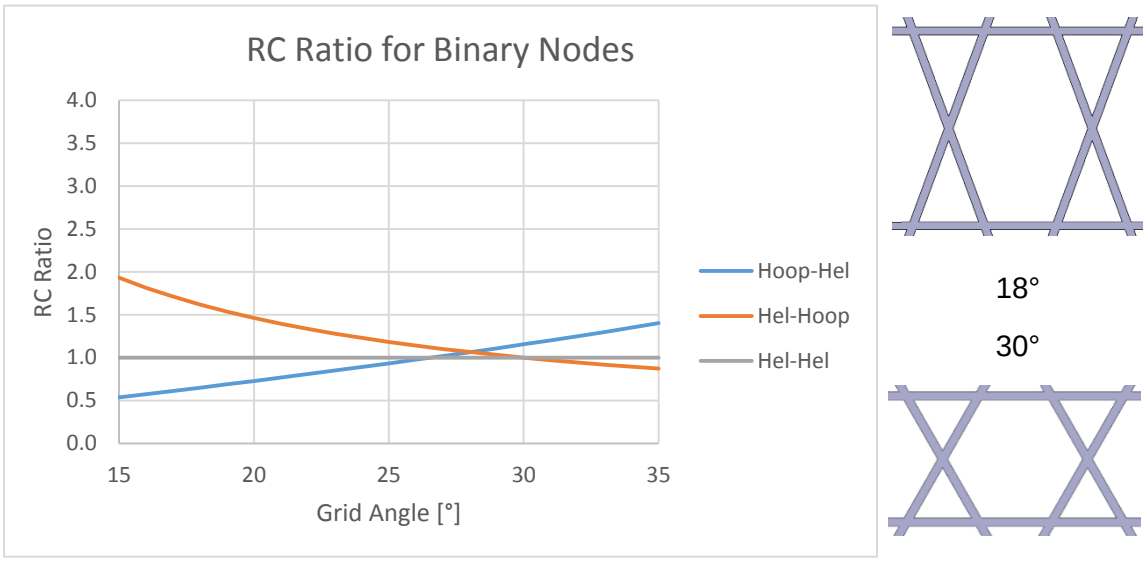

Figure 6-13 Compaction ratio for a binary node with associated lattice geometry

Binary nodes transitions also have three characteristic transition types, however the RC ratio for each transition type is lower for each transition for all grid angles compared to a collected node design presented in Figure 6-11. This is not surprising since the member lengths are all of a similar length. Overall this suggests that binary node designs will have a transition quality advantage for similar grid angles. As for collected nodes, the RC ratio is not sensitive to the helical rib spacing parameter.

6.5 Correlation to second panel

The second manufactured panel was sectioned and 30 ply waviness measurements were taken at transition regions. The geometry of each transition was used to determine the quality index based on the model calibrated from the first manufactured panel without any adjustments applied. The comparison of the data is presented in Figure 6-14.

Figure 6-14 Measured waviness severity from second panel compared to fit calibrated with the first manufactured panel data

Overall the correlation of the data to the fit is good with the *Binary Nodes* and *Ply Ratio* groups, with an 84% regression fit for these groups. The ply ratio group consists of measurements of transition regions where the interleave ratio is not equal, while the binary node group is consists of measurements from binary nodes.

The node ratio group consists of measurements of transition regions where the node consolidation is the independent variable. The *Node Ratio* and *Thin Ribs* groups are less consistent with the calibrated curve, with the waviness typically being over predicted. This means that the modifications generally resulted in lower waviness compared to the first panel, with the few high waviness severity measurements as expected for the *Ply Ratio* group.

Based on the findings from the first panel, it can be expected that the measured waviness values are above the fit due to the effect of greater rib height (15% increase in rib height). However, the slight change may not be apparent compared to the manufacturing and measurement tolerances.

Manufacturing and measurement tolerances generally seem to account for up to 0.5 p.p variation in measured waviness values for transitions with the same index. Tooling tolerance was greater for the second panel due to the novel manufacturing technique as discussed in 5.1.6. It is possible that the lattice geometry could be more sensitive to variations compared to the collected node samples due to the similar and shorter rib element lengths, particularly in the binary node region. Further investigation and manufacturing trials would be required to support this idea.

The discussion of outliers is concerned with two groups: *Thin Ribs* and *Node Ratio.* Specifically, the *Node Ratio* group shows 6 measurements that fall below the calibration curve, of which 4 are hoop-helical node transitions, highlighted in blue. Together they

have an average deviation of 1.2 p.p between the predicted and measured values. Meanwhile, the measurement for the *Thin Rib* group is shows a deviation of 1.5 p.p. Together, there is a systematic overestimation of the quality index for these transition regions, meaning that the measured quality is better than expected.

The commonalities for these two groups are that they are hoop ribs and that they form collected nodes. The RC ratio calculation for this transition could be too conservative because the one side of the principle member is very short, whereas the amount of expansion material available is in fact considerable. An improvement is discussed in the following section.

The other outlier of note is highlighted in red. As in the first panel, there is a discrepancy with two points with the same geometric values but with a measured waviness severity that differs by almost 1 percentage point. Again, this could be related to manufacturing tolerances or process that has not been accounted for.

Fewer measurements are recorded for the second panel but it should be noted that the measurements do correlate with the results from the C-scan. As an example, the *Thin Ribs* group only has one sample, but it can be expected that other measurements would have similar values based on the similar c-scan result pattern.

6.6 Discussion and Improvement

This section will discuss the outliers noted in the correlation of both panels and explore two changes to the geometric model which aim to improve the fit to measured values.

The first correction is related to the normalization of the calculated index in relation to the rib height. It is thought that the measured waviness amplitude does depend on the height of the rib, where taller ribs could have a greater waviness amplitude for a given arrangement and geometry. In the first panel the half height ribs showed a significant departure from the model, with an average absolute deviation from the model of *3.8* p.p below the curve. Since the rib heights are half the nominal value, it is proposed to scale the index value by a factor *0.5*. This would reduce the average absolute deviation to *0.5* p.p, which seems acceptably within the manufacturing and measurement tolerance to justify that the transition quality can be estimated using the process model.

Given the small sample of ribs and measurements with a significantly different height, it is difficult to extrapolate this effect without further trials. Therefore the correction is only applied to the above mentioned index values.

The second modification primarily concerns hoop rib transitions that typically have low measured waviness and are systematically over-predicted by the quality index. This was most clearly visible in the second panel, although the effect is also present in the first panel. As discussed, using a the described definition of the RC ratio to determine the member lengths could lead to a conservative index for hoop-helical transition regions due to one side of the intersection having an unrealistic short member. This is illustrated in Figure 6-15.

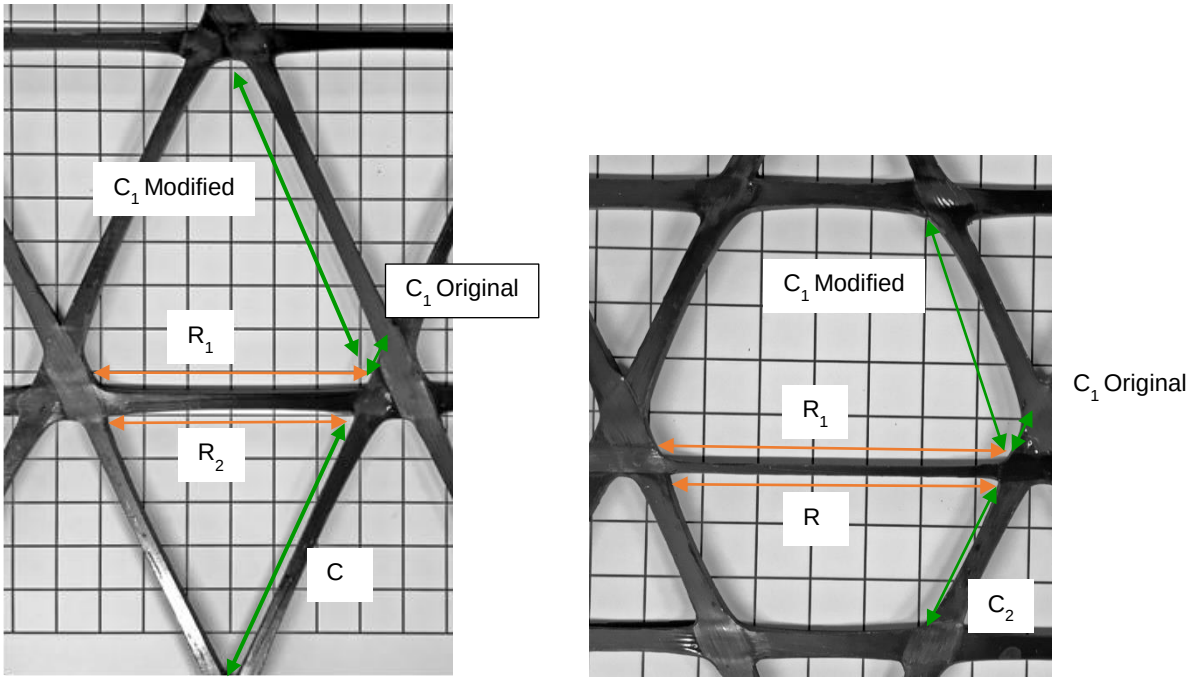

Figure 6-15 Modification to the RC ratio calculation for hoop-helical transitions

The diagram shows the intended modification to the measurement C_1 that would affect the RC ratio for hoop-helical transitions. The change increases the value of C_1 by effectively ignoring the short section next to the node and instead measuring the length up to the next hoop rib. This provides a more physical representation of the quantity of expansion tooling that will provide compaction force at the transition region, as is the intent of the RC ratio. The inclination of the new measurement vector to the compaction direction of the tows (perpendicular to the fibres) is approximately equal to the grid angle, and in this respect is the same as the original measurement vector. Therefore the measurement is consistent with the other vectors considered in the calculation of the ratio. Overall the RC ratio for these transitions is significantly improved with the modified measurement definition. No change is made to the other measurement vectors for the hoop-helical transition.

It is not valid to change the RC measurement definitions for other transitions types, although they also use short C values. Regarding the helical-helical transition, the short vector is valid to describe the small quantity expansion tooling and no other vector can be reasonably drawn to describe the behaviour on that side of the transition. Concerning the helical-hoop transition, one cannot draw another vector that better describes the quantity of expansion tool material that contributes to the rib compaction at the transition with a reasonable inclination angle. For practical lattice designs with grid angles less than 30°, no other modifications to the RC measurement definitions are required for the described transitions.

With the above changes implemented, as well as removing 4 outlier values (3 from the first panel, 1 from the second), the overall correlation for all points with the linear regression improved, as shown in Figure 6-16. The improvement is also tabulated in Table 13, showing the R^2 values.

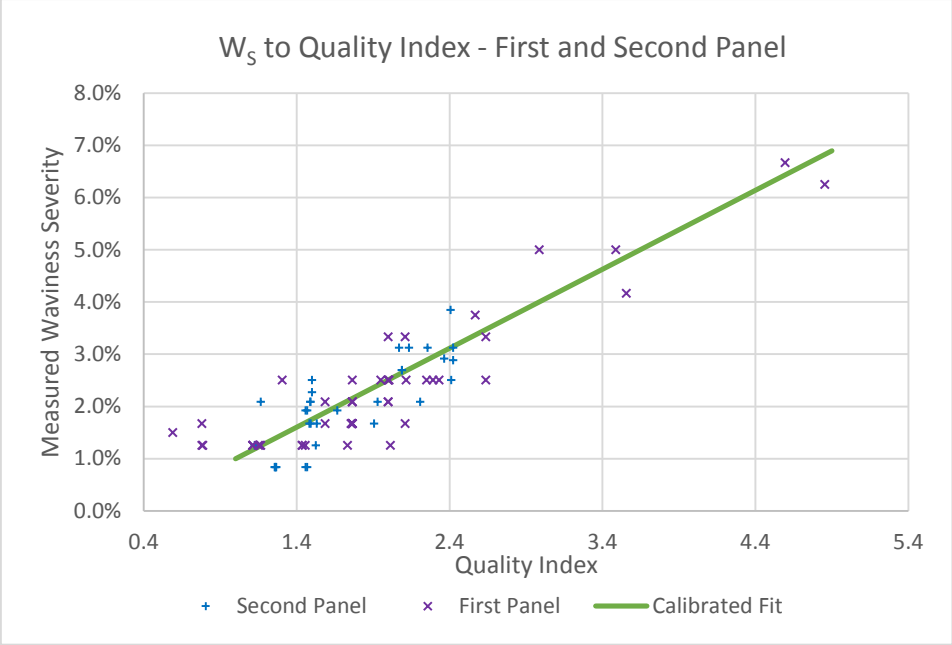

Figure 6-16 Measured waviness severity from both panels compared to calibrated fit

Table 13 Effect of modification to model fit

Panel		Regression Fit	
	# of Points	Original	Improved
First	60	47%	84%
Second	29	15%	76%

The two modifications have significantly improved the fit of the model to the measured values. The updated RC ratio chart for various grid angles is presented below:

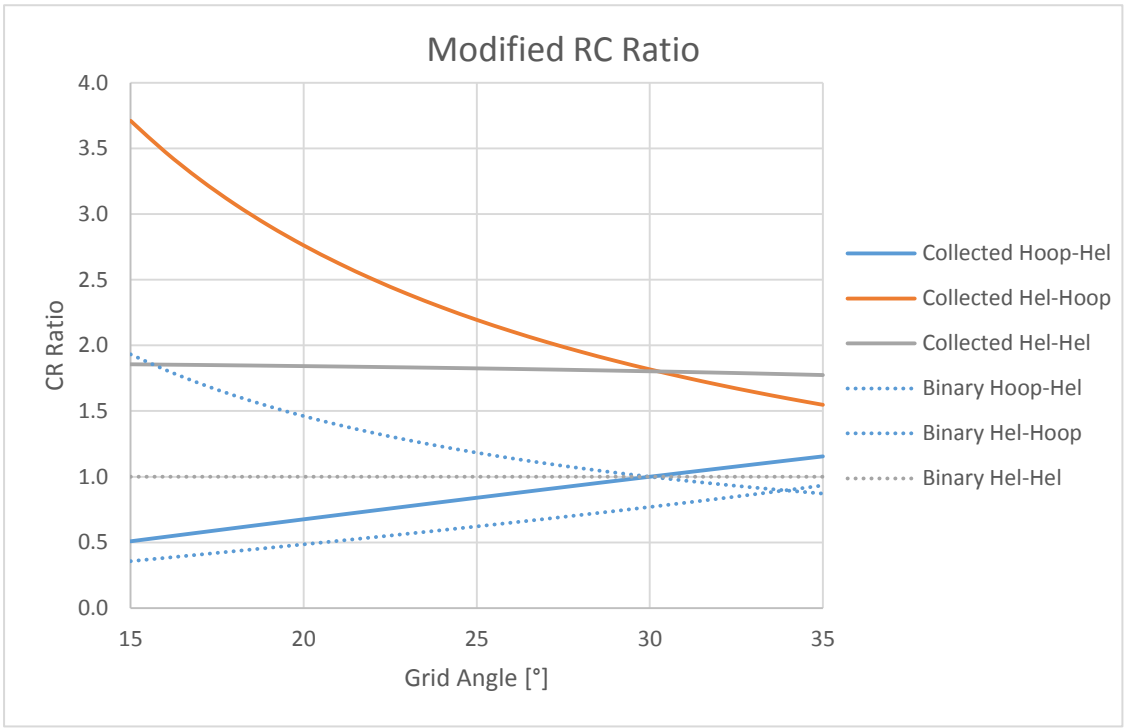

Figure 17 Modified compaction ratio for collected and binary nodes

The change from the previous RC ratio charts is simply that the Hoop-helical transition ratios are translated to a lower value. As expected, they show the lowest ratio compared to the other transitions.

Overall, the improvements demonstrate that a geometric model can be used to quantitatively describe the node transition quality of general lattice designs, including the various additional ribs and lattice arrangements with a reasonable accuracy. Furthermore, this result provides support for the process description and understanding that the model is based on.

6.7 Conclusions

The following conclusions can be drawn regarding the process model:

- A description is presented that physically describes the consolidation and compaction behavior at an intersection that results in ply waviness.
- A geometric model is able to estimate the transition quality of general lattice designs.
- The model can be calibrated based on a known manufacturing process.
- The model can be adjusted for some changes in rib height.
- The model accurately evaluates:
    - Collected nodes, differentiating between each rib element and transition type
    - Binary nodes, for each transition type
    - Additional members, whether they terminate at nodes or rib elements
- The model is calibrated for measured waviness severities from 1-7%, which covers the desirable and realistic range for practical lattice designs.
- The accuracy of the model is within the manufacturing and measurement tolerances that are typically 0.5 p.p of waviness severity for the studied lattices.
- A qualitative explanation is suggested for the quality of transitions in ribs that are under-compacted, but at the design rib height.

7. Closing Remarks

In the context of the presented research, the conclusions will be presented in terms of those relating to the research question followed by those relating to manufacturing and quality characterisation of pre-preg fibre-placed structures with expansion tooling. Following this, the future work suggested by the conclusions will be detailed.

7.1 Primary Conclusions

The goal of the research was to develop a model to understand the manufacturing process that could be used to determine which lattice designs, geometry and modification were manufactureable with high quality using the pre-preg fibre-placed manufacturing process.

The work provided is a first step towards answering the research question. This can be summarised with the following points:

- Significant differences of micro-structural quality at rib-node transitions of collected node lattice structures were identified, where collected nodes are defined as points where 3 rib elements intersect. These quality differences are characterised by ply-waviness, or lack of, and resin rich pockets.
- A novel description is proposed to explain the systematic deviation in lattice rib widths based on a concept of resin flow, where resin is migrating from rib sections and node overlaps to the transition region next to nodes. This local process is related to a pressure differences that arises due to disparate compaction response in rib-sections compared to node transitions.
- A description is proposed to explain the lack of variation in the manufactured rib height that is related to the stability of consolidation behaviour around the design height. This global process is related to the nearly incompressible behaviour of silicone tooling below the design height.
- A novel description is proposed to explain the observed transition quality patterns based on the consolidation and compaction in the region around a node. Generally, transition quality is compromised by asymmetric and unbalanced compaction behaviour that is largely determined by lattice geometry. Other factors identified are the interleaving of unequal numbers of tows at a node.
- The quality of rib-node transition regions can be quantitatively predicted with a model based on lattice geometry parameters. This has been demonstrated for the range of lattice structures studied, which represents the spectrum of lattice designs seen in literature.
- The model accurately predicts the effect rib width modifications and additional members have on the rib-node transition quality. These modifications are demonstrated to be incorporated into a regular lattice without compromising transition quality by following recommendations proposed by the model. FEM analysis indicates well incorporated modifications improve the performance of lattice designs around an attachment point.
- A minimum cell size is suggested based on the limits of tooling to provide adequate compaction. Exceeding this limit in small areas of the lattice results in the local formation of voids but is not associated with an increase in waviness, by a process that is explained in detail in the work.

7.2 Secondary Conclusions

The following conclusions are more specific conclusions from the research that are directly related to manufacturing or quality characterisation of the lattice designs in this research.

A basic framework for applying topology optimisation tools to composite lattice structures was presented. Results from an optimisation using isotropic materials are interpreted as composite lattice designs using 3 modification principles: rib width modification, rib angle modifications and additional rib members. Initial analysis suggests this optimisation process can improve the performance of the local lattice for a point load introduction.

7.2.1 Lattice dimensions

Overall the lattice dimensions in the two panels are consistent with the described equilibrium model of compaction and consolidation, with isolated exceptions that are thought to be the result of manufacturing variation. The model suggests that approximations in modelling and manufacture account for a small portion of deviations in lattice dimensions, while resin migration is responsible for larger systematic variations in lattice dimensions, particularly rib width. Other conclusions are:

- Collected node types are associated with thinner relative rib widths that suggest the requirement for resin is greater compared to binary nodes.
- Rib widths are sensitive to local lattice geometry, element lengths and node types.
- Measurements of lattice dimensions should be evaluated within the context of the lattice design, process and in comparison to local cells.
- A requirement for void free manufacturing could determine limits for lattice design with regard to minimum rib element length for a given node type.

Two methods were explored for silicone tooling design that are based on the ideal cell shape that is reduced with a specified scaling factor. The first method reduces the shape volume by scaling in all directions, such that the in-plane and out-of-plane dimensions are reduced. The second method only scales in the in-plane direction. This method reduced the minimum cell size that will allow the silicone tool to be inserted at room temperature. It is an important conclusion to note that no deviation in lattice geometry is associated with the different scaling methods employed.

7.2.2 Quality evaluation and quality model

Several non-destructive testing techniques were evaluated in this research. The value of the techniques is in supporting dimensional measurements of the lattice structure. Isolated deviations in lattice dimensions, such as rib width and node height, indicate issues with the manufacturing process, while consistent and small deviations can be expected based on the explanation presented above. Generally:

- C-scan techniques were not able to distinguish the presence of typical voids in transition regions as the voids coincide with other transition effects that are highlighted in the c-scan results.
- There is a qualitative correlation between the c-scan results and micro-sections in terms of waviness. Larger regions of highlights in the c-scan were related to regions with extended ply waviness.
- Isolated highlights in a c-scan can indicate issues in the manufacturing process, such as in the mid-section of a rib.

- CT scan techniques are effective in evaluating the quality of transition regions for small samples, for example a node. Their applicability as a qualification procedure for practical lattice structures is questionable.

The quantitative model is based on the compaction and consolidation process description and is calibrated for the specific material and process in this research. The model showed good correlation with tow widths of 1/8” as well as 1/4”. Regarding the range of applicability of lattice geometry, the quantitative quality model has demonstrated a good correlation for the following geometry parameters.

- Rib height: 3 – 7 mm
- Rib width: 3.5 to 5.2 mm
- Grid angles 23° & 25°
- Binary nodes and collected nodes
- Nodes with additional rib elements

This list does not represent qualitative limit for the model, as it may well provide quality insights for lattice structures that fall outside the above limits.

7.3 Recommendations

7.3.1 Mechanical Testing

The research has identified distinct differences in node transition quality related to ply waviness in the transition region. Understanding precisely how node transition quality effects the mechanical properties of lattice structures would be valuable knowledge for design and analysis, allowing the initial performance of variations and modifications of lattice geometry to be estimated without costly mechanical test campaigns. Detailed design analysis will still require mechanical test verification, but lattice modifications or novel geometries can be explored with some confidence regarding the performance of node transitions.

Current testing has found that the performance of node transitions is less than predicted by material strength specifications alone, and the reduced performance must be accounted for in model predictions. Now that it is possible to explore novel lattice geometry that has not been mechanically tested and predict the quality of the node transitions in terms of ply waviness, it is desirable to know to what extent reduced ply waviness can improve the mechanical performance of node transitions. If increased ply waviness is predicted, it is desirable to know to what extent the performance might be reduced.

It is therefore recommended to manufacture node transitions with specified and predictable waviness and to use these samples for a test campaign that aims to correlate measured waviness to a mechanical performance knockdown.

One method to produce samples with predictable waviness severity is proposed in Figure 7-1. This sample uses the geometry to manipulate the RC ratio, as this was identified as a primary factor in predicting transition quality. The sample consists of cells with an increasing aspect ratio that is predicted to result in incrementally increasing ply waviness. The range of waviness severity of the node transitions is estimated to be from 1.0% - 4.0%, that qualitatively represents the “best” to “worst” of practical lattice designs.

Such a sample could be separated into 11 individual ribs with a transition region. Each rib will have a known transition quality, either by prediction or by measurement. Each

sample can be mechanically tested, most likely in pure compression as lattice structures are generally loaded in this scenario.

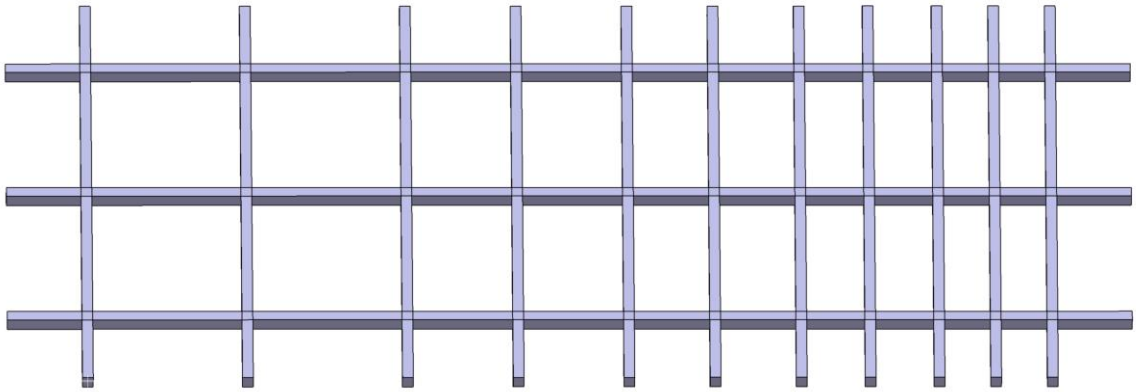

Figure 7-1 Proposed waviness severity sample

Due to the ply waviness being concentrated in the centre of the rib section, it is expected that samples with high waviness will also have a high sensitivity to bending effects. Bending loads will strain the fibres on the upper and lower surface of the rib, where the fibres are practically straight, whereas the distorted fibres are near the neutral axis and experience less strain due to bending. Thus the difference in performance between a node transition with high waviness compared to a transition with low waviness will be less apparent when loaded in bending because the distorted fibres will be lightly loaded. Therefore care must be taken to ensure that samples are loaded in uniform compression to obtain an accurate compression knockdown factor.

Another point to investigate is the effect of rib height and the impact on measured waviness severity. It has been seen in this research that ribs with half height had a corresponding waviness severity that was half the predicted. Again the question is how does this observation affect the mechanical performance of the transition. If the performance reduction is proportional to the absolute waviness severity measurement, then ribs with a lower height should experience less strength knockdown. However this means that increasing rib height would result in diminishing improvements in strength, as high ribs are expected to have greater absolute ply waviness that is associated with performance reduction. Conversely, if the knockdown is proportional to the waviness severity normalised for the rib height, higher or lower rib height should not have a significant effect on performance reduction at node transitions.

A test campaign would require lattice samples with the same geometry and different rib heights to be manufactured. Having rib height as the independent variable would identify the relationship to mechanical performance reduction.

7.3.2 Modelling

With a better understanding of the node transition micro-structure, efforts to model the transition region with improved detail could be explored in order to improve the accuracy of simulations for complex loading scenarios. The transition region is currently modelled with a reduced material stiffness to simulate the fibre distortion and resin pockets with reduced mechanical properties. This method has demonstrated a good correlation for tests with in-plane axial loading. Besides its good correlation, this modelling modification can be implemented with minimal effort.

However, due to the simplicity of the approximation, it could be over-conservative when predicting the rib behaviour under bending loads. In bending, the maximum normal stress occurs at the extreme fibre from the neutral axis i.e. the upper and lower surface of the rib. Characterisation of the transition region shows that fibre distortion is concentrated in the centre of the rib section, while the plies near the upper and lower surfaces have negligible distortion. Therefore it is expected that the performance under bending loads will be closer to a rib with nominal properties compared to a rib under axial loading. These changes are illustrated in Figure 7-2.

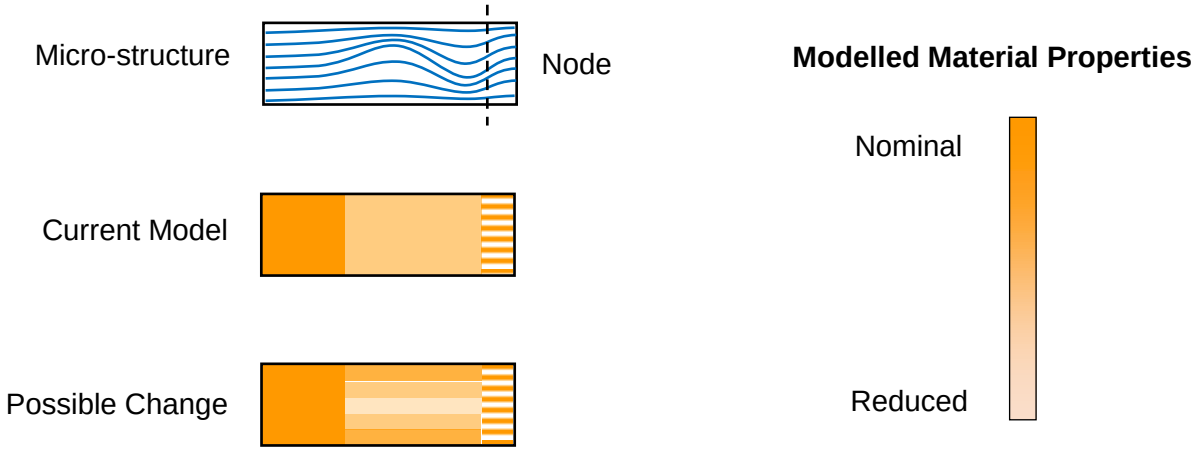

Figure 7-2 Microstructure compared to modelling method

The presented modelling change will approximate the observed waviness distribution with layered properties that represent the degree of fibre distortion. In the centre of the rib, the material properties are significantly reduced, more so than in the current modelling approach. Moving from the centre to the outer surface of the rib, the material properties increase linearly to near nominal material properties, that is greater than the current modelling approach. This modelling method should be applicable for axial loading as well as bending loads, and provide a more accurate simulation for combined loading situations.

The magnitude of material property reduction should be proportional to the waviness severity noted in the ribs. High waviness severity would be related to a greater reduction at the centre of the rib, while the outer fibres are essentially unchanged, as noted in the transition characterisation. Mechanical testing of manufactured samples with measured waviness severity would be required to correlate the property reduction of the proposed model. The level of detail and quantization of layers is to be determined depending on the results of mechanical testing.

7.3.3 Material and Process

The quality model has been calibrated for this particular material and process, as described in section 5.1.2. Different composite materials may exhibit node transition behaviour to a greater or lesser extent than is measured with the current material and process. Changes in the transition behaviour would result in a systematic deviation in quality predictions if they are not accounted for with modification to the quality model.

Material factors that could change the characteristic behaviour could be the initial tow thickness, resin viscosity and flow behaviour and other factors. Further work could investigate how these material parameters influence the expected transition behaviour, and account for the changes with modifications to the quality model.

Factors related to the process that could influence transition behaviour could be autoclave pressure. Out-of-autoclave processes that use a significantly lower pressure are an attractive process due to an associated reduction in manufacturing cost. However their applicability for composite lattice structures is currently unknown. Trials that compare the two processes could be evaluated, among other metrics, on the manufactured transition quality using the framework and characterisation techniques presented in this research. A brief exploration of possible outcomes is presented in the following paragraphs.

Regarding node consolidation, the vacuum applied to the completed layup is known to consolidate the nodes to near the design height. It is reasonable to expect that at elevated temperatures, resin flow would allow further consolidation under vacuum pressure alone. Silicone tooling would be slightly resized to account for the lower applied pressure. Therefore consolidating nodes to the design height should be possible.

However rib compaction is a local effect that is essential in transporting resin to transition areas to provide a void free structure. It is not clear how lower processing pressures will impact this process. It is not clear what pressure is required to compact rib sections and form them to the design dimension. Insufficient compaction of rib sections would result in widespread formation of voids, not only at node transitions but also in rib mid-sections.

If vacuum bag pressure is sufficient to compact and form the ribs, there remains a question about resin migration from rib sections to the node transition regions. These regions have a requirement for resin to fill spaces where plies diverge and interleave at the node. Without sufficient resin migration, it can be expected that these node transition regions would show a high propensity for void formation. Such void formation would reduce the mechanical properties of the node transition and compromise the strength of the lattice structure such that the performance is not comparable to structures manufactured with the current process.

Furthermore, a reduction in the ability for resin to migrate could also limit the lattice designs that are currently manufactureable with low void content. It has been shown that short rib sections may limit the manufactureable lattice geometry based on the resin reservoir-sink relationship and migration process. If the migration process is hindered by the reduced processing pressure, the manufactureable geometry may become more restricted in terms of minimum rib lengths.

Exploration of the out-of-autoclave requires samples to be manufactured and evaluated.

8. References

[1] V. V. Vasiliev, V. A. Barynin and A. F. Razin, "Anisogrid composite lattice structures - Development and aerospace applications," *Composite Structures,* no. 94, pp. 1117-1127, 2012.

[2] L. Pavlov, B. Smeets and S. M. Simonian, "Optimization of a composite lattice satelllite central cylinder structure using an efficient semi-automated approach," in *57th AIAA/ASCE/AHS/ASC Structures, Structural Dynamics, and Materials Conference*, San Diego, California, 2016.

[3] S. M. Huybrechts, S. E. Hahn and T. E. Meink, "Grid stiffened structures: a survey of fabrication, analysis and design methods," *Proceedings of the 12th International Conference on Composite Materials,* 1999.

[4] B. J. Smeets, "Development of an in-panel attachment method for fibre-placed composite lattice and grid-stiffened structures," Delft University of Technology, Delft, NED, 2016.

[5] P. M. Wegner, J. E. Higgins and B. P. van West, "Application of Advanced Grid-Stiffened Structures Technology to the Minotaur Payload Fairing," in *43rd AIAA/ASME/ASCE/AHS/ASC Structures, Structural Dynamics and Materials Conference*, Denver, Colorado, 2002.

[6] K. Terashima, T. Kamita, G. Kimura, T. Aoki and T. Yokozeki, "Experimental and analytical study of composite lattice struture for future Japanese launchers," in *The 19th International Conference on Composite Materials*, Montreal, Canada, 2013.

[7] G. Totaro and F. De Nicola, "Recent advance on design and manufacturing of composite anisogrid structures for space launchers," *Acta Astronautica,* vol. 81, pp. 570-577, 2012.

[8] B. Smeets, T. Papenhuijzen, L. Pavlov and M. Koot, "Development logic and building block testing approach for pre-preg lattice satellite central cylinder applications," in *ECSSMET 2018*, Noordwijk, Netherlands, 2018.

[9] Y. O. Bakhvalov, S. A. Petrokovsky, V. P. Polynovsky and A. F. Rasin, "Composite irregular lattice shells designing for space applications," in *17th International Conference of Composite Materials*, Edinburgh, 2009.

[10] J. Higgins and B. van West, "NDE and repair of damaged Minotour fairing shell," *Composite Structures,* vol. 67, pp. 189-195, 2005.

[11] S. M. Huybrecht, T. E. Meink, P. M. Wegner and J. M. Ganley, "Manufacturing theory for advanced grid stiffened structures," *Composites Part A: Applied Science and Manufacturing,* no. p.155-161, 2002.

[12] V. Michaud, S. Sequeria Tavaresm, A. Sigg, S. Lavanchy and J.-A. E. Manson, "Low pressure processing of high fiber content composites," *The 8th International Conference on Flow Processes in Composite Materials (FPCM8),* 2006.

[13] T. G. Gutowski, Advanced Composites Manufacturing, New York: John Wiley & Sons Inc., 1997.

[14] M. S. Rouhi, M. Wysochi and R. Larsson, "Modelling of coupled dual-scale flow-deformation processes in composites manufacturing," *Composites: Part A,* Vols. p 108-116, 2013.

[15] F. De Nicola and G. Totaro, "Recent advance on design and manufacturing of composite anisogrid structures for space launchers," in *62nd International Astronautical Congress*, Cape Town, 2011.

[16] A. S. Wronski and T. V. Parry, "Compressive failure and kinking in uniaxially aligned fibre composites," *Journal of Material Science,* no. 3656-3662, 1982.

[17] S. Horrmann, A. Adumitroaie, C. Viechtbauer and M. Schagerl, "The effect of fibre waviness on the fatigue life of CFRP materials," *International Journal of Fatigue,* vol. 90, pp. 139-147, 2016.

[18] J. Wang, K. D. Potter, K. Hazra and M. R. Wisnom, "Experimental fabrication and characterization of out-of-plane fiber waviness in continious fiber-reinforced composites," *Composite Materials,* vol. 46, no. 17, pp. 2041-2053, 2012.

[19] W. J. Christian, F. A. DiazDelaO, K. Atherton and E. A. Patterson, "An experimental study on the manufacture and characterization of in-plane fibre-waviness defects in composites," *Royal Society Open Science,* 2018.

[20] S. N. Nair, A. Dasari, C. Y. Yue and S. Narasimalu, "Failure behavior of unidirectional composites under compression loading: Effect of fibre waviness," *Materials,* vol. 10, no. 8, p. 909, 2017.

[21] R. Smith, L. Nelson, M. Mienczakowski and R. Challis, "Automated non-destructive analysis and advanced 3d defect characterisation from ultrasonic scans of composites," in *ICCM International Conferences on Composite Materials*, 2009.

[22] J. Martin-Herrero and C. Germain, "Microstructure reconstruction of fibrous C/C composites from X-ray microtomography," *Carbon,* vol. 45, pp. 1242-1253, 2007.

[23] S. Huybrechts and S. W. Tsai, "Analysis and behaviour of grid structures," *Composites Science and Technology,* vol. 56, pp. 1001-1015, 1996.

[24] Y.-L. Hsu, M.-S. Hsu and C.-T. Chen, "Interpreting results from topology optimization using density contours," *Computers & Structures,* no. 1049-1058, 2001.

[25] R. Smith, Z. Qureshi, R. Scaife and H. El-Dessouky, "Limitations of procesing carbon fibre reinforced plastic/polymer material using automated fibre placement technology," *Journal of Reinforced Plastics and Composites,* vol. 35, no. 21, pp. 1527-1542, 2016.

[26] I. te Kloeze, "Design, analysis, manufacturing and testing of load introductions in grid-stiffened composite structures," Delft University of Technology, Deflt, NED, 2015.

[27] S. W. Yurgartis, "Measurement of small angle fibre misalignments in continious fiber

composites," *Composites Science and Technology,* vol. 30, pp. 279-293, 1987.

[28] J. Schindelin and I. &. F. E. e. a. Arganda-Carreras, "Fiji: an open-source platform for biologial-image analysis," *Nature methods,* vol. 9, no. 7, pp. 676-682, 2019.

[29] V. V. Vasiliev, V. A. Barynin and A. F. Rasin, "Anisogrid lattice structures - survey of development and application," *Composite Strucutres,* vol. 54, pp. 361-370, 2001.

[30] O. Sigmund, "A 99 line topology optimization code written in Matlab," *Struct Multidisc Optim,* Vols. 120-127, 2001.

[31] Y. Bakhvalov, V. Molochev, S. Petrokovskii, V. A. Barynin, V. Vasiliev and A. F. Razin, "Proton-M composite interstage structures; design, manufacture and performance.," *European Conference for Aerospace Structures (EUCASS),* 2005.

Appendix A. Modelling of rubber expansion

An initial investigation was conducted to determine what could be learned about how the rubber tooling interacts with the composite to determine the cured cell shape. Since it was known that the manufactured cell shapes deviated from the ideal design, it was thought that the compaction provided by the silicone expansion tooling could be responsible. In this respect, it was desired to find the contact pressure the tooling should be exerting on the composite material at the point of cure.

Several assumptions were made:

Firstly, an assumption was made that the manufactured shape did not change significantly from the point of curing. The formation of the cell shape should occur at the cure temperature (180°C), while the cell shape is measured at room temperature. The difference is thought to be negligible given the low thermal expansion coefficient (CTE) of the composite. As stated on the data sheet, the fibre has a CTE of -1.1×10^{-6}/°C.

Secondly, assumptions of the silicone material properties were made since properties were not precisely known. The CTE of the material was measured in laboratory conditions and can be considered accurate. However, the elastic modulus was estimated based on the manufacture specified Shore hardness value. The value used was 3.2 MPa that is in the typical range for silicone rubber. A Poisson ratio of 0.45 was used for modelling the rubber as a representative value for this class of material as no measurement was made.

Lastly, it was assumed in the simulations that the volume and size of the silicone material was equal to the ideal designed manufactured volume. In retrospect, it was found that during the high temperature post-cure of silicone tools (a process that is carried out before the tools are used with the composite), the mass of the silicone tools reduced by approximately 2%. Although the manufacturing process is known to be accurate, the shape, volume or properties of the tools may have changed as a result of the post-cure operation.

The investigation involved detailed measurements of the manufactured cell geometry such that a representative surface could be created in FEM software. The rigid surface represents the cured composite part. Measurement of the bounded volume of this surface showed that it was approximately 2.6% smaller than the design. The silicone tooling at room temperature was simulated to expand a uniform temperature load such that it filled the space bounded by the rigid surface. Frictionless contact was defined between the silicone and the rigid surface, while the silicone tool was constrained in the out of plane directions to simulate the caul plates. This is illustrated in Figure 8-1.

The illustration shows the rigid surface in grey and the silicone material in green. A hybrid formulation element was used to model the silicone material due to its high Poisson ratio. A linear static solver was used. The output shows the contact pressure results for the silicone tool. The sides of the tool are in contact with the composite material surface, while the surface of the tool is in contact with the caul plate.

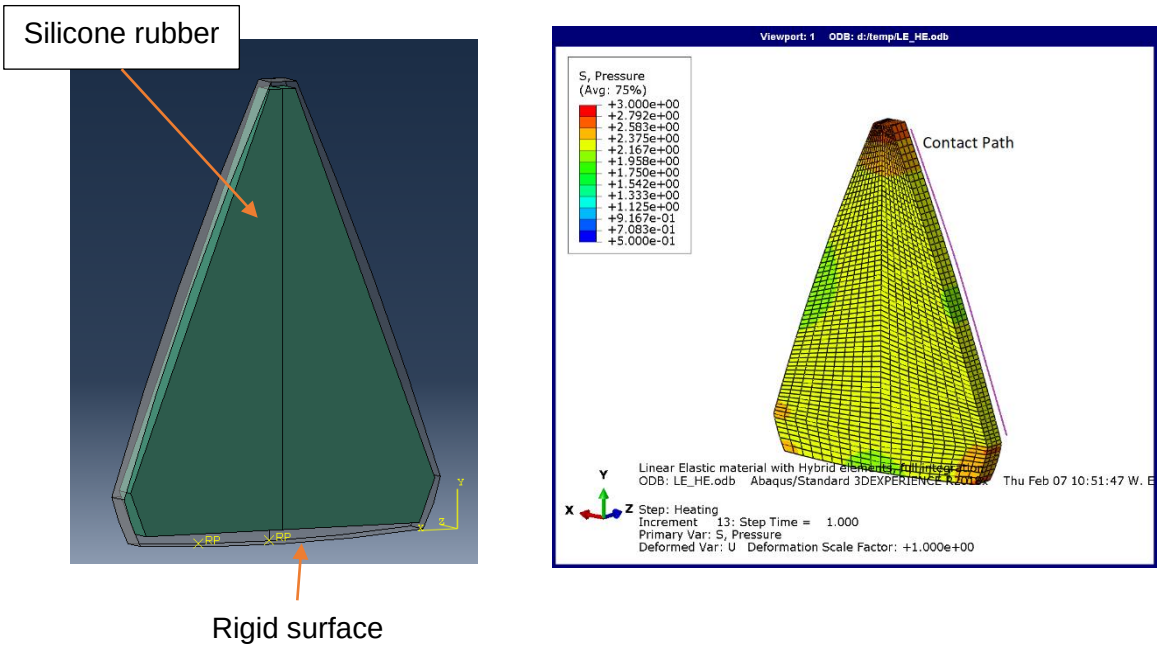

Figure 8-1 Modelling of silicone tool expanding into the cured composite shape, at room temperature (left) and at the cure temperature (right)

The contact pressure ranges from a maximum value of approximately 28 Bar in the corners of the block, to the minimum value of approximately 15 Bar at the mid-point of the edge. These pressures are significantly higher than the differential pressure of the autoclave and vacuum bag (6.8 Bar), due to the fact that the cured cell volume is approximately 2.6% smaller than the design volume used to determine the tooling size. Again, the assumption for the tooling sizing calculation is that the expansion tool and composite are at the hydrostatic pressure this is clearly contradicted by the above result.

One explanation for the discrepancy, that the contact pressure should be so much greater than the autoclave pressure, is related to the mass loss during post cure. Had the expansion tool been smaller in volume, the resulting pressure at high temperature would be less and therefore closer to the processing conditions. This is a systematic deviation. Other deviations could come from incorrect application of material properties, such as the elastic stiffness being set too high. The measurement of the cell size could also have a small influence. These factors would provide a result with a lower pressure that, on initial inspection, seems a more acceptable description of expansion tool-composite interaction.

On the other hand, it may not be necessary to strictly adhere to the processing conditions to validate the result. The autoclave pressure must be resisted by the silicone tooling and composite part to satisfy equilibrium in a global sense, but local pressures in once cell do not need to be equal. Comparison to the adjacent cell shows that the pressure results are significantly lower, with an average of 7.7 Bar, and could be lower still given the factors mentioned above. In this case, the global pressure condition is satisfied with local variations. This explanation is rather unsatisfying and rests a great deal on measurements of limited precision. The conclusions it leads to are also difficult to validate.

Though the magnitude of pressure may be disputed, the variation along the contact surface is rather clear. The lowest pressure is at the middle of the rib section and the

highest pressure is at the node regions. In other words the composite material experiences a pressure gradient that should result in encourage resin to flow towards the mid-rib. Since the opposite is true, another process must be active as presented in section 5.2.1.

Appendix B. CT scan images

This section presents detail of the scanning and additional CT images from the investigated node. Some explanation will be made of the visible features.

The scans were performed on a *phoenix nanotom® m*, which required around 1.5 hours to expose 1440 images. The results were filtered to reduce beam hardening effects with the accompanying software suite (a value of 8 was used). The montage images and directionality analysis was performed using the open source software Fiji (Fiji Is Just ImageJ).

The directionality analysis in this research was done on a stack of images in the transition area of investigation. A stack is an ordered sequence of images that represent a part of the scanned material. Of course directionality analysis can be performed on a single image. The analysis is based on the Fast Fourier Transform of the image that transforms the spatial image into the frequency domain. Details of the analysis tool are available on the ImageJ distribution [28].

The example of the directionality analysis is shown with a cropped section from the conducted CT scan, Figure 8-2.

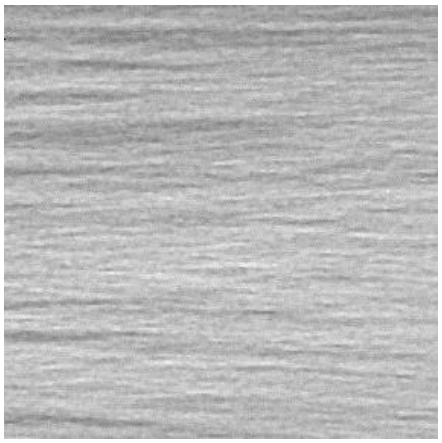

Figure 8-2 Sample of fibres visible in CT scan

The output from the directionality analysis is shown in Figure 8-3. The analysis shows the orientation map for identified directionality in the stack of images. A results table with several statistics is presented based on the fitted directionality distribution. The fit is based on a Gaussian function. The results table lists the average directionality (in degrees) that represents the peak of the Gaussian distribution, also listed is the standard deviation of the distribution.

Observations of the orientation map suggest that the analysis tool is biased to image patterns in the centre of the image. Therefore comparisons of ply directionality must be made with images that relate to similar locations i.e. making like-to-like comparisons. Analysis of different locations or image sizes may influence the result of image directionality analysis.

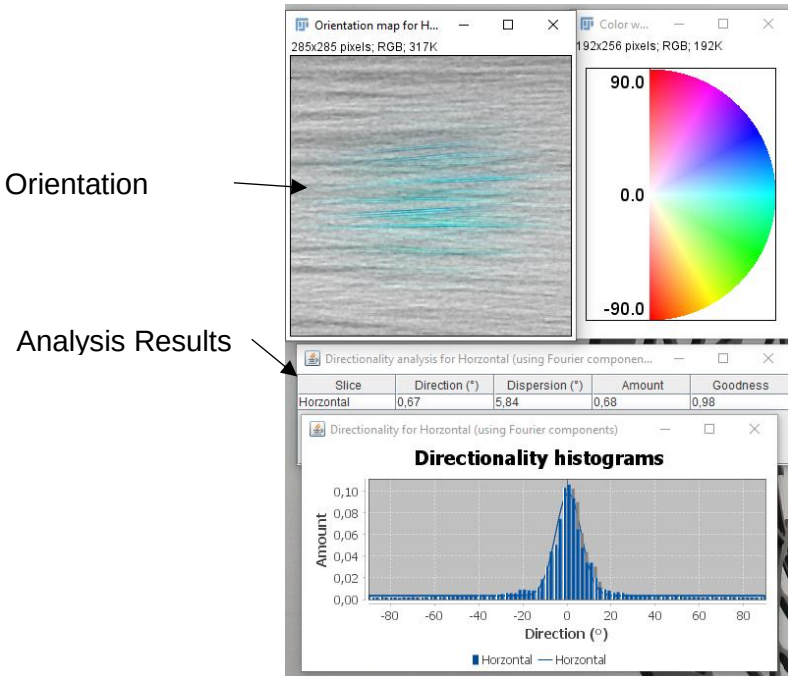

Figure 8-3 Output of Fiji directionality analysis for an example image

The first image shows the development of waviness though the angle change rib, Figure 8-4.

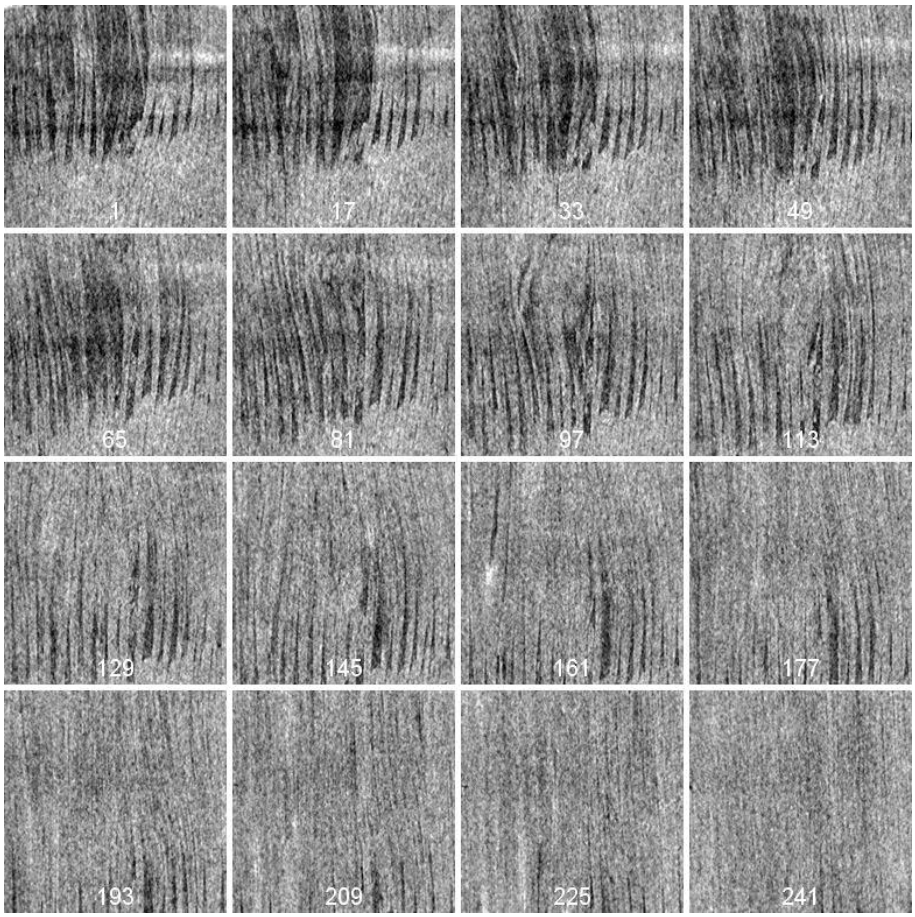

Figure 8-4 Montage of images showing waviness development in an angle change rib (helical-helical)

The first images are taken from the “inside” of the angle change, where the fibres were initially bucked and creased in the layup stage. Some of this effect seems to remain in the cured sample, as the ply directionality shows more distortion compared to the later images in the sequence. These later images show improved alignment, as can be seen in the image directionality analysis in Figure 8-5.

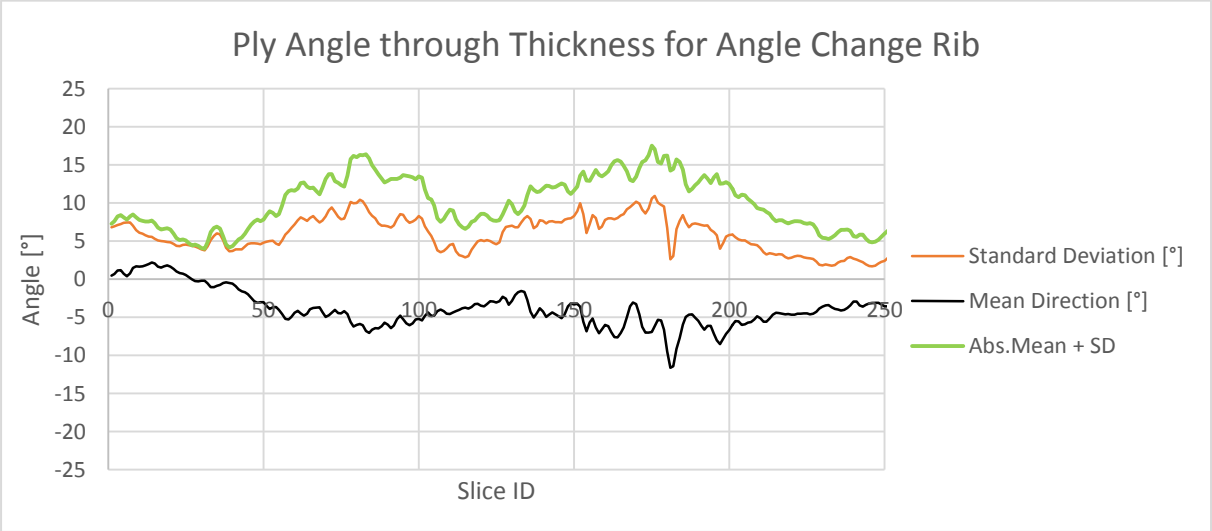

Figure 8-5 Waviness development for angle change rib

The ply directionality chart in Figure 8-5 shows a progression through the width of the rib that is dissimilar from unmodified rib-node transitions. The distinct peaks in the *Absolute Mean + Standard Deviation* marker are uniquely observed in this transition with an angle change, and demonstrate the change in ply directionality at different section points.

Below in Figure 8-6 is the montage for the corresponding un-modified rib, without the angle change, and shows the clear difference in waviness development. The nominal rib has a visually smoother transition region in comparison to the above, as well as the general sense. The ply direction distortion is low. This is also visible in the ply angle chart presented in Figure 8-7.

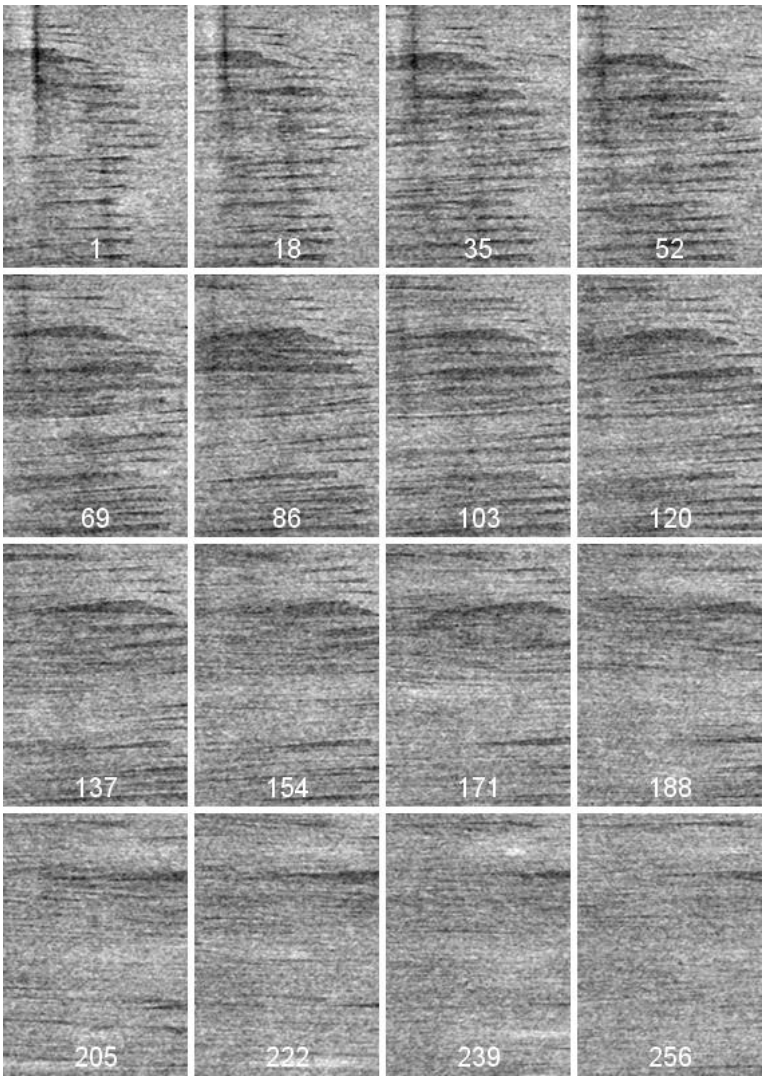

Figure 8-6 Montage of images showing waviness development through an unmodified helical-helical rib

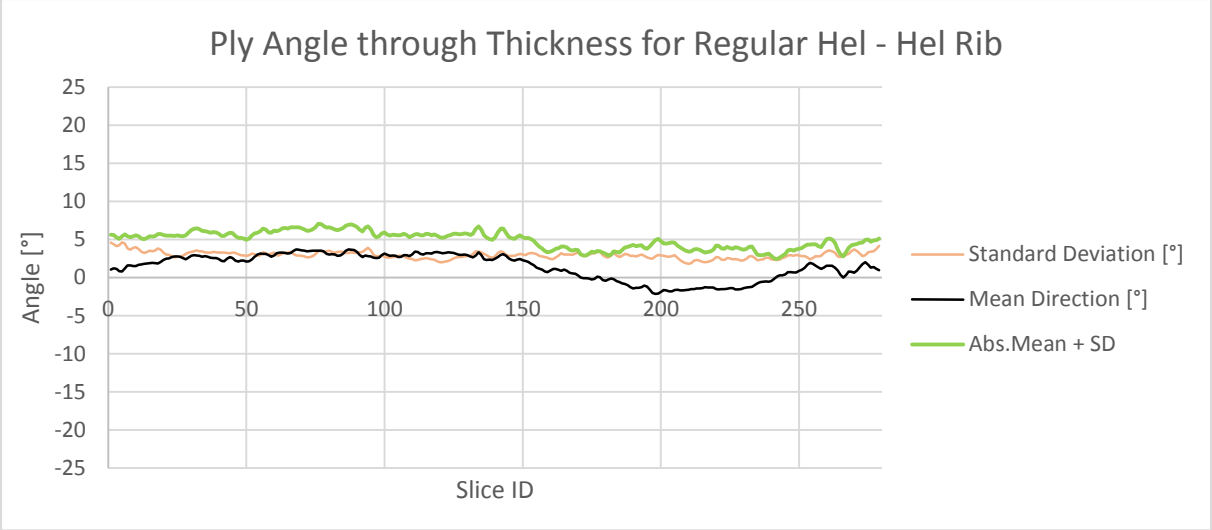

Figure 8-7 Waviness development for a helical-helical rib

The hoop to helical rib transition was generally observed to have the lowest waviness in micro-section analysis. The CT image montage in Figure 8-8 demonstrates this as the image progression shows very low ply distortion in the transition region.

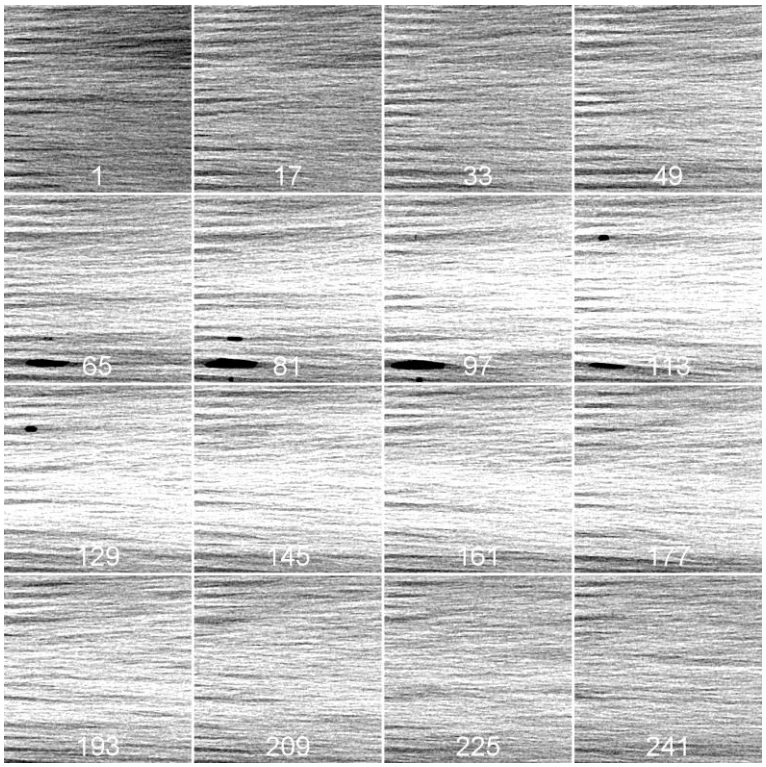

Figure 8-8 Montage of images showing the waviness development through a hoop-helical rib

The voids in the transition area are conspicuous and remarkable in that they did not appear in any of the other rib-node transitions for the sampled node. CT analysis and the above montage supports general observations of the high propensity of void formation in the hoop-helical node transition. Regarding the ply waviness, the image directionality analysis supports the observations of the montage. The chart in Figure 8-8 shows the mean direction is well aligned to the axis of the rib, while there is a fairly constant standard deviation through the width of the rib.

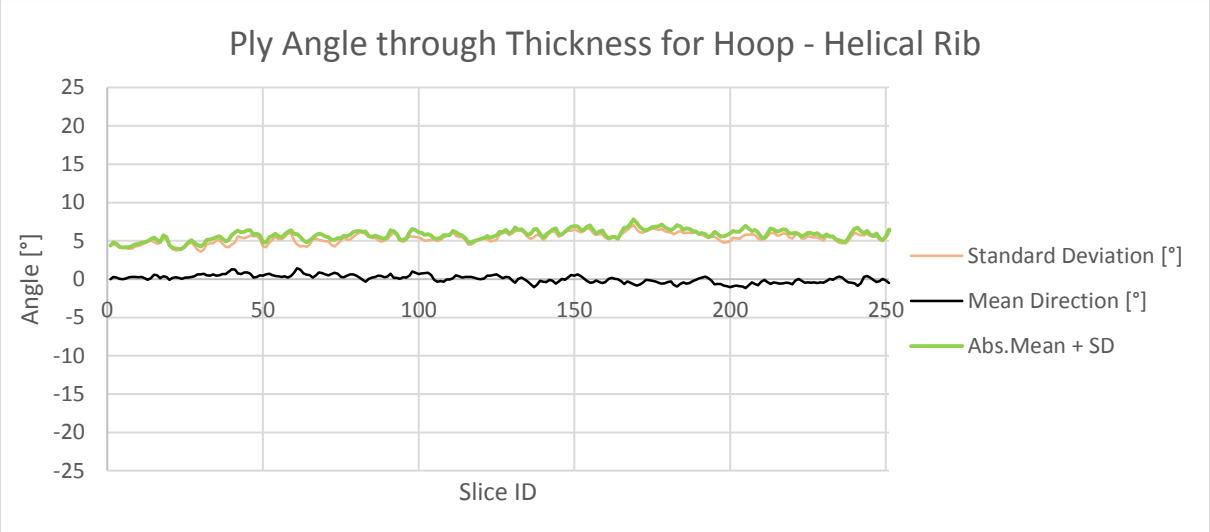

Figure 8-9 Waviness development for a hoop-helical rib

The last image montage in Figure 8-10 is from the thickness change rib, where additional tows were included to produce a rib member with increased width. Overall the distribution and quality of the rib is similar to the corresponding helical-hoop rib presented in Figure 5-28

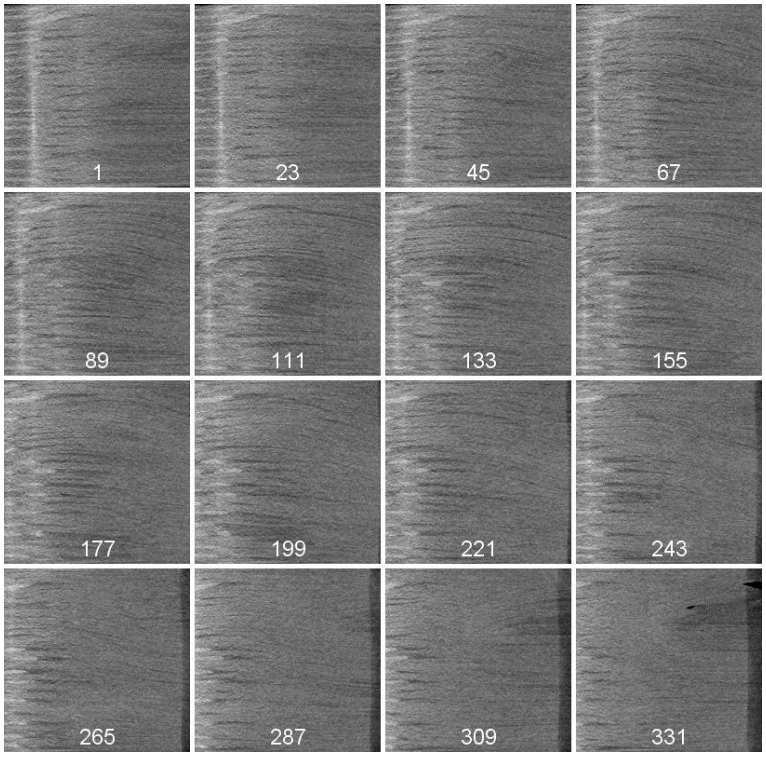

Figure 8-10 Montage of images showing the waviness development of a thickness change rib

The ply directionality chart for the thickness change rib in Figure 8-11 shows a regular development of ply angle deviation through the width of the rib. The magnitude of the deviation in the centre of the width for this sample is comparable to unmodified rib.

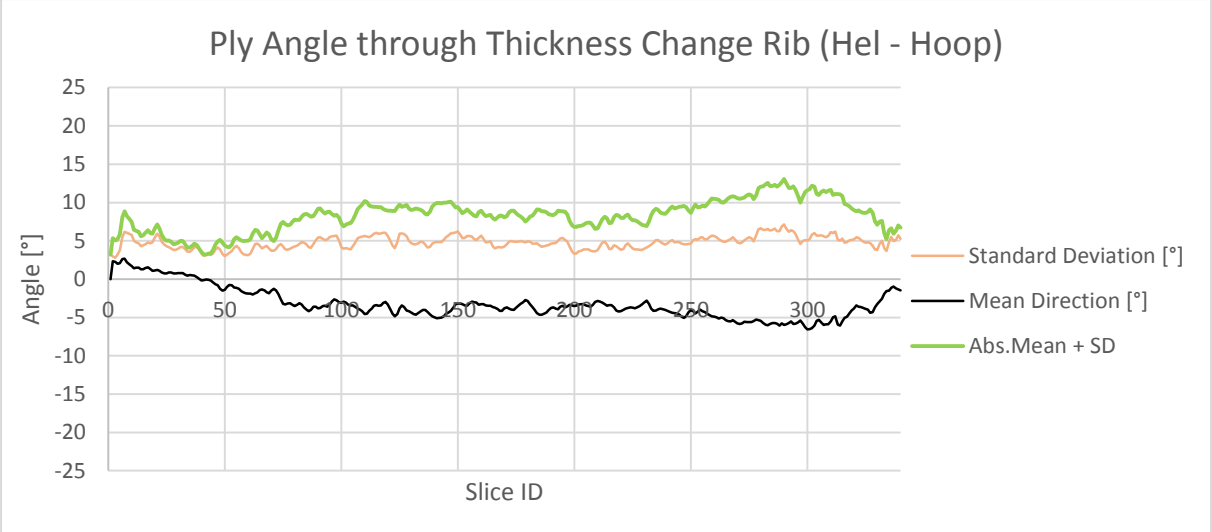

Figure 8-11 Waviness development for a thickness change rib (helical-hoop)

Overall the CT image montages provide a qualitative comparison of the transitions regions that represent the lattice structure manufactured in the first trial. They also highlight the effect lattice modifications have on the transition region by direct comparison for angle changes and rib width changes. The ply directionality analysis provides support for the qualitative conclusions by quantifying the general ply directionality. Comparisons of the magnitude and distribution of the ply angle deviations between the rib-node transitions are used to explain general behaviour in the manufactured panel.

Appendix C. Angle Change Modifications

As discussed in the modelling section, the angle change ribs displayed a different waviness characteristic that could not be described within the model the measurements are presented in this section and discussed.

From the first manufactured panel that explored modified rib angles, 8 measurements were made for angle modifications between 2.5 and 10°.These measurements are presented in Figure 8-12 and are segmented by transition type. For comparison, the average values for a *helical-hoop* and a *helical-helical* transition are 2.9% and 1.9% respectively.

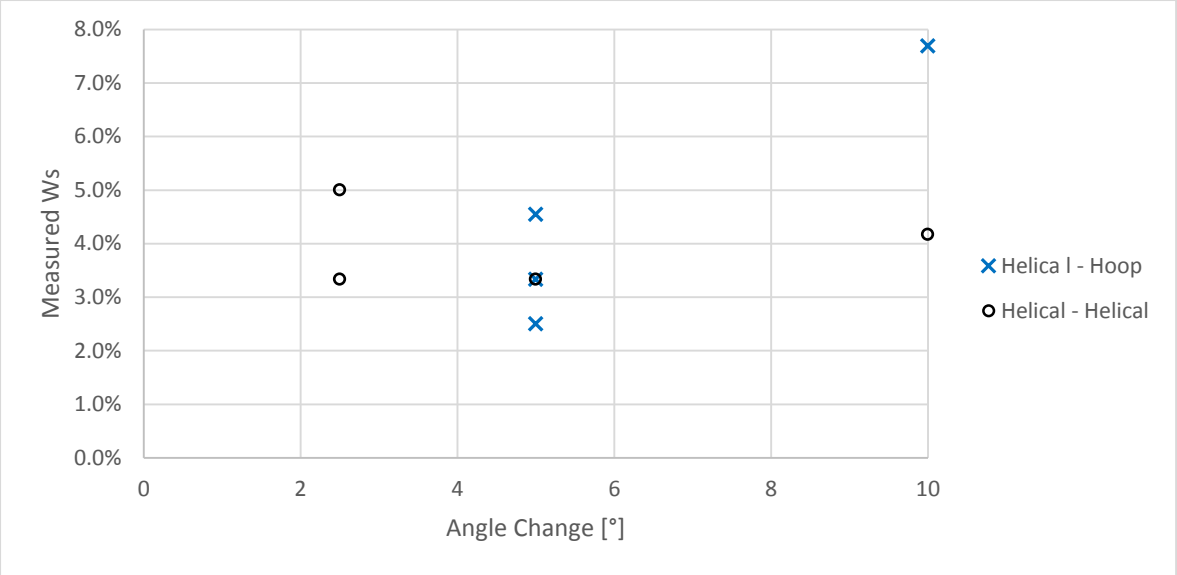

Figure 8-12 Angle change transition waviness measurements

The chart shows a poor correlation since there are several values with the same apparent angle change that were measured to have significantly different waviness severity (>2p.p.). Segmenting the results by transition type does not improve the correlation. Other factors are believed to influence the observed transition waviness that were not accounted for.

One such factor is the section location. The waviness characteristics of angle change ribs were not known at the time the sections were made, so section location was not controlled or accounted for. Moreover, the section technique does not provide fine control over the location of the section cut, given the thickness of the blade. Comparing sections in the same relative location could provide results that result in a clearer correlation.

However the asymmetric nature of the angle change ribs may exclude the possibility of describing a node transition with a single waviness severity value in the way that regular ribs can be. Characterisation of angle change ribs might require additional factors to describe the degree of imbalance, location or relative severity compared to an unmodified transition.

Precise understanding of the ply behaviour in angle change ribs is lacking given that only one sample has been investigated with a CT scan. Furthermore, conclusions based on this analysis may only be valid for the particular method used to produce these angle modifications, described in section 5.1.5. A different manufacturing technique could

eliminate the wrinkling of tows during layup that is likely related to the observed transition quality.

Appendix D. Rib Compaction Ratio

The node consolidation ratio is related to the rib width compaction ratio. Starting from the equation used to calculate the number of required tows as presented in section 5.

$$T_n = \frac{R_W R_H}{T_A} = \frac{R_W R_H}{T_W T_t}$$

Where the tow area T_A is simply the product of the tow width T_W and the tow thickness T_t, as shown below.

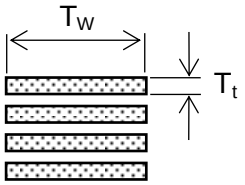

Tow Layup

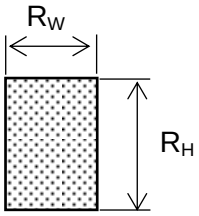

Consolidated rib

The rib compaction ratio is defined as the width of the rib compared to the tow width:

$$C_R = \frac{R_W}{T_W}$$

Using the equation for the node consolidation ratio:

$$C_n = \frac{2 \cdot T_N T_t}{R_H}$$

And substituting the equation to calculate the number of tows:

$$C_n = \frac{2 \cdot R_W R_H T_t}{R_H T_W T_t}$$

Cancelling like terms:

$$C_n = 2\frac{R_H}{T_W} = 2C_R$$

Thus the node consolidation ratio is twice the rib compaction ratio.

Appendix E. Micro-section Analysis Results

The helical ribs are marked in purple and are numbered separately from the hoop ribs marked in blue. The Additional ribs are marked in orange. Each node is sequentially numbered starting from the top left, working along the hoop rib.

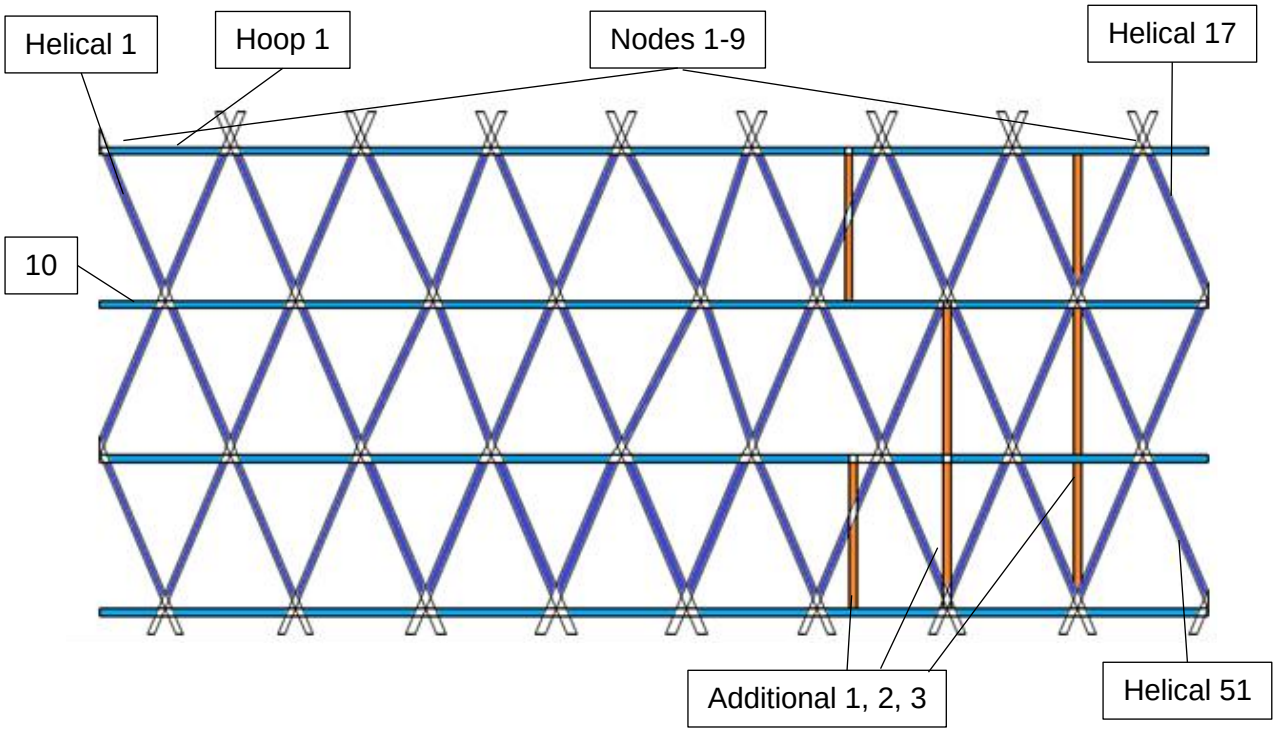

Figure 8-13 First panel naming convention

The table is divided in 4 sections as explained in the diagram below:

Identification			Index Calculation								Measured Waviness			Comparison to Model	

Identification is based on the rib and node number, using the convention described in Figure 8-13. Index calculations are based on the geometric factors identified in section 6.2 . The measured waviness is based on the model described in section 5.4.1. Lastly, the comparison is made to the linear fit parameters shown in Figure 6-16. The fit shown the predicted values and then the difference in percentage points from the measured waviness severity.

Table 14 Micro-section analysis for the first manufactured panel with Quality index values

	Rib #	Node #	α	C1	C2	R1	R2	*R*	*I*	*N*	Index	A [mm]	L [mm]	W_S	*Fit*	*+/- p.p.*
Helical	*19*	*20*	0	36	5	36	39	1.8	1.0	1.3	**1.76**	0.5	15	**1.7%**	*2%*	*0.5*
	37	*29*	0	36	5	36	39	1.8	1.0	1.2	**1.59**	0.5	12	**2.1%**	*2%*	*-0.2*
	2	*10*	0	36	5	36	39	1.8	1.0	1.3	**1.76**	0.5	12	**2.1%**	*2%*	*0.1*
	2	*2*	0	28	3	36	39	2.4	1.0	1.3	**2.00**	0.5	10	**2.5%**	*3%*	*0.0*
	7	*4*	0	28	3	36	39	2.4	1.0	1.3	**2.00**	0.5	12	**2.1%**	*3%*	*0.4*
	7	*13*	0	36	5	36	39	1.8	1.0	1.3	**1.76**	0.8	15	**2.5%**	*2%*	*-0.3*
	3	*2*	0	28	3	36	39	2.4	1.0	1.3	**2.00**	0.5	12	**2.1%**	*3%*	*0.4*
	3	*11*	0	36	5	36	39	1.8	1.0	1.3	**1.76**	0.5	12	**2.1%**	*2%*	*0.1*
	24	*13*	0	28	3	36	39	2.4	1.0	1.3	**2.00**	1.0	15	**3.3%**	*3%*	*-0.8*
	24	*22*	0	36	5	36	39	1.8	1.0	1.3	**1.76**	0.5	12	**2.1%**	*2%*	*0.1*
	25	*13*	0	28	5	36	39	2.3	1.0	1.3	**1.95**	1.0	12	**4.2%**	*2%*	*-1.7*
	25	*23*	0	36	5	36	39	1.8	1.0	1.3	**1.76**	0.5	15	**1.7%**	*2%*	*0.5*
	30	*16*	0	5	5	36	39	7.5	1.0	1.3	**3.56**	1.0	12	**4.2%**	*5%*	*0.7*
	30	*25*	0	36	5	36	39	1.8	1.0	1.3	**1.76**	0.5	15	**1.7%**	*2%*	*0.5*
	32	*17*	0	28	5	36	39	2.3	1.0	1.3	**1.95**	0.8	15	**2.5%**	*2%*	*-0.1*
	32	*26*	0	36	5	36	39	1.8	1.0	1.3	**1.76**	0.5	15	**1.7%**	*2%*	*0.5*
	33	*17*	0	5	36	36	39	1.8	1.0	1.3	**1.76**	0.5	15	**1.7%**	*2%*	*0.5*
	33	*27*	0	36	5	36	39	1.8	1.0	1.3	**1.76**	0.5	15	**1.7%**	*2%*	*0.5*
	36	*28*	0	36	5	36	39	1.8	1.0	1.2	**1.59**	0.5	15	**1.7%**	*2%*	*0.2*
	40	*30*	0	36	5	36	39	1.8	1.0	1.6	**2.12**	0.5	10	**2.5%**	*3%*	*0.2*
	42	*31*	0	36	5	36	39	1.8	1.0	1.7	**2.29**	0.5	10	**2.5%**	*3%*	*0.5*
	47	*25*	0	28	3	36	39	2.4	1.0	1.3	**2.00**	0.5	10	**2.5%**	*3%*	*0.0*
	47	*34*	0	5	5	33	39	7.2	1.0	1.3	**3.49**	1.0	10	**5.0%**	*5%*	*-0.2*
	41	*31*	0	36	5	36	39	1.8	1.0	1.7	**2.29**	0.8	10	**3.8%**	*3%*	*-0.8*
Hoop	*23*	*23*	0	43	36	30	28	0.7	1.0	1.3	**1.11**	0.3	10	**1.3%**	*1%*	*-0.1*
	25	*25a*	0	31	40	13	13	0.4	1.0	1.3	**0.79**	0.3	10	**1.3%**	*1%*	*-0.6*
	12	*11*	0	36	43	30	32	0.8	1.0	1.3	**1.15**	0.3	10	**1.3%**	*1%*	*0.0*
	11	*10*	0	43	36	30	28	0.7	1.0	1.3	**1.11**	0.3	10	**1.3%**	*1%*	*-0.1*
	11	*11*	0	43	36	30	28	0.7	1.0	1.3	**1.11**	0.3	10	**1.3%**	*1%*	*-0.1*
	12	*12*	0	43	36	30	28	0.7	1.0	1.3	**1.11**	0.3	10	**1.3%**	*1%*	*-0.1*
	6	*6a*	0	21	15	22	22	1.2	1.0	1.3	**1.44**	0.3	10	**1.3%**	*2%*	*0.4*
	16	*15a*	0	10	25	22	22	1.3	1.0	1.3	**1.46**	0.3	10	**1.3%**	*2%*	*0.4*
	16	*15*	0	36	5	28	5	0.8	1.0	1.3	**1.17**	0.3	10	**1.3%**	*1%*	*0.0*
	26	*26a*	0	31	40	13	13	0.4	1.0	1.0	**0.59**	0.3	10	**1.5%**	*0%*	*-1.1*
	16	*16*	0	43	36	23	28	0.6	1.0	1.6	**1.31**	0.5	10	**2.5%**	*1%*	*-1.0*
	25	*25*	0	65	84	28	26	0.4	1.0	1.3	**0.78**	0.3	10	**1.3%**	*1%*	*-0.6*
	25	*26*	0	65	84	28	26	0.4	1.0	1.3	**0.78**	0.5	15	**1.7%**	*1%*	*-1.0*
	27	*27*	0	36	43	31	32	0.8	1.0	1.3	**1.16**	0.3	10	**1.3%**	*1%*	*0.0*
Thickness	*37*	*20*	0	28	3	36	39	2.4	1.1	1.2	**2.11**	1.0	15	**3.3%**	*3%*	*-0.7*
	36	*20*	0	28	3	36	39	2.4	1.1	1.2	**2.11**	0.5	15	**1.7%**	*3%*	*1.0*
	39	*21*	0	28	3	36	39	2.4	1.2	1.4	**2.64**	0.5	10	**2.5%**	*3%*	*1.0*

	Rib #	Node #	α	C1	C2	R1	R2	*R*	*I*	*N*	Index	A [mm]	L [mm]	W_S	*Fit*	*+/- p.p.*
	40	*22*	0	28	3	36	39	2.4	1.2	1.4	**2.64**	1.0	15	**3.3%**	*3%*	*0.1*
	42	*23*	0	28	3	36	39	2.4	1.3	1.5	**2.99**	1.0	10	**5.0%**	*4%*	*-1.0*
	41	*22*	0	28	3	36	39	2.4	1.3	1.5	**2.99**	1.5	12	**6.3%**	*4%*	*-2.3*
Additional	*Add2*	*16*	0	5	5	40	40	8.0	1.0	1.6	**4.60**	2.0	15	**6.7%**	*6%*	*-0.2*
	Add2	*25a*	0	13	13	31	31	2.4	1.0	1.3	**2.01**	0.5	10	**2.5%**	*3%*	*0.0*
	Add2	*25a*	0	13	13	40	40	3.0	1.0	1.3	**2.25**	0.8	15	**2.5%**	*3%*	*0.4*
	Add2	*34*	0	5	5	31	31	6.2	1.0	2.0	**4.86**	1.5	12	**6.3%**	*7%*	*0.6*
	Add1		0	5	15	26	22	2.4	1.0	1.3	**2.01**	0.3	10	**1.3%**	*3%*	*1.3*
	Add1	*33a*	0	22	5	26	22	1.8	1.0	1.3	**1.73**	0.3	10	**1.3%**	*2%*	*0.9*
	Add3	*26a*	0	14	14	21	40	2.2	1.0	1.0	**1.44**	0.3	10	**1.3%**	*2%*	*0.4*
	Add3	*17*	0	4	4	40	40	10.0	1.0	1.6	**2.57**	0.8	10	**3.8%**	*3%*	*-0.4*
	Add3	*17*	0	4	4	33	33	8.3	1.0	1.6	**2.33**	0.5	10	**2.5%**	*3%*	*0.5*
Angle	*26*	*14*	10	28	3	36	39	2.4	1.0	1.3	**2.00**	2.0	13	**7.7%**	*3%*	*-5.2*
	6	*12*	5	36	5	36	39	1.8	1.0	1.3	**1.76**	1.0	15	**3.3%**	*2%*	*-1.2*
	6	*4*	5	28	3	36	39	2.4	1.0	1.3	**2.00**	0.5	10	**2.5%**	*3%*	*0.0*
	22	*12*	5	28	3	36	39	2.4	1.0	1.3	**2.00**	1.5	10	**7.5%**	*3%*	*-5.0*
	9	*5*	0	28	3	36	39	2.4	1.0	1.3	**2.00**	1.0	12	**4.2%**	*3%*	*-1.7*
	9	*14*	10	36	5	36	39	1.8	1.0	1.3	**1.76**	1.0	12	**4.2%**	*2%*	*-2.0*
	23	*12*	5	28	3	36	39	2.4	1.0	1.3	**2.00**	1.0	11	**4.5%**	*3%*	*-2.0*
	23	*22*	2.5	36	5	36	39	1.8	1.0	1.3	**1.76**	1.0	15	**3.3%**	*2%*	*-1.2*
	22	*21*	2.5	36	5	36	39	1.8	1.0	1.3	**1.76**	1.0	10	**5.0%**	*2%*	*-2.8*
	26	*23*	5	36	5	36	39	1.8	1.0	1.3	**1.76**	0.5	10	**2.5%**	*2%*	*-0.3*
Outliers	*12*	*15*	0	5	36	17	20	0.9	1.0	1.3	**1.23**	0.5	12	**2.1%**	*1%*	*-0.7*
	12	*7*	0	4	4	11	18	3.7	1.0	1.3	**2.50**	1.0	12	**4.2%**	*3%*	*-0.9*

The naming convention for the second panel is as described in the figure below.

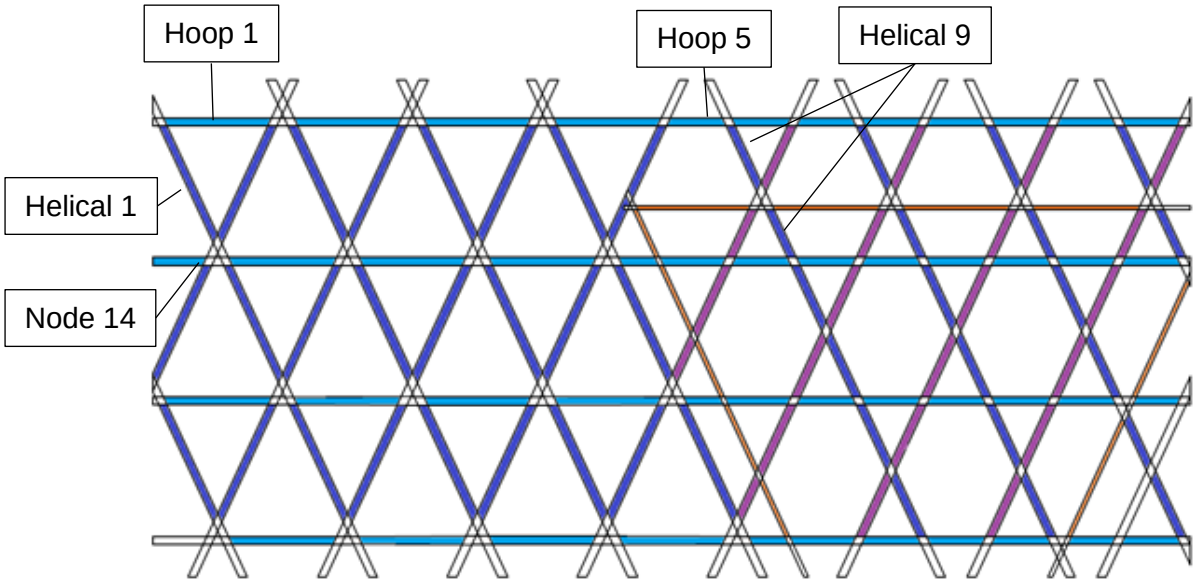

Figure 8-14 Second panel naming convention

	Rib	Node	C 1	C 2	R 1	R 2	*R*	*I*	*N*	Index	A [mm]	L [mm]	W_S	*Fit*	*+/- p.p.*
Binary	*12*	*T*	61	5	32	31	1.0	1.0	1.5	**1.64**	0.5	12	**2.1%**	*2.0%*	*-0.1*
Nodes	*12*	*20*	35	30	32	31	1.0	1.0	1.5	**1.65**	0.5	10	**2.5%**	*2.0%*	*-0.5*
	11	*T*	61	5	32	31	1.0	1.0	1.5	**1.64**	0.5	12	**2.1%**	*2.0%*	*-0.1*
	11	*21*	35	30	32	31	1.0	1.0	1.5	**1.65**	0.5	11	**2.3%**	*2.0%*	*-0.3*
	30	*-*	36	43	36	43	1.0	1.0	1.5	**1.68**	0.3	10	**1.3%**	*2.0%*	*0.8*
	30	*36*	31	6	36	55	2.4	1.0	1.5	**2.63**	0.5	12	**2.1%**	*3.5%*	*1.4*
	45	*35*	30	35	36	55	1.4	1.0	1.5	**1.98**	0.5	13	**1.9%**	*2.5%*	*0.6*
	45	*-*	36	42	36	43	1.0	1.0	1.5	**1.69**	0.5	15	**1.7%**	*2.0%*	*0.4*
	18h	*18*	42	78	31	35	0.6	1.0	1.5	**1.24**	0.3	10	**1.3%**	*1.4%*	*0.1*
	34h	*35*	42	77	31	35	0.6	1.0	1.5	**1.25**	0.3	10	**1.3%**	*1.4%*	*0.1*
	35h	*35*	79	42	35	31	0.5	1.0	1.5	**1.24**	0.3	10	**1.3%**	*1.4%*	*0.1*
	35h	*36*	36	77	35	31	0.6	1.0	1.5	**1.28**	0.5	12	**2.1%**	*1.4%*	*-0.7*
Ply	*1*	*14*	70	10	70	76	1.8	0.9	1.5	**2.35**	0.8	12	**3.1%**	*3.0%*	*-0.1*
Ratio	*3*	*15*	9	70	77	70	1.9	1.2	1.5	**2.65**	0.7	14	**2.5%**	*3.5%*	*1.0*
	4	*15*	9	70	77	70	1.9	0.9	1.5	**2.60**	0.7	12	**2.9%**	*3.4%*	*0.5*
	19	*15*	59	7	75	77	2.3	1.1	1.5	**2.65**	1.0	13	**3.8%**	*3.5%*	*-0.4*
Node	*25h*	*27*	70	83	60	63	0.8	1.0	1.4	**1.39**	0.3	15	**0.8%**	*1.6%*	*0.8*
ratio	*26h*	*27*	70	83	60	63	0.8	1.0	1.4	**1.39**	0.3	15	**0.8%**	*1.6%*	*0.8*
	33	*27*	7	60	77	70	2.2	1.0	1.4	**2.30**	0.7	13	**2.7%**	*3.0%*	*0.3*
	34	*27*	7	60	77	70	2.2	1.0	1.4	**2.30**	0.7	13	**2.7%**	*3.0%*	*0.3*
	33	*38*	9	71	71	75	1.8	1.0	1.4	**2.10**	0.3	13	**1.0%**	*2.7%*	*1.7*
	34	*39*	9	71	71	75	1.8	1.0	1.4	**2.10**	0.5	15	**1.7%**	*2.7%*	*1.0*
	27h	*29*	70	83	60	63	0.8	1.0	1.6	**1.62**	0.3	15	**0.8%**	*1.9%*	*1.1*
	28h	*29*	70	83	60	63	0.8	1.0	1.6	**1.62**	0.5	13	**1.9%**	*1.9%*	*0.0*
	37	*29*	7	60	77	70	2.2	1.0	1.6	**2.67**	0.8	12	**3.1%**	*3.0%*	*-0.1*
	38	*29*	7	60	77	70	2.2	1.0	1.6	**2.67**	0.8	13	**2.9%**	*3.0%*	*0.1*
	23	*29*	9	68	60	63	1.6	1.0	1.6	**2.28**	0.8	12	**3.1%**	*3.0%*	*-0.1*
	16h	*17*	70	83	77	70	1.0	1.0	1.5	**1.64**	0.5	15	**1.7%**	*2.0%*	*0.3*
	23	*17*	7	60	77	70	2.2	1.0	1.5	**2.48**	0.8	12	**3.1%**	*3.2%*	*0.1*
Thin Ribs	*1h*	*9,10*	31	49	66	62	1.6	1.0	1.5	**2.12**	0.5	12	**2.1%**	*2.7%*	*0.6*
Adjusted	*25h*	*27*	70	85	60	63	0.8	1.0	1.4	**1.38**	0.3	15	**0.8%**	*1.6%*	*0.7*
	26h	*27*	70	85	60	63	0.8	1.0	1.4	**1.38**	0.3	15	**0.8%**	*1.6%*	*0.7*
	27h	*29*	70	85	60	63	0.8	1.0	1.6	**1.61**	0.3	15	**0.8%**	*1.9%*	*1.1*
	28h	*29*	70	85	60	63	0.8	1.0	1.6	**1.61**	0.5	13	**1.9%**	*1.9%*	*0.0*
	16h	*17*	70	85	77	70	0.9	1.0	1.5	**1.63**	0.5	15	**1.7%**	*2.0%*	*0.3*